REGULATION AND FUNCTION OF AUTOPHAGY IN CIGARETTE SMOKE-INDUCED CELLULAR STRESS: IMPLICATIONS FOR CHRONIC OBSTRUCTIVE PULMONARY DISEASE

by

Hilaire Colletta Lam

BA, Wellesley College, 2006

Submitted to the Graduate Faculty of

School of Medicine in partial fulfillment

of the requirements for the degree of

Doctor of Philosophy

University of Pittsburgh

2011

UNIVERSITY OF PITTSBURGH

SCHOOL OF MEDICINE

This dissertation was presented

by

Hilaire Colletta Lam

It was defended on

September 8, 2011

and approved by

Dr. Michael T. Lotze, MD, Professor, Vice Chair, Department of Surgery; Assistant Vice Chancellor, University of Pittsburgh Schools of the Health Sciences

Dr. Tim D. Oury, MD, PhD, Professor, Department of Cellular and Molecular Pathology

Dr. Donna B. Stolz, PhD, Associate Professor, Department of Cellular and Molecular Pathology

Dr. Ora A. Weisz, PhD, Professor, Department of Cell Biology and Physiology

Thesis Advisor: Dr. Augustine M. K. Choi, MD, Parker B. Francis Professor of Medicine, Harvard Medical School; Chief, Pulmonary and Critical Care Medicine, Brigham and Women's Hospital

REGULATION AND FUNCTION OF AUTOPHAGY IN CIGARETTE SMOKE-INDUCED CELLULAR STRESS: IMPLICATIONS FOR CHRONIC OBSTRUCTIVE PULMONARY DISEASE

Hilaire Colletta Lam, PhD

University of Pittsburgh, 2011

Chronic obstructive pulmonary disease (COPD) is characterized by an abnormal inflammatory response to inhalation of noxious agents, particularly cigarette smoke (CS), which leads to a progressive and poorly reversible decline in lung function. Autophagy, a highly conserved adaptive response to cellular stresses, which removes cytoplasmic components such as organelles and long-lived proteins via encapsulation and lysosome-dependant degradation, has also been implicated in cell death pathways. We previously observed autophagy protein induction and autophagosome accumulation in *in vivo* and *in vitro* models of experimental COPD, as well as in COPD patients. The regulation and function of autophagy in CS-induced COPD have not been fully elucidated.

To delineate the role of autophagy in the response of lung epithelial cells to CS we developed a novel *in vitro* model of mainstream CS exposure in primary mouse tracheal epithelial cells (MTECs) differentiated at an air-liquid interface (ALI). MTEC cultures in response to CS *in vitro* recapitulated many features of CS exposure *in vivo*, including autophagosome accumulation, cilia shortening, misfolded protein aggregation, loss of tight junction integrity and cell death. *In vitro* we discovered that sublethal doses of CS enhanced selective autophagic flux, while CS-induced cytotoxicity was associated with decreased autophagic activity and autophagosome accumulation. We also discovered that autophagic flux is induced *in vivo* upon acute exposure, but is not significantly upregulated following chronic 6 month exposure to CS. Both $LC3B^{-/-}$ and $Beclin\text{-}1^{+/-}$ mice and MTEC cultures were protected from CS induced injury, indicating that these autophagy proteins promote epithelial cell death. Moreover, we investigated the effects of CS on autophagic substrates. HDAC6 regulates autophagosome-lysosome fusion, autophagic degradation of ubiquitinated protein aggregates, and cilia resorption. Cytotoxicity and protein aggregate accumulation were observed basally in $HDAC6^{-/Y}$ derived MTEC cultures, while CS-exposed mice were more vulnerable to

emphysematous changes. Evidence of autophagic degradation of cilia components was also observed following CS treatment. These data indicate that autophagy plays a complex role in COPD pathogenesis, in which CS-induced autophagy both removes deleterious protein aggregates and contributes to apoptosis.

TABLE OF CONTENTS

LIST OF FIGURES

PREFACE

ACKNOWLEDGEMENTS

I would like to begin by acknowledging my mentor, Augustine Choi, who has given me the necessary resources, guidance, and freedom to develop this project. I have grown exponentially in both technical and critical thinking skills working in his laboratory.

Augustine Choi has an incredible team and I would not be the scientist I am today without the members of his laboratory, past and present, who have played a critical role in my training. Working with them has been a great pleasure and privilege.

I would like to specifically acknowledge, Hong Pyo Kim, who assisted in the conception of this project and my initial training in the laboratory, Emeka Ifedigbo, who has been and ever present source of logistical support, Jeff Haspel, with whom I have had wonderful scientific discussions about flux, Suzanne Cloonan and Stefan Ryter for their critical reading of this manuscript.

Since the first week I arrived in Boston, numerous members of the Pulmonary and Critical Care Medicine Department of Brigham and Women's Hospital have provided invaluable assistance and advice. In particular, I would like to thank Shiva Tyagi for his technical training in the generation of the mouse tracheal epithelial cell cultures.

My dissertation committee has also provided great insight and guidance into this project. Even from a distance, emails have been exchanged that have significantly helped in the development of this project.

My family has been a great support throughout this journey. From moving me to Pittsburgh and back to Boston and then just being there through the ups and downs of graduate school, I am grateful for their love and support.

My husband, Quentin Lam, has been a sustaining force through it all, and everything I have accomplished belongs in part to his constant presence and encouragement.

Finally, my faith allows me to look outside of myself, to never be so caught up in my experiments, that I am unable to see the people around me and their needs both scientific and

personal. I ultimately work not for the esteem of my peers or my own personal satisfaction but to say:

> *Not to us, O LORD, not to us, But to Your name give glory because of your lovingkindness, because of Your Truth. Psalm 115:1*

1.0 INTRODUCTION

Chronic obstructive pulmonary disease (COPD) is a leading cause of mortality and morbidity worldwide (1). The primary etiological agent of COPD is cigarette smoke (CS), which promotes the pathogenesis of chronic bronchitis and emphysema (2). At the molecular level development of COPD is primarily attributed to imbalances in oxidant, inflammatory and protease pathways (3). Recently implicated in COPD, autophagy is a lysosome-dependent degradative process promoting both cytoprotection via degradation of damaged organelles and proteins as well as cell death (4-8). Since there are relatively few treatment options available to COPD patients, elucidating the roles of autophagy in this disease may yield valuable insights for future therapies.

1.1 COPD

COPD affects 10% of the global population over 40 years of age with billions of dollars spent each year on treatment in the US alone. Extrapolations predict that COPD will be the third leading cause of death worldwide by 2020 (1). In developing countries exposure to environmental pollution, particularly biomass fuels, is an increasingly prevalent cause of disease pathogenesis. Since only 10-20% of smokers develop COPD, this is a strong indication that genetic factors play a critical role in disease vulnerability. Rigorous genomic studies are underway to identify disease susceptibility loci (9-11).

1.1.1 COPD pathology

COPD pathology is complex with significant patient-to-patient variation, as the disease manifests degrees of emphysema, small airway remodeling, and chronic bronchitis (12-14). Patients with COPD experience an accelerated decline in forced expiratory volume in one second (FEV_1), as well as, increased resistance in the conducting airways and reduced lung compliance (2, 9). Chronic bronchitis is characterized by inflammation of the airways with mucus gland hypertrophy and hyperplasia. The resultant mucus hypersecretion further obstructs airways already narrowed by inflammation and fibrosis. Emphysema is defined as permanent enlargement of airspaces due to loss of alveolar cells, which leads to significant reductions in gas exchange area and contributes to loss of lung elastic recoil, thereby restricting airflow. Difficulty breathing, dyspnea, commonly associated with COPD reduces capacity for physical activity and promotes co-morbidities such as muscle weakness and osteoporosis. Recent studies have begun to focus on the systemic effects of COPD, including the contribution of increased inflammatory mediators in the serum to the disease process (15-18). Patients with COPD frequently have co-morbid cardiovascular disease including arterial stiffness, endothelial cell dysfunction, and a propensity for the formation of atherosclerotic plaques (19, 20). COPD is also correlated with increased risk of diabetes, suggesting that metabolic pathways are also affected in this disease (21, 22).

1.1.2 COPD molecular mechanisms of disease

Considerable insights into the molecular mechanisms of COPD have been gained through studying the imbalances in oxidative metabolism, inflammation and protease activity. These molecular pathways are interdependent, frequently acting in concert to promote disease pathogenesis.

CS contains thousands of free radicals in each puff and imposes a significant oxidative stress for epithelial cells; therefore, both intracellular and extracellular antioxidant metabolism is critical. The key transcription factor mediating the antioxidant stress response is nuclear factor E2-related factor 2 (Nrf-2). Expression of this protein, which binds to antioxidant response elements, is increased by CS, but decreased in the disease state. Nrf-2 deficient mice are

susceptible to CS induced airspace enlargement, suggesting that this transcription factor is a critical determinant of disease susceptibility (23-25).

Particulate and vapor phase constituents of CS activate chronic inflammatory pathways beginning with activation of macrophages and recruitment of neutrophils through the release of chemotactic factors, such as interleukin-8 (IL-8) and leukotriene B4 (LTB4) (26-28). Activation of cytotoxic T lymphocytes (CD8+), which target epithelial cells for destruction, has also been implicated in this inflammatory cascade. (29). Neutrophils release neutrophil elastase (NE) and the oxidative environment promotes the activity of macrophage-derived matrix metalloproteinases (MMPs), which degrade connective tissue components, such as elastin, collagen and fibronectin (30-32). Extracellular matrix loss then induces detachment associated epithelial cell death, anoikis.

Excessive protease activity contributes to the development of autoimmunity by producing an abundance of extracellular matrix self-antigens in an inflammatory setting (33). Protease activities in the lung are usually balanced by antiproteases, such as α-1 antitrypsin (A1AT), secretory leukoprotease inhibitor (SLPI), and tissue inhibitors of matrix metalloproteases (TIMPs) (34-37). Mutations in the A1AT gene were the first genetic factors implicated in the development of emphysema. There is complex interdependence among these three processes and variability between patients, which has impeded the development of effective therapeutics.

1.1.3 *In vivo* models of COPD

COPD, particularly emphysematous changes, have been studied in rodents, dogs, guinea pigs, monkeys, and sheep (38, 39). With the advent of modern genetic manipulations, mice have become the model of choice; however, there are noteworthy differences between mouse and human pulmonary anatomy (40). Mice have less extensive airway branching and do not normally have respiratory bronchioles. The majority of cells in the human bronchial tree are ciliated and there is an abundance of goblet cells, both of which decline in approaching the terminal bronchioles, while Clara-like cells dominate in the mouse respiratory tract and goblet cells are extremely rare. Only 37% of the murine airway cells are ciliated, which occur in heterogeneous patches. Bronchial glands, which are hypertrophied and hyperplastic in chronic bronchitis, are only present in the mouse trachea (41-43).

There are a number of methods used to produce emphysematous changes in mouse models. Intratracheal instillation into the lungs of lipopolysaccharide (LPS), elastase, and vascular endothelial growth factor (VEGF) inhibitors all induce varying degrees of apoptosis and inflammation (44-48). However, CS exposure to mice is most similar to human COPD and causes physiological alterations resulting in emphysema and airway remodeling. The disadvantage of this model is that disease development takes at least 3-6 mo to develop and is milder, nonprogressive, and certain features, such as goblet cell metaplasia, will regress after smoking cessation. Also, due to a lack of bronchial glands, mice are a poor model of mucus hypersecretion.

There are strain dependent variations in the development of CS-induced emphysema in mice, potentially providing insights into the mechanistic basis of this disease (49). The mouse strain AKR/J is most susceptible CS injury, showing 30% increase in airspace enlargement by mean linear intercept (Lm). AKR/J mice exposed to CS for 6 mo demonstrate a significant decrease in tissue elastance and increased compliance along with the production of proinflammatory cytokines and infiltration of neutrophils, macrophages, and Th1 associated lymphocytes. The C57BL/6 strain is less susceptible to emphysema with a 13% increase in Lm following 6 mo of exposure; however, lung mechanics remained unchanged in this strain. Finally, NZWlac/J mice are resistant to CS induced emphysema (49). Valuable insights have been gained from the mouse CS model due to the ease of genetic manipulation.

1.1.4 *In vitro* models of COPD

CS contains more than 4,000 chemicals and fundamental molecular mechanisms of this complex mixture have been elucidated from the development of *in vitro* cultures treated with specific toxic components such as paraformaldehyde, nicotine, and even general oxidative stressors such as H_2O_2 (50-57). In an effort to more fully mimic CS exposure, cells have also been treated with CS condensate (CSC) and CS extract (CSE), which involve solubilizing solid components that deposit following combustion and collecting hydrophobic constituents by bubbling smoke through media, respectively (58-60). These treatment strategies have been applied to numerous cell types including cell lines of epithelial, endothelial, mesenchymal, and hematopoietic lineages (16, 61-70). Recent studies have sought greater physiological relevance by growing

cells on transwells and treating the cells at an ALI with mainstream CS (71-73). From these studies careful dose and kinetic assays have been performed, evaluating the stress responses instigated to maintain cellular homeostasis, as well as, the identification of key players involved in mediating CS-induced cell death.

1.1.5 Effects of CS on the respiratory epithelium

In vivo and *in vitro* studies indicate that there are complex interactions between adaptive and pathological responses, which depend on the dose, time and duration of CS exposure (74-76). CS induces structural changes, activation of stress responses and cell death. Acute responses include regulated loss of epithelial barrier integrity via disruption of intercellular contacts (72, 77). Microarray analysis of epithelial cells exposed to CS report acute downregulation of transcription (73). There is also increased antioxidant pathway activation and RNA processing (73). A number of studies have demonstrated upregulation of the unfolded protein response (UPR) and endoplasmic reticulum associated degradation (ERAD) pathways with CS exposure (78, 79). Activation of prosurvival and proinflammatory transcription factor, nuclear factor κ-light-chain-enhancer of activated B cells (NFκB), has also been implicated, promoting the transcription of IL-6, IL-8 and other proinflammatory cytokines (80-85).

Ciliated cells represent a large proportion of the apical surface area of the respiratory epithelium and are vulnerable to CS-induced injury (86-89). Cilia are microtubule-based organelles formed by specialized centrioles, called basal bodies, which dock at the plasma membrane and nucleate the axoneme. While the ciliary membrane is continuous with the plasma membrane, cilia are discrete organelles due to transition fibers at the base of each cilium that regulate protein import and export (90, 91). Motile ciliary axonemes are comprised of 9 outer doublet microtubules and a central pair, a 9+2 structure. Cilia are dynamic organelles dependent on intraflagellar transport (IFT). Continuous kinesin dependent anterograde trafficking adds cilia components to the distal tip of the cilium, while dynein-dependent retrograde trafficking recycles materials to the cell body (92, 93). Recently, ubiquitination of cilia components in the axoneme has been implicated in cilia resorption; however, lack of ciliary proteasomal activity suggests that tagged proteins are degraded in the cytoplasm (94).

Early studies demonstrated that CS can increase and decrease ciliary beat frequency through protein kinase C (PKC) and purinergic signaling, as well as evidence for both increased and decreased proportions of ciliated cells lining the airways (75, 76, 87, 89, 95). These data provide examples of the epithelium dynamically adapting to CS-induced stress. CS cytotoxicity also causes desquamation of the epithelium, which has been shown to induce squamous cell metaplasia through the dedifferentiation of neighboring viable cells, which then proliferate to regenerate an intact epithelium. Chronic CS exposure inhibits differentiation of ciliated cells and promotes repopulation with goblet cells producing a hyersecretory phenotype (**Figure 1**) (96, 97).

Recent studies in human populations have noted a significant change not only in ciliated cell number, but also, cilia length in the respiratory epithelium of healthy smokers. Modeling of these effects suggested a significant defect in mucociliary clearance even in healthy smokers (88). Since mucociliary clearance is the primary innate defense mechanism of the lung, CS-induced cilia injury leaves lungs vulnerable to disease-promoting infections.

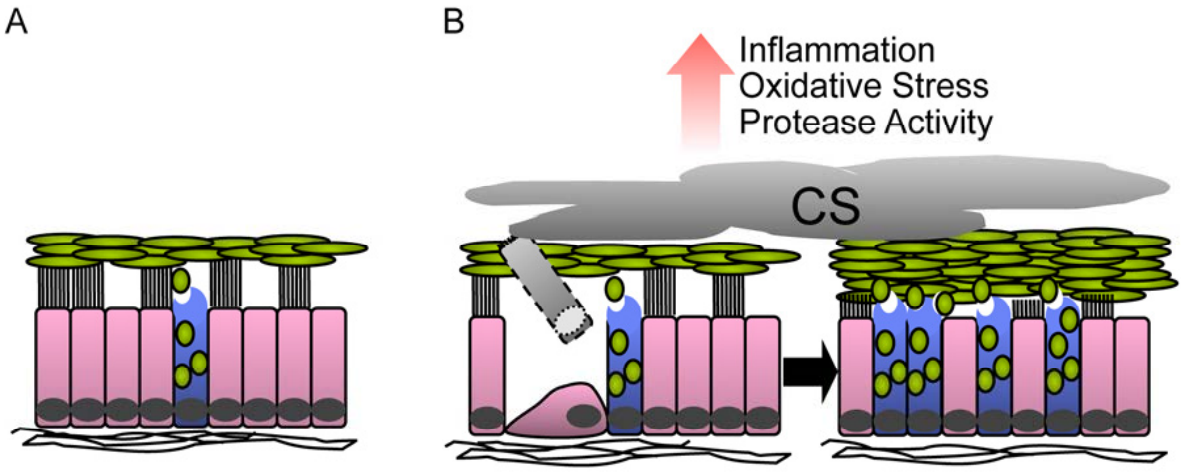

Figure 1. The effects of CS on mucociliary clearance in the respiratory epithelium. A) Mucociliary clearance is the primary innate defense mechanism of the lung. Goblet cells secrete mucins, which trap particulates and pathogens in the mucus layer. Ciliated cells push the mucus out of the lungs by coordinated beating of the cilia. B) Exposure to CS induces inflammation, oxidative stress, and protease activity. In this environment, epithelial cell apoptosis is increased and the remaining cells undergo dedifferentiation and squamous cell metaplasia to protect the underlying interstitium. Upon recovery of the intact epithelium, goblet cell differentiation dominates and cilia shorten leading to a disruption of mucociliary clearance, ultimately promoting airway obstruction.

1.1.6 COPD management and treatment

There are limited therapeutic options for the management of COPD. Smoking cessation is the first step in all treatment strategies, which reduces the rate of decline in remaining lung function, but fails to reverse established disease. Pulmonary rehabilitation through structured programs of education and physiotherapy has been shown to improve exercise capacity and quality of life in patients. Bronchodilators, such as anticholinergics and β2 andrenoreceptor agonists promote a less than 10% increase in FEV_1, as well as, reducing dyspnea and increasing exercise tolerance. Treatment with corticosteroids is controversial and seems most effective in patients with coexistant asthma. Generally, corticosteroids in combination with broad spectrum antibiotics are effective during acute exacerbations, but fail to prevent disease progression and are avoided for routine disease management. As lung function declines, long-term oxygen therapy is indicated (98-105). Lung transplantation remains a viable therapeutic option for some patients with end stage COPD.

1.2 AUTOPHAGY

The process of autophagy is named from the Greek “to eat oneself” and is a lysosome-dependent mechanism for the removal of cytoplasmic constituents (106-108). There are three distinct autophagic pathways, microautophagy, chaperone-mediated autophagy and macroautophagy. Small invaginations that pinch-off into the lysosomal membrane characterize microautophagy (109, 110). Chaperone-mediated autophagy requires chaperone proteins Hsc70, Hsp40, Hip and Hop interacting with lysosome–associated membrane protein (LAMP) 2 to specifically transport unfolded proteins containing the KFERQ targeting motif into the lysosomal lumen (111-113). The primary focus of these studies is macroautophagy, herein referred to as autophagy, which is responsible for the bulk degradation of cytoplasmic constituents including organelles, proteins and protein aggregates (114).

Autophagy initiation requires the formation of a phagophore, which elongates and matures into the double-membraned autophagosome. Once formed, autophagosomes fuse with various components of the endocytic pathway, such as endosomes, forming hemiphagsomes.

Ultimately these structures fuse with the lysosome, and the internal membrane and constituents are degraded by lysosomal hydrolases in the autophagolysosome (**Figure 2**). Freed amino acids along with other building blocks, are recycled to the cytoplasm via specialized permease channels (106). Autophagy plays both physiological and pathological roles in numerous processes including adaptation to starvation, protein and organelle clearance, development, aging, elimination of microorganisms, cell death, tumor suppression and antigen presentation (115-118).

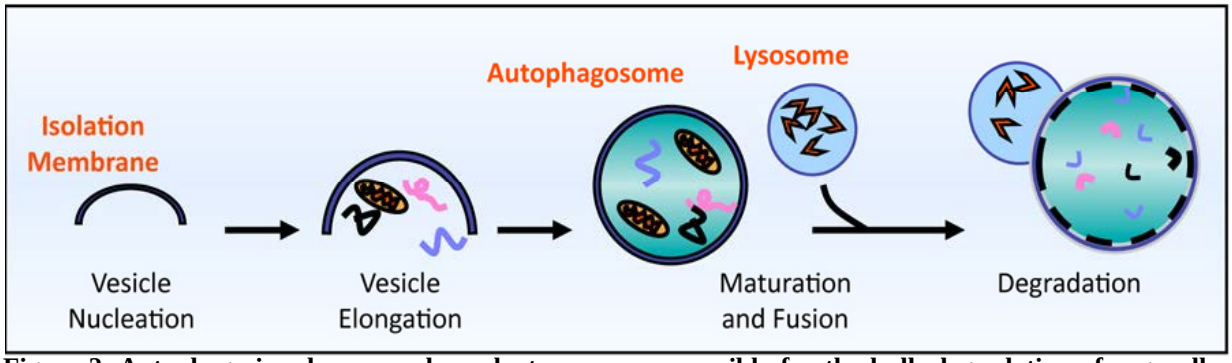

Figure 2. Autophagy is a lysosome-dependent process responsible for the bulk degradation of organelles and long-lived proteins. Autophagy involves the encapsulation of cytoplasmic constituents into a double-membraned structure called an autophagosome, which forms *de novo* in the cytosol. Mature autophagosomes fuse with lysosomes leading to the degradation of the inner membrane and sequestered cytoplasmic components by lysosomal hydrolases. Degradation products, including essential biological building blocks, are then recycled to the cytoplasm.

1.2.1 Molecular mechanisms of autophagy

Generally designated as Atg, more than 30 proteins have been implicated in autophagy regulation. Mammalian target of rapamycin (mTOR), the master sensor of metabolic status, inhibits autophagy under conditions of nutrient abundance (119-129). Other mediators of autophagic regulation identified to date include reactive oxygen species (ROS), B cell lymphoma 2 (Bcl-2), AMP-activated protein kinase (AMPK), $Ca2^{+}$, Bcl-2 and nineteen kilodalton interacting protein 3 (BNIP3), damage-regulated autophagy modulator (DRAM), calpain, tumor necrosis factor-related apoptosis-inducing ligand (TRAIL), Fas-associated death domain (FADD), and inositol triphosphate (IP_3) (130-141). While the sources of autophagic membranes are cell and context specific, the ER is believed to be the major contributor along with the mitochondrial, plasma and nuclear membranes (142-144).

Phagophore initiation begins with the ULK complex, composed of ULK1/2, Atg13, FIP200, and Atg101, which is negatively regulated by mTOR complex 1 (mTORC1)-mediated phosphorylation (126, 145, 146). Nucleation is further supported by a class III phosphoinositol(3)kinase (PI3K), Vps34, which is recruited in a complex with Beclin-1, VPS15, UVRAG, Ambra1, and Bif1, and regulates lipid components at the forming autophagic membrane (**Figure 3**). Beclin-1 contains a BH3 domain, through which interaction with Bcl-2 inhibits autophagy. Rubicon, another Beclin-1 interacting protein negatively regulates autophagosome-lysosome fusion (147-155). Two ubiquitin-like conjugation pathways promote autophagosome membrane elongation. Atg12 is covalently conjugated to Atg5 via activation by Atg7, an E1-like enzyme, and Atg10, an E2-like enzyme. Atg16L interacts with the Atg5-Atg12 complex and dimerizes on the outer membrane promoting proper elongation and curvature of the isolation membrane (156-160). Microtubule-associated protein light-chain 3B (LC3B) is conjugated to phosphatidylethanolamine and associates with both the inner and outer membrane

in the second conjugation system (**Figure 3**). LC3B is first hydrolyzed by Atg4A-D at the carboxyterminus revealing a terminal glycine residue, and can also be recycled from the outer surface of the autophagosome by similar proteolytic activity of Atg4. LC3 and related proteins GATE16 and GABARAP are then activated and conjugated via Atg7, E1-like enzymatic activity, and Atg3, E2-like enzyme (161-166). Since LC3B remains associated with the completed autophagosome until lysosome fusion and is a substrate of degradation, this protein is frequently used as a marker of autophagosome formation and activity (167). Fusion of autophagosomes with lysosomes depends on the microtubule and actin cytoskeleton, as well as LAMP2 and the GTPase Rab7 (168-171). Upon hydrolytic degradation, amino acids are recycled to the cytoplasm by the putative amino acid effluxer Atg22, while mechanisms of carbohydrate and lipid recycling are not fully elucidated (172-174).

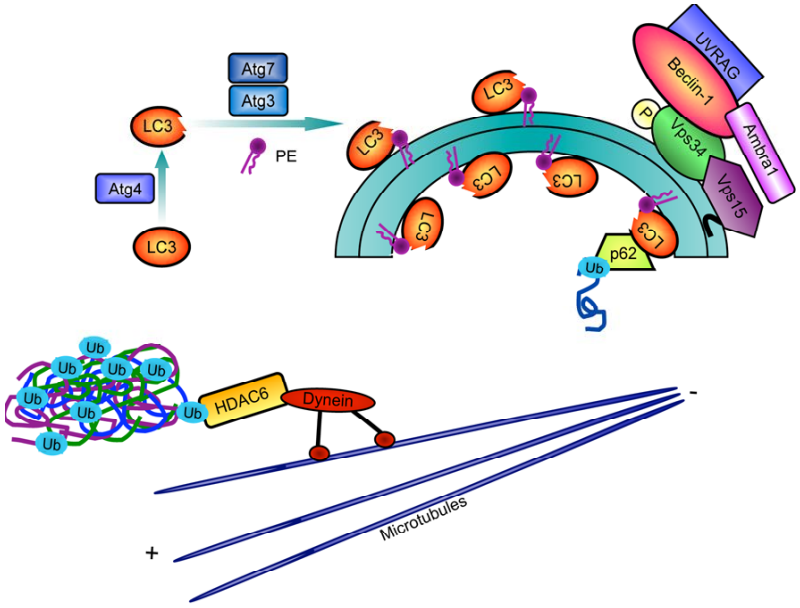

Figure 3. Molecular mechanisms of autophagy. Greater than 30 proteins have been implicated in autophagy. Beclin-1 is a key component of the class III PI3K complex, which is required for autophagosome nucleation. LC3 is covalently conjugated to phosphatidylethanolamine on the inner and outer membranes of autophagosomes by the proteolytic activity of Atg4, followed by the ubiquitin ligase-like activity of Atg7 and Atg3. Selective autophagy is mediated by a growing number of adaptor molecules, including p62 and HDAC6. A ubiquitin binding domain and LC3 interacting domain allow p62 to recruit ubiquitinated proteins to the forming autophagosome. HDAC6 has ubiquitin and dynein binding domains, which promote efficient autophagic clearance of misfolded proteins by centralizing ubiquitinated aggregates. Furthermore, HDAC6 mediated deacetylation of α-tubulin and cortactin regulate intracellular trafficking and autophagosome-lysosome fusion, respectively.

1.2.2 Selective autophagy

While autophagy was originally described as a nonselective process, a number of proteins, including p62/SQSTM1, histone deacetylase (HDAC) 6, neighbor of BRCA1 (NBR1) and Bag3 confer specificity to autophagic cargos. The chaperone protein Bag3 is upregulated with aging and promotes degradation of improperly folded proteins by autophagy (175-180). NBR1 was identified in a complex with Atg8, the yeast homologue of LC3B, in a yeast two-hybrid screen. NBR1 contains a conserved LC3 interacting motif, LIR, and an ubiquitin-binding domain. Both NBR1 and p62 localize to protein aggregates marking them for autophagic degradation, in a process by which these proteins are also selectively consumed (181-183).

The selective autophagy protein p62 plays a critical role in the degradation of ubiquitinated proteins by autophagy, via an ubiquitin binding and LIR motif (**Figure 3**) (181, 184). Also as a target of autophagic degradation steady state levels of p62 have been used to measure autophagic activity (185). Recently p62 was shown to be an important mediator of antioxidant activity via sequestration of Kelch-like ECH-associated protein 1 (Keap1) and release of Nrf-2 for transcription of proteins involved in antioxidant metabolism. From these studies p62 was shown to be transcriptionally regulated in a positive feedback loop by a Nrf-2 antioxidant response element (186-190). Regulation of Nrf-2 by p62 has added an additional layer of complexity to the study of autophagy. For example, inhibition of autophagy promotes robust ubiquitinated protein accumulation. However, further analysis of knockdown of both autophagy and p62 relieved the accumulation, and Nrf-2 was implicated in directly upregulating components of the ubiquitin pathway (191, 192). Similarly, Atg7 chimeric knockout mice are predisposed to hepatic tumors, which are likewise relieved by p62 or Nrf-2 double knockout suggesting that tumor formation and survival in this model requires loss of autophagy as well as upregulation of antioxidant capacity (193).

HDAC6 is another complex protein implicated at various stages of autophagy (**Figure3**). This protein is a cytoplasmic deacetylase with two catalytic deacetylase domains, a strong ubiquitin binding domain, and a dynein interacting domain (194-199). Targets of HDAC6 deacetylase activity include Hsp90, α-tubulin, peroxiredoxin and cortactin (196, 200-203). HDAC6 promotes efficient clearance of misfolded proteins by both concentrating substrates near the microtubule organizing center for autophagic degradation via ubiquitin binding and dynein

interactions, as well as assisting in autophagosome-lysosome fusion via deacetylation of the F-actin interacting protein cortactin (198, 204-207). Finally, acetylation of α-tubulin is associated with long-lived microtubules, such as is the case for the microtubules of the ciliary axoneme (208, 209). Microtubule acetylation enhances motor protein association, increasing the rate of trafficking and, while controversial, is generally believed to promote microtubule stability. Therefore, deacetylation and destabilization of microtubules by HDAC6 has been implicated in mediating intracellular trafficking and promoting growth factor induced cilia resorption (210-212).

1.2.3 Methods for detecting and monitoring autophagy

There are many complimentary methods for monitoring autophagosome formation (213, 214). Due to their distinct double membrane structure, autophagosomes are easily identified morphologically by transmission electron microscopy (TEM) (215-218). Quality of membrane architecture as well as care to distinguish between true autophagosomes and cytoplasmic constituents proximal to ER is essential in this analysis. Quantification of autophagosomes can be reported as both a number per area as well as a percentage of cytoplasmic area.

Since TEM provides a relatively small sampling of cells, immunofluorescence labeling is frequently employed (214, 219, 220). Endogenous labeling of LC3B, which remains associated with the autophagosome membrane from nucleation to lysosome fusion is most frequently utilized for autophagosome assessment. In these studies diffuse cytoplasmic LC3B staining becomes more punctate upon autophagosome formation. Regulation of autophagy genes and proteins are additional markers of autophagic activity. Immunoblot analysis of LC3, which migrates at a lower apparent molecular weight upon conjugation to phosphatidylethanolamine in association with the autophagosome membrane, is frequently used as an indirect marker of autophagosome numbers (221, 222). Since p62 is a direct target of autophagic degradation, a reciprocal relationship between protein levels and autophagic activity has been used in some studies (179, 223, 224).

Autophagic flux, the rate of protein turnover by autophagy, is an important readout for any study, since autophagosome accumulation could reflect either enhanced autophagosome formation or inhibited lysosomal degradation. A construct of LC3B tagged with both GFP and

mCherry was generated to assess the proportions autophagosomes and autophagolysosomes. While autophagosomes fluoresce yellow, the autophagolysosomes appear red because the acidic environment denatures and quenches the GFP activity (194, 213, 214, 220). Care must be taken with these studies as overexpression of the GFP tag may lead to protein aggregation and puncta formation independent of autophagy (225). Autophagic flux assays can also be conducted by comparing the accumulation of autophagic substrates in control and treated conditions following inhibition of degradation in the lysosome. Inhibitors such as Bafilomycin A_1, E64D, and chloroquine (CQ) prevent acidification of the lysosome, which is required for hydrolase activation. Leupeptin and pepstatin are specific inhibitors of lysosomal cathepsin activity. Using this approach, autophagic activity can be assessed both *in vivo* and *in vitro* (214, 219, 221, 226, 227).

1.2.4 Protein turnover in the lung

Cellular catabolism in the lung was studied in detail 30 years ago. From these studies two distinct classes of proteins were characterized, short-lived and long-lived. The short-lived proteins were rapidly transcribed, labeled with the radioisotope within 10 min and were degraded at a linear rate of 11% per h, while long-lived proteins required several hours of labeling and were then degraded at a rate of 1-3% per h (228). While starvation was shown to nearly double the rate of long-lived protein degradation, metabolite excess, such as glucose or insulin administration, was able to suppress protein turnover (229). At the time autophagy was not a focus of these early studies; however, the dynamic response to stress and energy status are hallmark features of autophagic regulation.

1.2.5 Autophagy in COPD

Over twenty years ago autophagosomes were observed by TEM analysis of the respiratory epithelium of beagle dogs exposed to CS (230). In microarray analysis, Atg5 and LC3B were significantly upregulated in primary human airway epithelial cells differentiated at ALI and exposed to CS (73). Furthermore, links between metabolism, particularly autophagy-activating malnutrition, and lung destruction are also evident in the literature. Malnutrition in humans alone

is able to promote emphysematous changes in the lung (231-233). Similarly, the only mouse strains susceptible to CS induced emphysema are strains that fail to demonstrate the usual age-related weight gain observed over 6 mo of chronic treatment (49). These data provide strong evidence implicating autophagy and metabolism in lung injury.

The first papers exploring the role of autophagy in COPD demonstrated transcriptional upregulation of autophagy proteins in COPD patients, as well as, autophagosome accumulation that positively correlated with COPD severity (6, 8). *In vitro* and *in vivo* models indicated that autophagosome accumulation was an acute response to CSE treatment and preceded cell death. Interestingly, knockdown of Beclin-1 and LC3B *in vitro* protected cells from CS-induced cell death (6, 8). While the role of macroautophagy in directly executing cell death is a greatly debated, there is ample evidence for crosstalk between apoptosis and autophagy (234).

The importance of disrupted protein folding homeostasis in airway epithelial cell stress has only recently moved to the forefront as a potential mediator of COPD pathogenesis. Recent studies have begun to elucidate the effects of CS on ER stress and protein turnover (66, 78, 79, 235-237). In particular CS contains ROS, which interfere with proper protein folding in the ER and elicits UPR and ERAD (78, 79). During the process of ERAD misfolded proteins are ubiquitinated and targeted for degradation by the ubiquitin proteasome system (UPS) and autophagy (238, 239). In particular, misfolded proteins that accumulate are sequestered into inclusion bodies and aggresomes in the cytoplasm for efficient autophagic clearance (240, 241). Recently, ubiquitin positive aggregates have been observed in Gold stage 4 smokers. These findings are reminiscent of the inclusion bodies comprised of misfolded proteins observed in neurodegenerative disorders (237). In the lung, accumulation of misfolded proteins has been associated with increased production of inflammatory mediators by epithelial cells. These findings have led to the speculation that mutant A1AT may promote emphysematous changes through the accumulation of misfolded protein aggregates (242). Based on these observations, autophagy is implicated as a key mechanism for the degradation of misfolded proteins (243).

Molecular mechanisms implicated in the upstream regulation of autophagy have also been correlated with the development of emphysema, in these studies CS was shown to inhibit mTOR via CS induced Rtp801 expression (7). While Rtp801 promoted inflammation, knockout mice were protected from CS induced inflammation, apoptosis and emphysema. Finally inhibition of mTOR directly promoted CS-induced proinflammatory pathways. While these

studies were not focused on autophagy, the finding of increased emphysema with mTOR inhibition, which activates autophagy, provides evidence for the relevance of these pathways in COPD.

The autophagic response appears to be cell type specific. In studies focused on the role of autophagy in smokers' macrophages, which are known to have reduced antimicrobial and enhance production of inflammatory mediators, autophagosomes accumulated due to decreased autophagic flux. This defect led to accumulation of damaged mitochondria and decreased ATP levels and a greater dependence on anaerobic respiration (244). These studies implicate autophagy in COPD; however, the relationship is complex and far from completely elucidated.

1.3 APOPTOSIS

Apoptosis is a regulated cell death pathway characterized by cell shrinkage, breakdown of the cytoskeleton, formation of apoptotic bodies, loss of mitochondrial membrane potential and DNA fragmentation (245-250). Apoptosis is primarily executed by a cascade of cystein proteases, which specifically cleave at C-terminal aspartate residues. In the caspase cascade stimuli activate initiator caspases 2, 8, 9, and 10, which then cleave effector caspases 3, 6, and 7 responsible for cellular disposal.

Intrinsic apoptosis is initiated by mitochondrial outer membrane permeability (MOMP), which is regulated by the Bcl family of proteins. Antiapoptotic members Bcl-2, Bcl-xL and Mcl-1, containing BH 1,2,3,4 domains, reside on the mitochondrial surface and balance the proapoptotic BH1, 2, 3 members, Bak and Bax. The BH3-only proteins Bid, Bim, Bad, and Noxa sense and respond to cell stress and damage by activating BH1,2,3 proteins and neutralizing BH1,2,3,4 proteins. Upon activation of the cell death program proapoptotic Bcl proteins are thought to oligomerize to promote MOMP and the release of cytochrome c. Cytochrome C promotes caspase 9 activation via formation of the apoptosome, a complex consisting of apoptotic protease activating factor 1 (Apaf-1), procaspase 9, and dATP. Caspase 9 cleaves and activates the effector caspases 3 and 7, which are responsible for execution of apoptosis. A second mitochondria-derived protein Smac/Diablo promotes efficient caspase activity by

inhibiting the proteasomal degradation of effector caspases by inhibitor of apoptosis proteins (IAPs).

Extrinsic apoptosis is regulated by cell surface receptors, including the tumor necrosis factor receptor (TNF-R) superfamily of death receptors and Fas. Upon TNFα or Fas ligand (FASL) binding the death inducing signaling complex (DISC) is formed by the recruitment of FADD and Caspase 8. DISC dimerization activates caspase 8, which directly activates caspase 3. FLIP is an endogenous inhibitor of caspase 8. Extrinsic and intrinsic apoptotic pathways converge upon caspase-mediated cleavage of the BH3 only protein Bid to tBid, which promotes MOMP. Both intrinsic and extrinsic apoptotic pathways have been implicated in COPD (251).

1.3.1 Apoptosis in COPD

Recent studies have demonstrated that apoptosis of epithelial, endothelial, mesenchymal, and inflammatory cells plays an integral role in COPD (252). Mouse models have shown that apoptosis leading to emphysematous changes can be induced without inflammation. For example, intratracheal administration of VEGF inhibitors, caspase 3, and ceramide are able to induce emphysematous changes in the lung via the direct activation of apoptotic pathways (253-256). Inflammation associated with COPD also promotes apoptosis. Increased cytotoxic CD8+ T cells release perforins, granzyme B and TNFα (257-259). Unmitigated protease activity promotes matrix degradation, basal membrane detachment and anoikis (260). NE also cleaves the phosphatidylserine receptor of alveolar macrophages reducing phagocytic activity and allowing damaging apoptotic cells to accumulate (261). MMP7 activity produces cleavage fragments that activate FAS (262). Finally, oxidative stress promotes apoptosis, and CS induced cell death *in vivo* and *in vitro* can been abrogated by the application of antioxidants (58, 263, 264). An apoptotic phenotype persists after smoking cessation in COPD patients indicating that this process may be an important therapeutic target (251, 265).

1.4 CROSSTALK BETWEEN AUTOPHAGY AND APOPTOSIS

The intersection of autophagy and apoptosis as these two processes promote regulated cell death is complex. Attempts to simplify these pathways into two distinct cell death processes, generally fail to fully describe the effects of a given stimulus. Instead a model is now arising in which autophagy and apoptosis are considered different facets of the same cell death continuum rather than two separate processes (234, 266). However, depending on the cell context and stimulus, the processes may be mutually exclusive. Pure autophagic cell death occurs when cells die with an intact cytoskeleton, an accumulation of autophagosomes without the activation or requirement of the caspase cascade; however, this is a relatively rare observation. Proteins implicated in both autophagy and apoptosis can be regulated by the same upstream molecules, such as p53 and the PI3K/Akt pathway, which induce and inhibit both processes, respectively. Recently calpain and caspase-dependent cleavage of autophagy proteins has been rigorously described (267). Some of these autophagy protein cleavage fragments, particularly Atg5 and Beclin-1, amplify the apoptotic stimulus by translocating from the cytosol to the mitochondria and promote MOMP (139, 268-270). In addition Beclin-1 contains a BH3 domain through which it interacts with Bcl-2 and Bcl-xL. This interaction at the ER membrane sequesters Beclin-1 away from the Vps34 kinase complex required for phagophore initiation (155, 271, 272). While overexpression of Bcl-2 inhibits autophagy, the overexpresion of Beclin-1 does not cause apoptosis (272). More recently we have published a role for caveolin-1 (Cav-1) in binding LC3B and Fas, thereby acting as a negative regulator of both apoptosis and autophagy (273). The interactions between apoptosis and autophagy proteins have proven to be both complex and at times contradictory, making this an exciting area of ongoing research.

2.0 RATIONALE & HYPOTHESIS

Autophagy is an essential homeostatic process in which organelles and long-lived proteins are encapsulated in double-membraned autophagosomes and subjected to bulk degradation by fusion with lysosomes. Starvation and other stress pathways induce autophagic degradation in order to provide essential building blocks required for adaptation to stress. Certain stress stimuli are characterized by cell death with autophagosome accumulation and markers of injury are reduced by autophagy deficiency in these models. As a critical mediator of homeostasis and cell fate, autophagy has been implicated in the pathogenesis of numerous diseases from cancer to neurodegeneration (274-278).

Recently, we determined that autophagy proteins are transcriptionally upregulated in COPD patients and that autophagosome formation is induced in *in vivo* and *in vitro* models of CS exposure. In these initial studies knockdown of autophagy proteins attenuated CS-induced cell death, while autophagy protein overexpression enhanced cell death (6, 8). These findings imply that autophagy and autophagic proteins mediate the fundamental molecular response of lung epithelial cells to CS-induced stress; however, these studies focused on specific autophagy proteins and less on the process of autophagy. Three recent discoveries make the study of autophagy in mediating CS-injury challenging: 1) Autophagy proteins, particularly autophagy protein cleavage fragments generated by activated caspases and calpains, promote apoptosis independent of autophagic activity (139, 267, 270, 279). 2) Autophagy deficiency enhances oxidant capacity by increasing p62 sequestration of Keap1 and promoting Nrf-2 antioxidant transcriptional activity (188-190). 3) Misfolded protein aggregates, targets of autophagic degradation, have been implicated in the sequestration of autophagic proteins (280, 281). These data suggest that autophagy and autophagy proteins may play a dual role in the response of epithelial cells to CS. Based on these observations **we hypothesized that autophagy is a crucial mediator of cell fate in response to CS, promoting cellular homeostasis and adaption**

during the initial cellular response, but instigating cell death during excessive or sustained CS exposure.

This hypothesis is addressed in the following specific aims:

1. To develop an *in vitro* model of the effects of CS on the airways

2. To assess the effects of CS on autophagic activity *in vitro* and *in vivo*

3. To examine the effects of CS on autophagic substrates (i.e. misfolded and ciliary proteins) using HDAC6$^{-/Y}$ cells and mice

4. Investigate the function of LC3B and Beclin-1 in autophagic and apoptotic pathways following CS exposure

3.0 MATERIALS AND METHODS

3.1 REAGENTS

Filtered research-reference cigarettes (3R4F) were obtained from The Tobacco Research Institute, University of Kentucky, Lexington, KY. Ham's F-12 with L-glutamine and DMEM/F-12 without L-glutamine and HEPES (MT-10-080-CM and MT-15-090-CM) were purchased from Cellgro by Mediatech Manassas, VA. Deoxyribunuclease I from bovine pancrease (DNase1, DN25-100MG), retinoic acid (R2625-50MG), HEPEs 1M in H_20 (83264-100ML), 200 mM L-glutamine (G7513-100ml), Insulin from bovine pancreas (I6634-50MG), human apo-transferrrin (T1147-100MG), SigmaFast Protease inhibitor cocktail tablets EDTA Free (S8830), leupeptin hemisulfate salt (L2884) and cholera toxin from *Vibio cholerae* (C8052-1MG) were obtained from Sigma-Aldrich, St. Louis, MO. Pronase from *Streptomyces griseus* (1016593100) was obtained from Roche, San Francisco, CA. Complete protease inhibitor cocktail tablets with EDTA (11 697 498 001) were purchased from Roche Diagnostics, Indianapolis, IN. Collagen I, mouse epidermal growth factor (EGF; 354001), bovine pituitary extract (354123), Nu-Serum (355100), and Primaria Falcon 100 mm cell culture dishes (353803) were obtained from BD Biosciences, San Jose, CA. Bovine serum albumin (BSA; BP1605-100), amphotericin B/fungizone (1672346), 12 mm Transwell® with 0.4 μm pore polycarbonate membrane (3401) and 12 mm Transwell® with 0.4 μm pore polyester membrane (3460) were obtained from Corning Inc Costar, Lowell, MA. Cell culture antibiotics penicillin/streptomycin (10,000U) were purchased from Lonza, Walkersville, MD. Dulbecco's Modified Eagle Medium with High Glucose (DMEM, 11965), phosphate buffered saline (1X; 10010), and gentamicin reagent (50mg/ml; 15750-060) were purchased from Invitrogen, Gibco, Auckland, NZ. TEM and SEM grade paraformaldehyde and gluteraldehyde were purchased from Electron Microscopy Sciences, Hatfield, PA. Histology grade formaldehyde, 37% solution was purchased from Mallinckrotd

Baker, Inc., Phillipsburg, NJ. Antibodies purchased from Santa Cruz Biotechnology, Santa Cruz, CA: acetyl α-tubulin (sc-23950), Beclin-1 (sc-11427), Bcl-2 (sc7382), BaxΔ21 (sc-6236). Antibodies from Sigma-Aldrich: LC3B (L7543), p62 (P0067), β-actin (A2228). Antibodies purchased from Cell Signaling Technology, Beverly, MA: LC3B (27735S), cleaved caspase 3 (9661S). Beclin-1 (612112) C-terminal specific antibody was purchased from BD Transduction Laboratories™, Sparks, MD. Centrin-1 (ab11257) antibody was acquired from Abcam, Cambridge, MA. Horseradish peroxidase (HRP) -conjugated secondary antibodies for immunoblot analysis were purchased from Santa Cruz Biotechnology: goat anti-rabbit IgG-HRP (sc-2004), goat anti-mouse IgG-HRP (sc-2005). Immunofluorescence reagents secondary antibodies Cy™3-conjugated donkey anti-rabbit (711-165-152) or anti-mouse (715-165-150) were from Jackson ImmunoResearch Laboratories, Inc., West Grove, PA. Alexa Fluor® 488 (A12379) and 647 (A22287) conjugated to phalloidin and Alexa Fluor® 488 secondary antibody anti-rabbit (A11034) and anti-mouse (A10667) and were purchased from Invitrogen, Molecular Probes, Eugene, OR. Remaining standard laboratory reagents were purchased from Sigma-Aldrich.

3.2 ANIMALS

Beclin-$1^{+/-}$ mice were provided by Beth Levine (The University of Texas Southwestern Medical Center at Dallas, Dallas, TX). The HDAC$6^{-/Y}$ mice were provided by Bin Shan (Tulane University, New Orleans, LA). LC3B$^{-/-}$ were provided by Marlene Rabinovitch (Stanford University, Stanford, CA), and backcrossed into a pure C57BL/6 background in our laboratory. The GFP-LC3B mice were purchased from Riken BioResource Center (3-1-1 Koyadai, Tsukuba-shi, Ibaraki 305-0074, Japan). WT C57BL/6 and Cav-$1^{-/-}$ were purchased from Jackson Laboratories (Bar Harbor, ME). All animal experimental protocols were approved by the Harvard Standing Committee for Animal Welfare or the University of Pittsburgh Institutional Animal Care and Use Committee.

3.3 *IN VIVO* CS EXPOSURE AND HARVEST PROTOCOL

Age and sex matched mice starting at 6-12 wk of age were exposed to total body CS in a 71 cm X 61 cm X 61 cm stainless steel chamber using a smoke machine (Model TE-10 Teague Enterprises) 5 d/wk for 1wk, 2 mo, and 6mo or room air (RA). The CS treatment required approximately 2 h each day as the mice were exposed to the mainstream and sidestream smoke of 100 3R4F cigarettes with an average TPM of 150 mg/m^3. The carboxyhemoglobin levels were typically less than 8% following exposure. Mice were also exposed to CS from 4 unfiltered cigarettes 5 d/wk using the nose-only method. At the end of the exposure regiment mice were euthanized by CO_2. The left lung was isolated with a suture, dissected and flash frozen in liquid nitrogen. The mouse was then tracheally cannulated and the right lungs were inflated with 2% formalin in PBS at 25 cm of H_20 pressure, dissected from the mouse and fixed in 4% formalin at 4°C for 2 d. The proximal trachea up to the larynx and a portion of proximal portion of the left lung were fixed for TEM analysis.

3.4 LUNG MORPHOMETRY

Lungs fixed for histology were further processed for morphological analysis of airspace enlargement by paraffin-embedding of midsaggital sections. Following a modified Gills staining 10-12 random 20X fields were imaged and processed to remove large airways, blood vessels and other nonalveolar structures. Images were acquired using brightfield microscopy on a Leica DM LB using a DFC480 3CCD Color Vision Module camera (Buffalo Grove, IL). The mean linear intercept was determined using a previously described algorithm, which has been automated in a modified ImageJ program available on the National Institute of Health website (http://rsb.info.nih.gov/ij/) (282-284).

3.5 CELL CULTURE AND CSE TREATMENT

Beas-2B cells, a human lung epithelial cell line, were maintained in complete media DMEM supplemented with 10% fetal bovine serum (FBS) and gentamicin (50 μg/mL). Cigarette smoke extract (CSE) was prepared using a peristaltic pump (VWR International) to bubble mainstream smoke from four 3R4F cigarettes with filters removed through 40 mL DMEM. Each cigarette was smoked within 6 minutes until approximately 17 mm remained. The extract was adjusted to a pH of 7.5 filter sterilized, stored at -80°C, and used immediately upon thawing. The CSE generated in this fashion was considered 100% strength was diluted in complete DMEM for cell treatment.

3.6 GENERATION AND CS EXPOSURE OF MTEC CULTURES

Methods for MTEC isolation and culture generation were described previously (71, 285, 286). For each isolation, age and sex matched mice 6-12 wk were euthanized by CO_2 necrosis. The tracheae were isolated and stored on ice in Ham's F-12 containing antibiotics (1X penicillin/streptomycin and fungizone). Careful dissection was used to remove all connective tissue and the tracheae were cut longitudinally to expose the luminal surface for overnight digestion at 4°C in 0.15% pronase in Ham's F-12 with antibiotics. Six tracheas were digested in 10 mL of solution in a 50 mL conical tube. The next day the tracheal digests were inverted 12 times and allowed to incubate for an additional hour at 4°C. The enzymatic activity was stopped by adding 10 mL of Ham's F-12 containing 20% FBS and antibiotics and gently inverted 12 times. The tracheae were spooled onto a pasture pipette and transferred to a new 15 mL conical tube containing 10 mL of Ham's F-12 with 20% FBS and antibiotics and inverted 12 times. This mechanical disruption of the tracheas was repeated two times more using fresh 15 mL conical tubes and media. Finally, the tracheae were discarded and the contents of the three 15 mL tubes were collected in the original 50 mL conical tube. The cells were pelleted at 350 x*g* for 10 min at 4°C. The media was aspirated and the cells were incubated for 5 min on ice in 100-200 μL per trachea of DNase solution (0.5 mg/ml DNase, 10 mg/ml BSA, in Ham's F-12 with antibiotics). The cells were then pelleted at 350 x*g* for 5 min at 4°C and then the media was aspirated. The

cells were seeded onto 100 mm Primaria plates in MTEC Basic Media (1 M Hepes, 200 mM Glutamine, 7.5% NaHCO3, 0.25 μg/ml Fungizone, 10^2 U/ml Penecillin Streptomycin in DMEM:Ham's F-12) containing 10% FBS and incubated for 5-6 h in a humidified incubator at 37°C, 5% CO_2. Cells that did not attach to the plate were collected by centrifugation at 350 x*g* for 10 min at 4°C and the cells were resuspended in MTEC proliferation media (10 μg/μl insulin, 5 μg/ml transferrin, 0.1 μg/ml cholera toxin, 25 ng/ml epidermal growth factor, 30 μg/ml bovine pituitary extract, $10X10^{-8}$ retinoic acid, and 5% FBS in MTEC basic media). In the 12 well transwell dish 1.5 mL of MTEC proliferation media was added to the basal compartment and 75-100 $X10^3$ cells/well were seeded in 500 μL onto the transwells, which were previously coated with 400 μl of 100 μg/ml type 1 rat tail collagen, incubated overnight, excess solution was aspirated and allowed to dry before washing twice with PBS. Cells proliferated for 10 d in submerged culture conditions with media changes every other day and fresh media made every fifth day. Cultures with a resistance over 1000 Ω/cm^2, as measured using an ohmvoltometer (EVOM™, World Precision Instruments, Sarasota, FL), were put at an ALI by removing all apical media and replacing the basal media with 750 μl of MTEC differentiation media (2% Nu-Serum and $10X10^{-8}$ M retinoic acid in MTEC basic media) in the basal compartment. The cultures then differentiated for 14 d at ALI with media changes every other day. CS treatment was conducted in a custom designed humidified chamber (EMI Services, Glenwillard, PA) at 37°C by exposing the cells for 10 min to 50 or 100 mg/m^3 of mainstream CS from 3R4F research-reference filtered cigarettes.

3.7 PROTEIN EXTRACT PREPARATION, IMMUNOPRECIPITATION AND IMMUNOBLOT ANALYSIS

All protein extractions were done on ice with ice-cold homogenization buffer. Protein extracts were made by lysing and scraping cells using cell RIPA buffer (400 mM HEPES, 5 M NaCl, 0.5 M EDTA, 1 M Na_3VO_4, 1 M NaF, 100 mM glycerol 2-phosphate, 3% Chaps w/v) or for tissues, tissue RIPA buffer (300 mM NaCl, 50 mM Tris(pH 7.6), 1% NP-40, 10% glycerol, 1 mM EDTA, 1 mM NaF, 1 mM Na_3VO_4) made with a fresh complete protease inhibitor tablet (Roche Diagnostics, Indianapolis, IN). The samples were homogenized by sonication 5 times 10 min (60

Sonic Dismembrator, Fisher Scientific). Cells were spun once for 20 min at 14,000 x*g* while tissue protein extracts were prepared by centrifuging 5 times 10 min each time at 14,000 x*g* and transferring to a new eppendorf for each consecutive centrifugation. The supernatants were collected after the final centrifugation and the protein concentrations were determined by a Coomassie Plus (Bradford) protein assay (Pierce Biotechnology Inc., Rockford, IL) by measuring the absorbance at 595 nm and linear regression form a BSA standard curve. The protein samples were then normalized using homogenization buffer. For co-immunoprecipitations cell extracts were incubated with 1 μg of antibody into 500 μg of total protein in 500 μl and incubated overnight on a rotor at 4°C. Then the extracts were incubated with 20 μL of protein A-sucrose beads (Santa Cruz Biotechnology) for an additional 2 hours, spun down at 500 x*g*, and washed by resuspending and centrifuging 5 times in RIPA buffer. All protein extracts were made in 1X NuPage loading buffer, 20 μl were added to the immunoprecipitation samples, and then boiled for 10 min. Approximately 10-50 μg of the protein samples were subjected to electrophoresis using a 4-12% SDS-polyacrylamide gel (Invitrogen, Carlsbad, CA). The proteins were electro-transferred onto polyvinylidene diflouride membrane (PVDF; Invitrogen). After the membranes were blocked in 5% nonfat milk in 0.2% Tris-buffered saline with 0.1% Tween 20 (TTBS) for 1 h at room temperature, the blots were incubated overnight at 4°C in primary antibodies diluted in TTBS. Membranes were washed three times for 5-7 min with TTBS, and incubated at room temperature for 2 h in the corresponding HRP-conjugated secondary antibody. Membranes were washed three times for 5-7 min again in TTBS and developed with ECL reagent (Amersham Biosciences, Piscataway, NJ).

3.8 *IN VIVO* AUTOPHAGIC FLUX ASSAY

A detailed protocol for *in vivo* autophagic flux has been described previously (227). Briefly, mice exposed to CS or RA were given an intraperitoneal injection of 40 mg/kg leupeptin in pharmaceutical grade saline at 1 h or 24 h following last the last CS treatment. Control mice received an equal volume of the vehicle. The leupeptin treated RA and CS mice were then

harvested 2 h later in parallel. Tissues were flash frozen and LC3B turnover was assessed in the lysosome-enriched (LE) fraction described section 3.9.

3.9 TISSUE AND CELL HOMOGENIZATION TO OBTAIN A LYSOSOME-ENRICHED FRACTION

Subcellular fractionation for the LE fraction was previously described in detail (227). Briefly, tissues were flash frozen upon harvesting and stored at -80°C until processing, which was all done at 4°C or on ice. Cells were trypsinized and pelleted at 300 x*g* 8 min at 4°C. Lysates were made with homogenization buffer (10 mM Tris, pH 8.0, 5 mM EDTA, 250 mM sucrose, protease inhibitor tablet without EDTA). Cells were mechanically disrupted by dounce homogenization ten times with the loose and ten times with the tight pestle. The tissue was mechanically homogenized (7X95mm Saw Teeth Generator, Omni International The Homogenizer Company, Kennesaw, GA). The homogenate was then centrifuged at 700 x*g* for 10 min and transferred to a new tube. If debris was still present an additional 700 x*g* spin was implemented. The protein was then normalized to 1-2 mg/ml using the homogenization buffer. An aliquot was saved for the whole cell fraction. The sample was then centrifuged at 20,000 x*g* for 30 min. Supernatant was saved for the cytoplasmic fraction. The pellet was washed twice with homogenization buffer and resuspended in sample buffer. All cell fractions were prepared with 1X NuPage LDS sample buffer (NP007, Invitrogen, Carlsbad, CA) boiled for 10 min and subjected to subsequent immunoblot analysis.

3.10 *IN VITRO* AUTOPHAGIC FLUX ASSAY

Cells were exposed to CS or CSE and treated 10 min later with lysosome acidification inhibitors chloroquine (25 μM) or bafilomycin A1 (100 nm). Control cells were treated with the inhibitor without CS or CSE treatment. The samples were then harvested using cell RIPA buffer from control and treated cells at the same time 0, 1, 3, or 6 h later and analyzed by standard immunoblot analysis described in section 3.7.

3.11 CELL VIABILITY AND CYTOTOXICITY ASSAYS

Cell viability was determined by the 3-(4-5-dimethylthiaxol-2-yl)-2,5-diphenyl tetraxolium bromide (MTT) assay. Cytotoxicity was assessed by measuring lactate dehydrogenase (LDH) activity in the basal media of the MTEC cultures according to the manufacturer's protocol (Cytotoxicity Detection Kit^{PLUS}, Roche Diagnostics, Indianapolis, IN). This assay measures LDH released into the media upon plasma membrane permeability, the assay determines LDH content by a coupled enzymatic reaction in which the tetrazolium salt INT is reduced to formazan dye, which is measured at 500 nm. The assay was performed in duplicate in a 96-well format and the absorbance was measured using a Multiskan EX Microplate Photometer from Thermo Scientific (Waltham, MA). The Annexin V FITC Apoptosis Detection Kit was purchased from BioVision (Mountain View, CA). The assay was performed on both detached and attached cells, by collecting all detached cells and trypsinizing the attached cells, washing once with PBS, centrifuging at 200 x*g* and resuspending the cell pellet in the manufacturers assay buffer. The cells were then stained according to the manufacture's protocol. The proportion of viable and apoptotic cells were assessed using a FACS Canto II (BD Bioscience) and FlowJo analytical software (Tree Star, Inc., Ashland, OR).

3.12 INTRACELLULAR ATP ASSAY

Intracellular ATP was assessed using the ATPlite luminescence assay system (Perkin Elmer, Waltham, MA). The assay measures light produced by the reaction of ATP with D-luciferin and luciferase. The amount of light produced is proportional to the ATP concentration. The assay was performed according to the manufacturer's instructions with some scaling to accommodate the surface area of the transwells. Total protein was normalized and the ATP concentration in the cell lysis solution was quantified on luminometer (1420 Multilabel Counter, Victor3^{TM}, Perkin Elmer, Waltham, MA) and determined by linear regression based on the standard provided in the kit.

3.13 SUCROSE-GRADIENT SUBCELLULAR FRACTIONATION

Generation of sucrose gradient-derived fractions was described previously (249). Briefly, cells were lysed in ice-cold MBS buffer (25 mM Mes (pH 6.5), 150 mM NaCl, 1% Triton X-100, 1 mM Na3VO4, with protease inhibitors). Lysates were adjusted to 4 mL of 40% sucrose by mixing with 80% sucrose and overlaid with 35% sucrose and 4 mL of 5% sucrose in MBS buffer. Twelve subfractions were obtained following ultracentrifugation at 39,000 rpm for 18 h (SW41 rotor, Beckman Instruments, Palo Alto, CA).

3.14 DNA CONSTRUCTS

Human WT LC3B cDNA (pCMV6-XL5-LC3B) was obtained from Origene (Rockville, MD), and mutagenesis was performed using the QuickChange II Site-directed Mutagenesis Kit (Stratagene-Agilent Technologies, La Jolla, CA). The Cav-1 WT (WT-Cav-1) expression clone and the Cav-1 CSD (residues 82-101)-deleted mutant (ΔCSD) were gifts from C. Tiruppathi (University of Illinois at Chicago, Chicago, IL). The Fas wt and Fas C199S expression clones were kind gifts from M.E. Peter (University of Chicago, Chicago, IL).

3.15 IMMUNOFLUORESENCE STAINING

Cells were fixed with 4% paraformaldehyde in 1X PBS directly on transwells for 1 h at 4°C then washed with PBS and stored at 4°C. Staining was done following a standard protocol. The cells were permeabilized for 15 min in 0.01% Triton-X 100 then washed in PBS twice and 0.5% BSA in PBS twice. The cells were blocked for 45 min with 2% BSA in PBS. The cells were washed once in 0.5% BSA and then incubated for 1 h at room temperature in primary antibodies, LC3B (1:50) and acetylated α-tubulin (1:250). The samples were washed 5 times with 0.5% BSA and then incubated for 1 h at room temperature in secondary antibody, Alexa 488 anti-rabbit (1:1000), Cy3 anti-mouse (1:500) and or phalloidin conjugated to Alexa-647 or Alexa-488 (1:1000). Misfolded protein aggregates were stained using a recently developed dye, ProteoStat

Aggresome Detetction kit for flow cytometry and microscopy, ENZO® Life Sciences, Farmingdale, NY. The cells were washed 3 times with 0.5% BSA and then twice with PBS. Nuclei were then stained with Hoechst for 30 s and washed 3 times with PBS. The samples were then mounted onto slides using and imaged using epifluoresence (Leica DM LB microscope and DFC 480 3CCD Color Vision Module) or confocal (Zeiss LSM 510 with two-photon).

3.16 TRANSMISSION ELECTRON MICROSCOPY

Cells were fixed for 1 h and tissues were fixed overnight at 4°C using TEM grade fixative solution of 2% formaldehyde and 2.5 % glutaraldehyde in 0.1 M Sodium Cacodylate buffer, pH 7.4. The samples were washed and stored in 0.1 M cacodylate buffer and kept at 4°C until processing. Sample embedding followed a standard protocol, in which all steps were done at room temperature unless otherwise indicated. The samples were post-fixed for 1 h in the dark in 1% osmiumtetroxide / 1.5% potassiumferrocynide in H_2O. The samples were washed 3 times in H_20 or maleate buffer pH 5.15, then incubated in 1% uranyl acetate in H_2O or maleate buffer for 30 min. The samples were washed three times in H_20 and dehydrated by a graded series of ethanol: 70% for 15 min, 90% for 15 min, then 100% twice for 15 min. The samples were then further dehydrated in propyleneoxide for 1 h. Infiltration was done with a 1:1 ratio of Epon:propyleneoxide for 2-3 h. The samples were then embedded in freshly mixed Epon and polymerized 24-48 h at 60°C. Ultrathin sections were then absorbed onto hydrophilic formvar/carbon coated grids and negatively stained with 1-2% aqueous uranyl acetate, dried and imaged using a Technai™ G^2 Spirit BioTWIN transmission electron microscope.

3.17 SCANNING ELECTRON MICROSCOPY

MTEC cultures were washed with PBS twice with gentle agitation on a vortex to disrupt mucus coating then fixed for 1 h at 4°C in 4% paraformaldehyde in 1X PBS (pH 7.4). The samples were then washed thoroughly in three changes of PBS and stored at 4°C. The tissue was post fixed in

1% osmiumtetroxide for 1 h then washed three times with PBS. The samples were dehydrated in a graded series of ethanol by 15 min incubations with: 30%, 50%, 70%, 90%, and three times at 100%. The samples were then critical point dried and mounted onto studs with the epithelial cell layer facing upwards and then sputter coated and stored in the desiccator. Specimens were imaged with a JEOL 9355 Field Emission Zeiss Gun scanning electron microscope with backscatter detector.

3.18 STATISTICAL ANALYSIS

Statistical analysis was conducted using GraphPad Prism software (GraphPad Software, La Jolla, CA). Data are presented as the means ± standard deviation (SD) or standard error of the mean (SE) from at least three independent experiments. Differences in measured variables between experiment and control groups were assessed using the Student's t test and between multiple groups and conditions using one-way and two-way ANOVAs and Bonferroni post tests. Statistically significant differences * $p<0.05$, highly significant differences ** $p<0.01$ and very highly significant differences *** $p<0.005$ are indicated.

4.0 RESULTS- DEVELOPMENT OF A PHYSIOLOGICAL MODEL OF CS-INDUCED CELL INJURY IN THE AIRWAY EPITHELIUM

4.1 MTEC CULTURE GENERATION, CHARACTERIZATION, AND CS TREATMENT

Since airway-derived immortalized cell lines lose the ability to differentiate into the various cell types lining the respiratory tract, C57BL/6 MTECs were isolated and grown at an ALI to produce highly differentiated pseudostratified cultures. This method was adapted from previously described protocols, in which cultures were created by digesting mouse tracheas with pronase, subjecting all detached cells to a brief negative selection step for fibroblasts, and then seeding the epithelial cell population onto transwells (71, 285, 287). In this study, cells proliferated under submerged conditions for 10 d and differentiated for an additional 14 d at an ALI (**Figure 4A**). Apical exposure to air is critical for differentiation and also induces fibroblast cell death, thereby ensuring culture homogeneity. Transepithelial electrical resistance (TER) was monitored every other day following seeding and used as a measure of culture confluence, purity, and differentiation. As the cells form an intact pseudostratified epithelium the TER peaked at approximately 3500 Ω/cm^2 just following conversion to an ALI, then the resistance dropped and stabilizes to approximately 2500 Ω/cm^2 as the cells differentiate and acquire ion channels (**Figure 4B**). MTECs that achieve a TER greater than 1000 Ω/cm^2 are confluent enough to be put at an air-liquid interface, while resistance measurements below 1000 Ω/cm^2 after day 10 are generally indicative of fibroblast or microbial contamination (285, 287). Therefore, TER was measured prior to removal of the apical media and just before CS-exposure on day 24 to ensure the quality and consistency of the cultures in every experiment.

Twenty-four days after seeding, ciliated, non-ciliated and basal cells were observed in the cultures by transmission electron microscopy (TEM) (**Figure 4C**). While the cells differentiated

into the correct representative cell populations, the morphology is more cuboidal than columnar. Ciliated cells comprised about 25% of the total cell population present in the MTEC cultures, which is consistent with previously published literature (285, 287). Goblet cells were also present in these cultures, but were rare, and with the other respiratory secretory cells were able to produce a discernable mucus layer; therefore the apical surface was also gently washed with fresh media during each media change, in particular, the apical surface was washed and the media changed at least 10 h prior to CS exposures.

MTEC cultures with the culture plate cover left on were exposed to mainstream CS for 10 min in a custom designed humidified chamber at 37ºC (**Figure 4D**). The average total particulate matter (TPM) achieved in the chamber during treatment was 50 mg/m^3 or 100 mg/m^3,

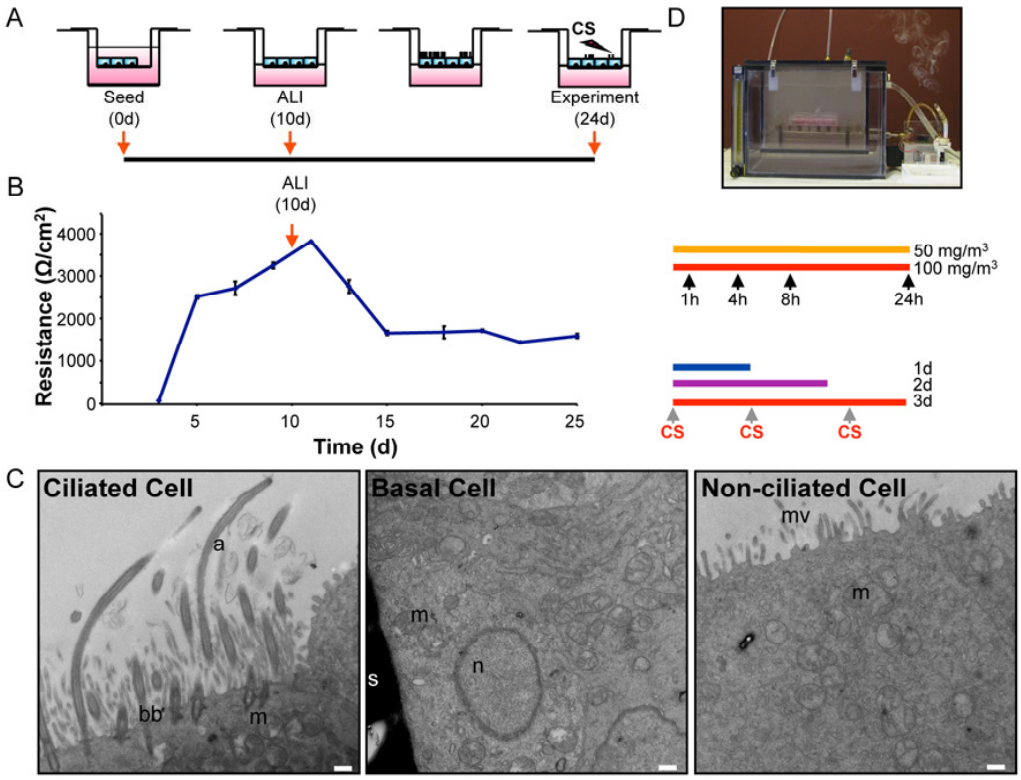

Figure 4. MTECs that have proliferated on transwells and differentiated at an ALI are a physiologically relevant *in vitro* model of the respiratory epithelium. A) MTEC culture generation requires cell proliferation under submerged conditions for 10 d, followed by removal of apical media and differentiation at an ALI for 14 d. B) Cells were treated with mainstream CS in a custom designed humidified chamber at 37ºC. Cells were either treated once for 10 min with 50 or 100 mg/m^3 of CS and harvested at 1, 4, 8, 24 h or treated up to 3 days with 50 mg/m^3 and harvested at day 1, 2 and 3. C) Following seeding on day 0, TER was measured to monitor the confluence, purity and differentiation state of the cultures. D) TEM analysis of ALI cultures confirmed the formation of a pseudostratified epithelium with ciliated, basal, and non-ciliated cells. (a-ciliary axoneme, bb-ciliary basal bodies, m-mitochondria, n-nucleus, s-substrate, mv-microvili; Bar=500nm)

generated by pumping in the mainstream smoke from 1 or 2 research-grade University of Kentucky 3R4F reference cigarettes, respectively. Following treatment, the cells were returned to a standard cell culture incubator with constant 37ºC, 5% CO_2 and humidity. Cells were exposed to CS with either a single dose of 50 or 100 mg/m^3 for 10 min or multiple doses 10 min each of 50 mg/m^3 every day for 3 d. In the single-dose model, cells were treated with CS and assessed at 1, 4, 8 and 24 h following exposure. In the multiday chronic model, the cells were treated with CS once a day with 50 mg/m^3 TPM over the course of three days and cells were harvested at 24, 48 and 72 h following the first treatment (**Figure 4D**). Since MTEC cultures are highly differentiated and can be treated at the ALI with whole mainstream smoke, these cells represent a suitable model for studying the effects of CS on the respiratory epithelium, particularly ciliated cells. Additionally, cultures can be generated from transgenic or gene deleted null mice to study the functional role of a specific protein or pathway in the response of the airway epithelium to CS.

4.2 CS-INDUCED DISRUPTION OF INTERCELLULAR CONTACTS AND CILIA

Following CS treatment, MTEC injury was first assessed by fluorescence microscopy (**Figure 5A**). Cells were stained for nuclei using Hoechst, F-actin using phalloidin conjugated to Alexa Fluor® 488 and for cilia using Cy™3 conjugated secondary antibody for acetylated α-tubulin, a posttranslational modification of long lived microtubules. While acetylated α-tubulin is not specific for cilia, acetylated α-tubulin is a sufficient cilia marker when combined with the distinct tuft-like morphology and apical localization of this organelle. F-actin is an integral component of both tight and adherens junctions; therefore, this stain delineates the nature of intercellular contacts. In control cells the ring of F-actin at the apical-basal junction was essentially continuous from one cell to the next and fields of ciliated cells were present. Four hours after treatment with 100 mg/m^3 of CS, dramatic remodeling of intercellular contacts was apparent, as the F-actin became discontinuous between neighboring cells and the intensity of staining increased. By 24 h, the F-actin stain indicated that the cells were rounder and larger. Previous studies using an epithelial cell line, Calu-3, grown on transwells and treated with CS at an ALI showed that CS alters tyrosine phosphorylation of tight junction proteins (72, 288). Similarly,

adherens junction disruption by CSE treatment has also been investigated in human-derived primary cultures (77). These findings are in marked contrast to the intercellular junction remodeling in MDCK II cells, which upon treatment with chemicals to shed cilia, have increased resistance (289). Furthermore, microarray analyses of CS-treated human ALI cultures have shown a decrease in junction protein expression (73). These studies demonstrate the importance of crosstalk between cilia and tight junctions, which are markers and mediators of epithelial cell polarization.

Immunofluorescence observations were further confirmed by scanning electron microscopy (SEM; **Figure 5B**). SEM of cells treated with 50 mg/m^3 demonstrated that cilia injury induced by CS occurred independent of apparent intercellular junctional remodeling. These results imply that general loss of apical-basal polarity does not account for all cilia disruption in this model. Intercellular contact disruption was most apparent by SEM in cells treated with 100 mg/m^3, in which cells appeared disconnected from one another and the matrix. Some cilia loss was apparent in these cells, but more pronounced was the complete loss of microvili, actin-based structures, observed on the surface of other epithelial cell types. These data support a significant impact of CS on cytoskeletal structures. Consistent with the above observations, CS-induced disruption of monolayer integrity was apparent in TER measurements, in which there was an acute drop in TER that fully recovered in cultures treated with 50 mg/m^3 TPM (**Figure 5C**). Cultures treated with 100 mg/m^3 had a rapid and sustained loss of resistance. Control cultures maintained a resistance of ~2500 Ω/cm^2 over the entire experiment. TER demonstrated a threshold effect, in which the pseudostratified epithelium either recovered to control levels, or resistance was completely lost without intermediate resistance measurements by 24 h following CS exposure. These data confirmed the time and dose dependent changes in intercellular contacts, and the recovery of intercellular contacts further demonstrated that CS-induces a highly regulated change in the nature of intercellular contacts.

Quantification of total ciliated cells remaining 24 h after CS exposure was determined by counting the number of acetylated α-tubulin cilia stained cells as normalized to total cells determined by counting nuclei in each field (**Figure 5D**). Based on these data, CS caused a dose dependent decrease in the percentage of ciliated cells; however, this method was not sensitive to changes in cilia length and number per cell. These data over accentuate changes in ciliated cell numbers caused by cell sloughing and failed to detect more subtle CS-induced cilia changes.

These data provide insights into the major morphological changes and regulated responses of epithelial cells exposed to CS.

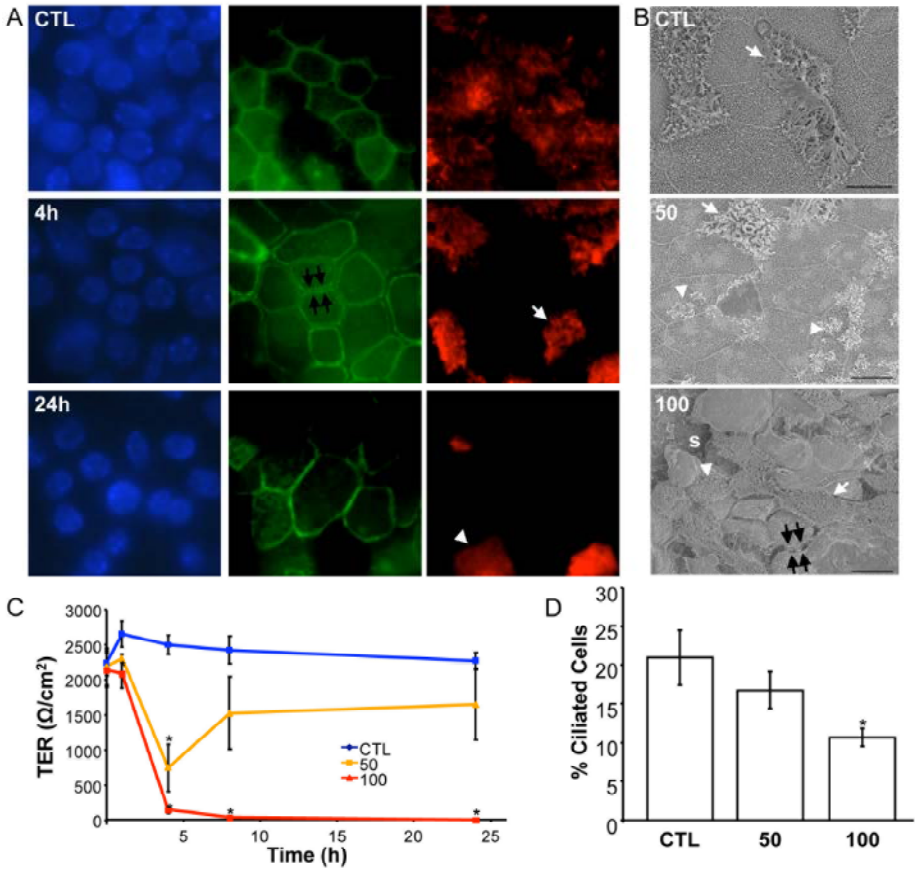

Figure 5. Acute exposure of MTEC cultures to CS disrupts intercellular contacts and induces cilia shortening and loss. A) ALI cultures were treated with CS at 100 mg/m^3 TPM, fixed at the indicated times and then stained for nuclei (blue, Hoescht), F-actin (green, Alexa-488 conjugated phalloidin) and cilia (red, acetylated α-tubulin). Epifluorecence images were acquired at different focal planes of the same field at 100X. (black arrows-disrupted intercellular contacts, white arrows- ciliated cells, white arrow heads-shortened/injured cilia) B) MTEC cultures 24 h after treatment with the indicated CS TPM (mg/m^3) were analyzed by SEM. (black arrows-disrupted intercellular contacts, white arrow-ciliated cells, white arrow heads-shortened/injured cilia, s-substrate; Bar=10 μm) C) Epithelial integrity was monitored by measuring TER at the indicated times after CS exposure. D) Percentage of ciliated cells was determined by quantifying the number of ciliated cells for total number of nuclei in 5-10 fields. TER and ciliated cell measures were assessed in 6 independent experiments and results are presented as the mean ± SE and *$p<0.05$ by student's unpaired *t* test.

4.3 CS-INDUCED CELL DEATH IN MTEC CULTURES

Cytotoxicity was assessed in MTECs treated with CS by assaying lactate dehydrogenase (LDH) activity in the basal media (**Figure 6A**). LDH activity was not detected in control cultures and cultures treated with 50 mg/m^3 TPM, while an average of 700 mU of LDH activity was detected in cultures treated with 100 mg/m^3. To correlate the levels of LDH activity to the proportion of cells undergoing late and early apoptosis, cells were trypsinized from the transwell membranes and collected with all detached cells and subjected to flow cytometry for the apoptotic indices, Annexin V (AV) and propidium iodide (PI) (**Figures 6B & C**). AV positive PI negative cells were considered early apoptotic cells and AV positive PI positive are cells were considered late apoptotic cells. While apoptotic cells were generally rare in the control MTEC cultures, the harsh conditions required for epithelial cell disassociation caused a marked increase in the cell death response; however, the difference between control and 50 mg/m^3 TPM treated cells was not significantly different supporting the findings of the LDH assay. In contrast, the majority of cells treated with 100 mg/m^3 entered either early apoptosis (~50%) or late apoptosis (~40%) (**Figure**

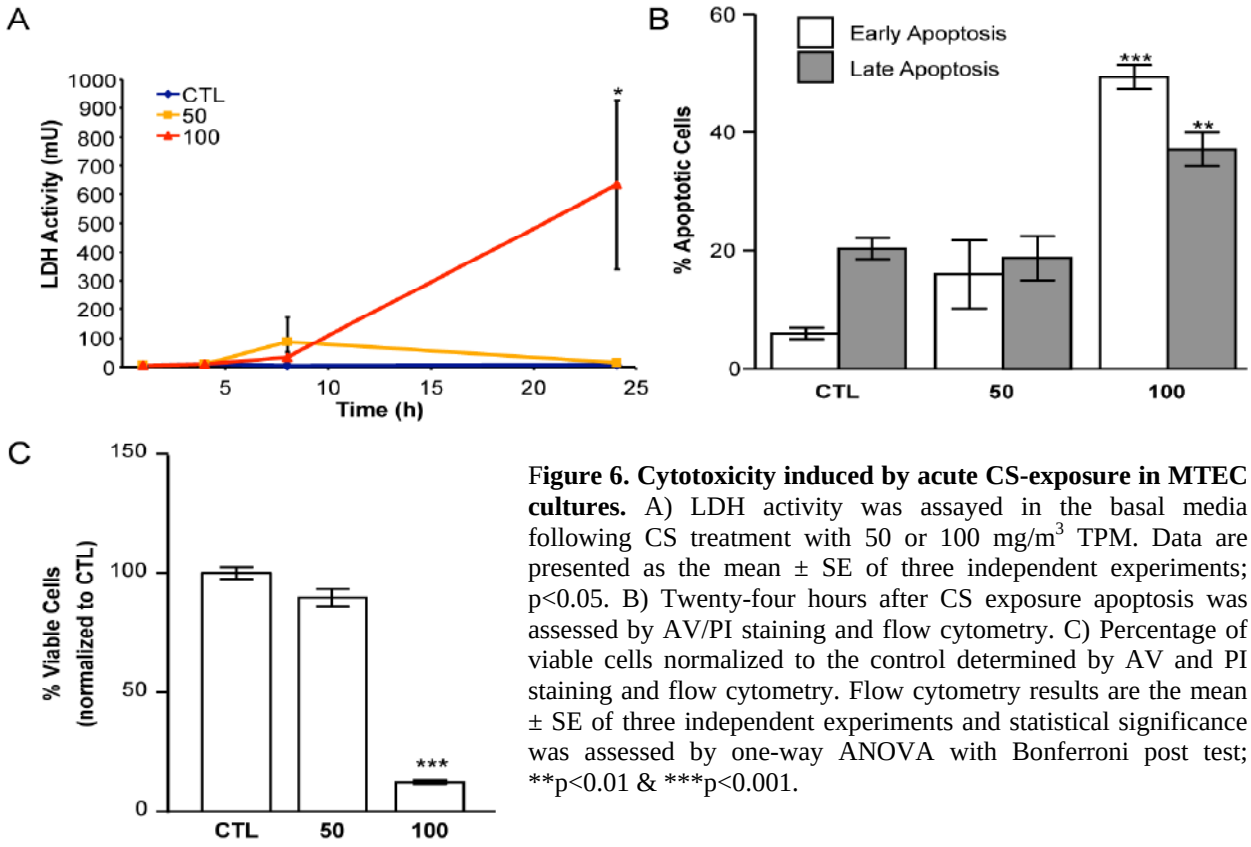

Figure 6. Cytotoxicity induced by acute CS-exposure in MTEC cultures. A) LDH activity was assayed in the basal media following CS treatment with 50 or 100 mg/m^3 TPM. Data are presented as the mean ± SE of three independent experiments; $p<0.05$. B) Twenty-four hours after CS exposure apoptosis was assessed by AV/PI staining and flow cytometry. C) Percentage of viable cells normalized to the control determined by AV and PI staining and flow cytometry. Flow cytometry results are the mean ± SE of three independent experiments and statistical significance was assessed by one-way ANOVA with Bonferroni post test; **$p<0.01$ & ***$p<0.001$.

6B). The percentage of viable cells, Annexin V and PI negative, was determined relative to controls. Viability was maintained in cells treated with 50 mg/m^3**,** while less than 15% of the cells were viable 24 h following exposure to 100 mg/m^3 TPM (**Figure 6C**). These data indicate that this model is ideal for studying the effects of both subtoxic and toxic doses of mainstream CS on highly differentiated MTEC cultures.

4.4 A CHRONIC MODEL OF CS TREATMENT

To recapitulate the effects of chronic exposure to CS in the MTEC cultures, cells were treated with 50 mg/m^3 for 10 min once a day over the course of 3 d and cultures were harvested 24 h after each smoke treatment. The morphology of the cells was again assessed by confocal microscopy at each time point after staining for nuclei, F-actin, and acetylated α-tubulin (**Figure 7A**). There was a time dependent disruption of cilia as cells treated for multiple days appear to have fewer and shorter cilia by this analysis; however, intracellular contact disruption was only observed following CS treatment for 3 d, when large intercellular gaps became apparent. This observation was corroborated by loss of TER in the cultures treated with 50 mg/m^3 on the third day (**Figure 7B**). While quantification of the percentage of ciliated cells after smoking is not a sensitive measure of CS-induced cilia shortening and loss, there was a statistically significant decrease in ciliated cells following 3 d of CS treatment (**Figure 7C**). Cytotoxicity over the multiple days of CS exposure was determined by measuring the LDH activity in the basal media (**Figure 7D**). LDH activity was not detected in control cells or cells exposed to CS for one and two days; however, a significant increase in LDH activity was detected 24 h after the third smoke exposure. In both the single and chronic CS exposures ciliated cell loss was only significant with the induction of cell death. These data present strong evidence for the role of epithelial cell sloughing in CS-induced ciliated cell loss, and also suggest that ciliated cells are more susceptible to CS-induced injury. These data are consistent with the basal cell population, which is protected underneath the ciliated and nonciliated cells, playing a critical role in re-epithelialization following desquamation (290, 291).

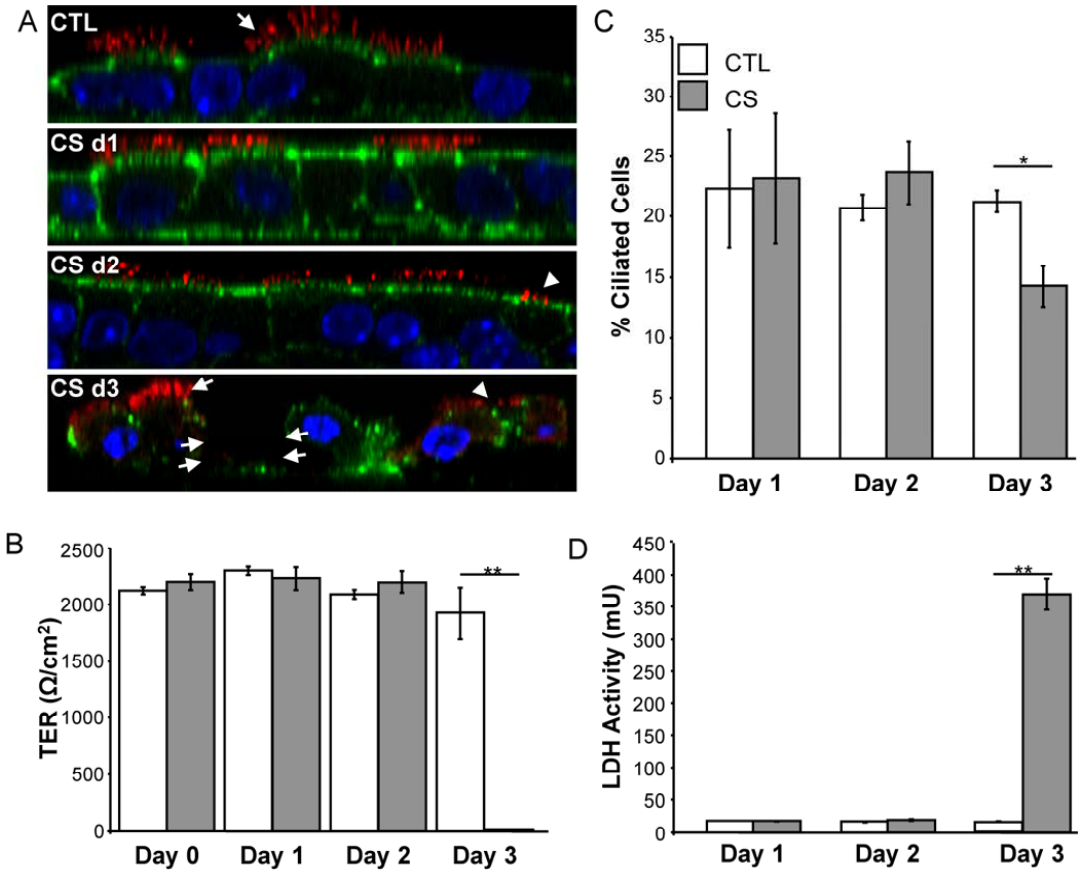

Figure 7. Cilia loss, intercellular contact disruption and cytotoxicity are observed following multipule doses of CS at 50 mg/m^3 TPM. A) Confocal analysis of MTEC culture z-sections stained for nuclei (blue, Hoescht), F-actin (green, Alexa488-conjugated phalloidin) and cilia (red, acetylated α-tubulin). (arrows-cilia, arrow heads-shortened/injured cilia, double arrows- disrupted intercellular contacts. B) TER was measured prior to CS exposure and then 24 h following CS exposure. C) Loss of ciliated cells in the MTEC cultures was observed following three continuous days of CS treatment. D) Cytotoxicity was assessed by measuring LDH activity in the basal media 24 h after CS exposure. All data are presented as the mean ± SE with statistical significance determined by student's unpaired *t* test; *p<0.05 & **p<0.01.

5.0 RESULTS- EFFECTS OF CS ON AUTOPHAGY

5.1 CS-INDUCED ACCUMULATION OF AUTOPHAGOSOMES IN MTEC CULTURES

To investigate the effects of CS on autophagy in the respiratory epithelium, TEM was used to visualize autophagic structures in ciliated cells of MTEC cultures 24 h following CS treatment (**Figure 8A**). There was an increase in autophagosomes in cultures treated with 50 and 100 mg/m^3 TPM. The cells treated with the sublethal CS dose contained both autophagosomes and autolysosomes, while the cells treated with the acutely lethal dose appear apoptotic with an accumulation of autophagosomes and other vacuoles. Additionally, cultures treated with 100 mg/m^3 were completely devoid of ciliary axonemes, while the nucleating basal bodies remained docked at the apical surface. In order to confirm CS-induced autophagosome accumulation, MTEC cultures were generated from GFP-LC3B mice and treated with CS (**Figure 8B & C**). While there was a significant ~30% increase in GFP-LC3B puncta/μm^2, a dose dependent accumulation was not observed. These imaging studies confirm that CS induces autophagosome accumulation in MTEC cultures. Autophagy and cell death markers were assessed by immunoblot analysis for LC3B II, p62, and cleaved caspase 3 (**Figure 8D**). Cultures treated with 50 mg/m^3 TPM had similar steady state levels of LC3B II and p62 as the control. In contrast, the LC3B immunoblot showed a rapid accumulation of LC3B II in cultures treated with 100 mg/m^3 TPM, which preceded induction of cell death as assessed by production of cleaved caspase 3. Furthermore, high molecular weight p62 positive aggregates were produced in cultures treated with 100 mg/m^3 TPM. These SDS-insoluble aggregates appear in autophagy deficient cells and are frequently used as a marker of decreased autophagic flux (179, 224).

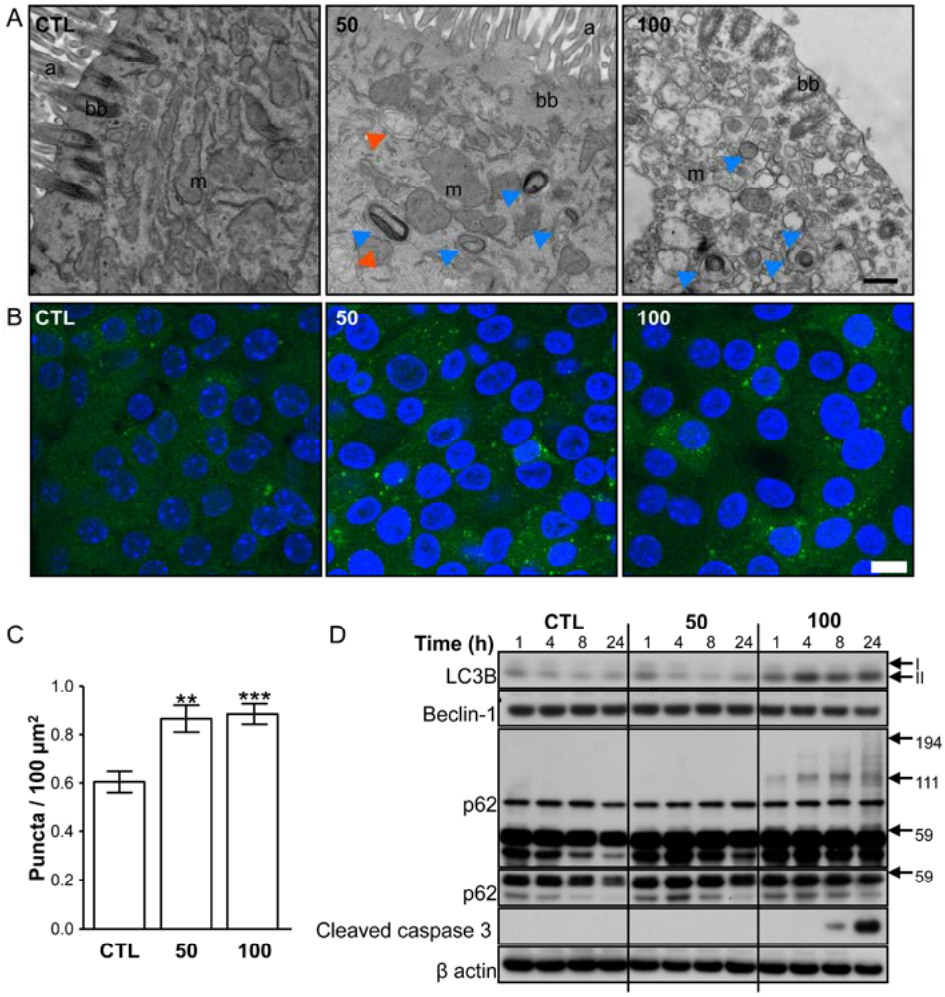

Figure 8. CS causes autophagosome accumulation in MTEC cultures. A) Autophagosomes (blue arrows) and autolysosomes (red arrows) accumulate in MTEC cultures treated with CS at the indicated TPM (mg/m^3). Axonemes are completely absent in some ciliated cells treated with CS at 100 mg/m^3 TPM. (a-axoneme, bb-basal bodies, m-mitochondria, bar=500nm). B) Representative images of MTEC cultures generated from GFP-LC3B mice show an accumulation of GFP-LC3 puncta. (bar=10µm) C) GFP-LC3B puncta were quantified in 10 fields at 63X magnification from three independent experiments and tested for significance by one-way ANOVA using Bonferroni post test **p<0.01, ***p<0.005. D) Autophagy and cell death markers were assessed in MTEC cultures by immunoblot at the indicated time points after treatment with 50 mg/m^3 or 100 mg/m^3 CS TPM. Cytoplasmic (I) and autophagosome-associated (II) LC3B bands, with apparent molecular weights (kDa) are indicated to the right of the blots.

5.2 INDUCTION OF AUTOPHAGIC FLUX BY CS EXPOSURE IN MTEC CULTURES

Steady state measurements of autophagosome accumulation and autophagy markers are unable to distinguish between autophagy induction and inhibition of lysosome fusion/degradation. To assess CS-induced changes in autophagic flux following a single treatment with 50 or 100 mg/m^3 TPM, accumulation of LC3B II and p62 were measured by immunoblot following the addition of the lysosome acidification inhibitor bafilomycin A1 (**Figure 9A**). As described previously, LC3B II, which coats both the inner and outer autophagic membrane, is degraded in the inner compartment following autophagosome lysosome fusion. The protein p62 is a target of autophagic degradation. Via an LC3 interaction motif, an ubiquitin binding motif and other protein interacting motifs, p62 selectively recruits other proteins for autophagic degradation. This activity of p62 is generally considered a complementary mechanism to the proteosomal pathway for the removal of ubiquitinated proteins. While control cultures and cultures treated with 50 mg/m^3 TPM had a similar rate of LC3B II accumulation, LC3B failed to accumulate in cells treated with 100 mg/m^3 TPM. These data indicated that overall flux was not changed in subtoxic CS exposure compared to control cultures, while flux is reduced in cultures in which cell death is acutely induced. The decrease in LC3B protein following bafilomycin A1 treatment likely reflected overall repressed transcriptional activity at this lethal dose of CS. The high basal level of autophagy in the control cells may be an artifact of the cell culture system, reflecting the surplus of nutrients available to these cells. Since the MTEC cultures are highly confluent, differentiated, and not highly proliferative, excess nutrients in the absence of proliferation may cause the cells to have high anabolic and catabolic activity, of which autophagy may play a critical role. In contrast to the rate of LC3B II accumulation by bafilomycin A1, p62 accumulation was augmented in the cells treated with 50 mg/m^3 TPM compared to control. The monomeric and SDS-insoluble p62 positive bands were both enhanced by CS exposure. Consistent with LC3B flux analysis, treatment with 100 mg/m^3 TPM inhibited selective autophagic flux, and induced acute cytotoxicity marked by an accumulation of autophagosomes, LC3B II, and SDS-insoluble p62 by immunoblot (**Figure 8D & 9A**).

Since autophagy is dependent upon ATP and mitochondria are particularly vulnerable to the oxidative stress caused by CS, ATP levels were measured in the MTEC cells following CS exposure to determine if lack of intracellular ATP could account for the block in autophagic

activity (**Figure 9B**). While there was a time dependent drop in cellular ATP, the kinetics of this drop were much slower and not significant compared to the acute block in autophagic flux observed with 100 mg/m^3 TPM. These data indicate that the block in autophagic activity caused by lethal CS treatment is not a consequence of inadequate energy availability.

To confirm these findings autophagic flux was also assayed in the multiday model of CS treatment using chloroquine (CQ), which also prevents lysosome acidification (**Figure 9C**). Consistent with the single dose studies LC3B II turnover was not altered, while p62 turnover was enhanced by CS treatment. The SDS-insoluble p62 positive aggregates appear with CQ treatment in the CS treated cells, which suggests that these aggregates are produced as a result of CS exposure and are efficiently cleared by autophagy. However, p62 is a target of the oxidative stress transcription factor Nrf-2, and CS-induced p62 transcription may increase the p62 available for turnover and thereby contribute to the apparent increase in autophagic flux determined by this marker (188, 189, 191, 193, 292). These *in vitro* studies suggest that

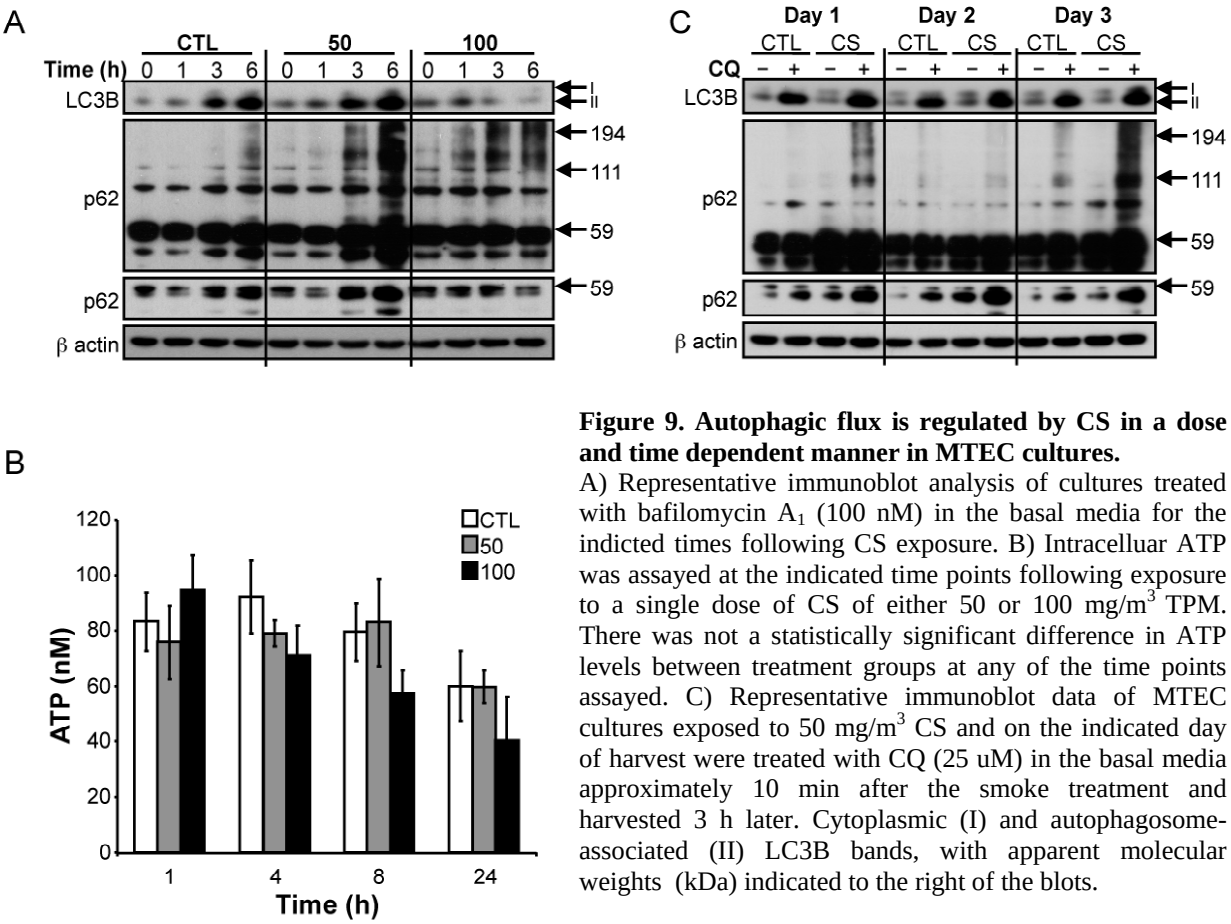

Figure 9. Autophagic flux is regulated by CS in a dose and time dependent manner in MTEC cultures.
A) Representative immunoblot analysis of cultures treated with bafilomycin A_1 (100 nM) in the basal media for the indicted times following CS exposure. B) Intracelluar ATP was assayed at the indicated time points following exposure to a single dose of CS of either 50 or 100 mg/m^3 TPM. There was not a statistically significant difference in ATP levels between treatment groups at any of the time points assayed. C) Representative immunoblot data of MTEC cultures exposed to 50 mg/m^3 CS and on the indicated day of harvest were treated with CQ (25 uM) in the basal media approximately 10 min after the smoke treatment and harvested 3 h later. Cytoplasmic (I) and autophagosome-associated (II) LC3B bands, with apparent molecular weights (kDa) indicated to the right of the blots.

autophagic flux, particularly selective autophagic flux, is activated by CS in two different models of subtoxic, 50 mg/m^3 TPM CS treatment. These data also indicate that lethal doses of 100 mg/m^3 TPM CS cause autophagosome accumulation associated with decreased autophagic flux, which is independent of a loss in cellular ATP and precedes detection of cell death markers.

5.3 INDUCTION OF AUTOPHAGIC FLUX BY CS *IN VIVO*

To validate the *in vitro* findings of the MTEC cultures treated with CS, mice were treated with CS for 1 wk or 2 mo and assessed for autophagic markers. Mice were exposed to CS 5 d/wk for approximately 2 h a day in a total body box in which the TPM was between 150 and 200 mg/m^3. TEM analysis of the tracheal epithelium of mice treated for 1 wk with CS contained ciliated cells which recapitulated the phenotypes observed in both the 50 and 100 mg/m^3 TPM treated MTEC cultures (**Figure 10A**). While the majority of cells contained autophagosomes and appeared viable as would approximate the sublethal treatment with 50 mg/m^3, an occasional apoptotic cell was observed that resembled the cells in the MTEC cultures treated with 100 mg/m^3. In these apoptotic cells intercellular contacts were disrupted, basal bodies docked at the apical membrane were devoid of axonemes, mitochondria were swollen, the cells were filled with vacuoles and there was evidence of nuclear condensation. Based on this imaging analysis, the MTEC cultures treated with CS appear to closely approximate the effects of CS on the respiratory epithelium *in vivo*. Mice treated with CS for 1 wk or 2 mo were injected with the lysosomal protease inhibitor leupeptin either immediately following (t=0h) or 24 h (t=24h) after the final CS treatment and tissues were harvested 2 h later, in order to assess the effects of CS on autophagic flux *in vivo* (**Figure 10B**). LC3B accumulation in the lysosome-enriched (LE) fraction was then compared between control and CS treated mice by densitometric analysis. The difference in LC3B levels for each mouse was calculated from an LC3B standard curve and the difference in flux between the room air (RA), 1 wk, and 2 mo CS treated mice was determined by subtracting the mean basal amount of LC3 in the PBS treated mice for each treatment group form the individual values of the leupeptin treated mice. The difference in LC3B was then graphed to show the change in LC3B II turnover in the LE fraction caused by CS. There was a time dependent increase in autophagic flux activated by CS exposure, as the 2 mo CS mice had the most autophagic flux.

The LC3B II levels in the PBS treated 2 mo CS mice was lower than the RA, suggesting that there are fewer autophagosomes accumulating in the lung tissue of these mice with this treatment. Finally, CS-induced autophagy was sustained as flux was significantly increased whether the activity was assayed immediately after exposure or 24 h later in the 2 mo CS treated mice.

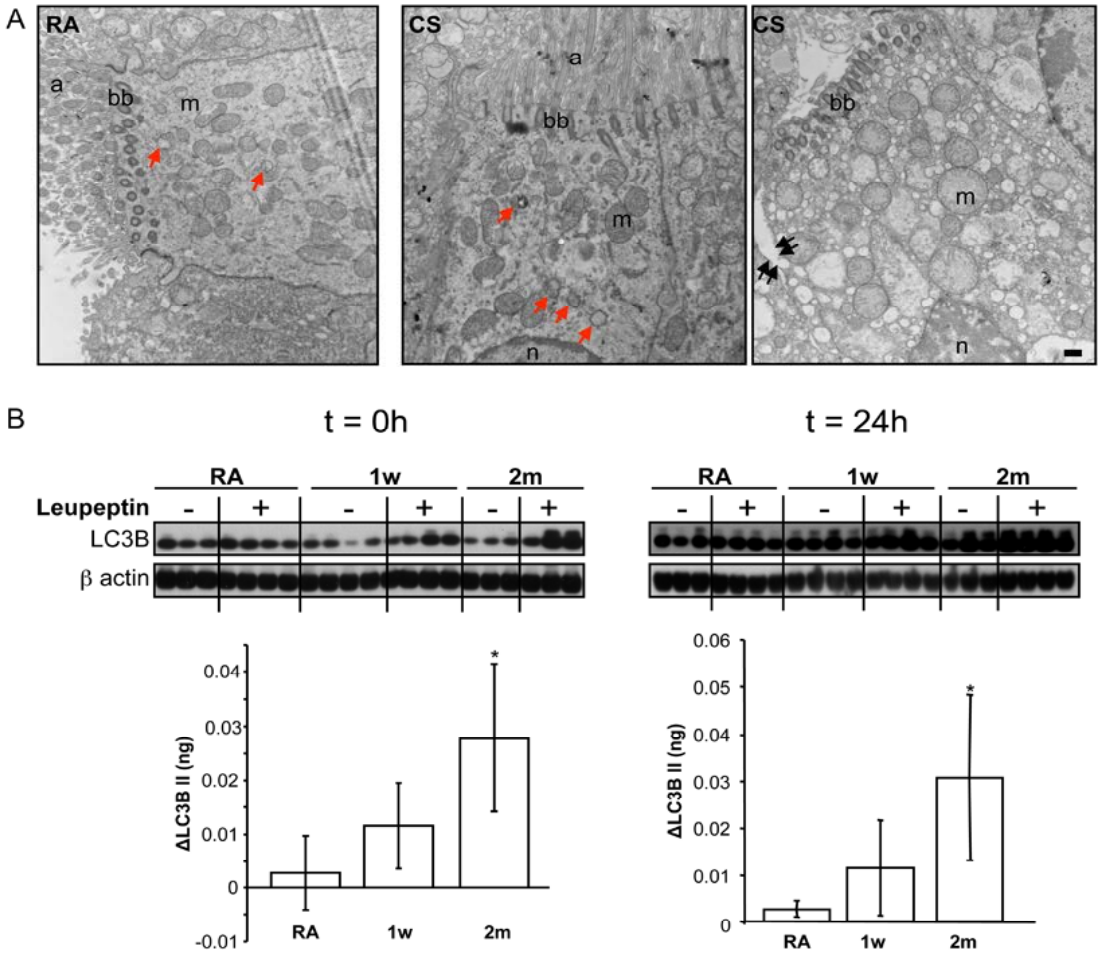

Figure 10. CS regulates autophagic activity *in vivo*. A) Representative TEM images show both morphologically healthy and dying cells, as well as autophagosome morphology in ciliated cells of the tracheae of mice exposed to RA or to CS for 1 wk (arrows-autophagosomes, a-axoneme, bb-basal bodies, m-mitochondria, n-nucleus. Bar=500nm). B) Mice exposed to CS for 1 wk or for 2 mo were injected with 40 mg/kg of leupeptin immediately following the last CS exposure (t = 0h) or 24 h later (t = 24h). Whole lungs were harvested and frozen 2 h subsequent to the leupeptin injection. Autophagic flux was assessed by densiometric analysis using an LC3B standard curve, following the isolation of the LE fraction. Flux was calculated by subtracting the average amount of LC3B II in vehicle treated mice from the amount of LC3B II that accumulated with leupeptin treatment (n=3-4, *p<0.05 by students unpaired *t* test).

6.0 RESULTS- EFFECTS OF CS ON AUTOPHAGIC SUBSTRATES

6.1 EVIDENCE FOR PROTEIN AGGREGATE STRESS IN PATIENTS WITH COPD

Recent studies have suggested that misfolded protein stress promotes proinflammatory pathways contributing to COPD pathogenesis (237). In one of these studies expression of mutant A1AT was shown to enhance inflammatory cytokine production; suggesting that this mutation may promote emphysematous phenotype by an additional mechanism to altering the lung protease balance (237, 242, 243). More recently a survey of COPD patients' lung tissue for markers of UPR and ERAD, demonstrated a marked accumulation of ubiquitinated aggregates in late disease (237). Since protein folding may be a key molecular mechanism underlying CS-induced changes in epithelial cells and autophagy is a critical mechanism for protein aggregate removal, we investigated this pathway in human tissues. Using ProteoStat™ protein aggregation dye to stain protein aggregates, also called inclusion bodies, we observed an increase in cells containing large numbers of red staining puncta, which positively correlated with COPD severity (**Figure 11A) (293)**. These findings are in agreement with the recently published paper in which ubiquitin positive aggregates were observed in late stage COPD. Furthermore, expression of HDAC6, which has been implicated in efficient autophagic degradation of protein aggregates, was also significantly upregulated in the lungs of smokers, but was not correlated to COPD severity (**Figure 11B**). These findings suggest that pathways implicated in protein aggregate removal may be upregulated in smokers as a fundamental physiological response to CS. These data support a role for protein aggregate stress in COPD pathogenesis and suggest that inefficient removal of protein aggregates may be a hallmark feature of late stage disease.

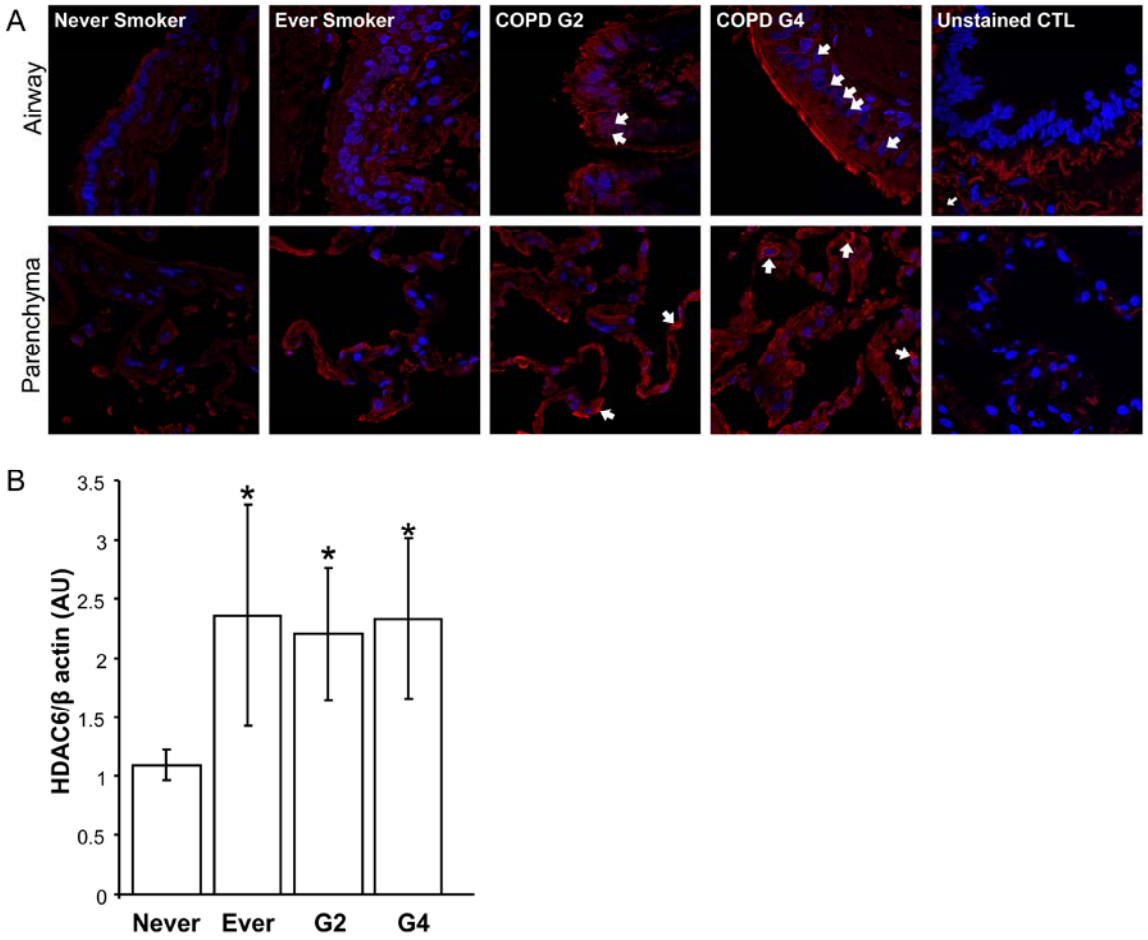

Figure 11. Misfolded protein aggregates accumulate in late stage COPD patients and HDAC6, a protein critical for aggregate removal, is acutely upregulated in smokers. A) Protein aggregates were stained in human lung tissue using ProteoStat™ protein aggregation assay from ENZO. Protein aggregates (arrows) appear in both the airway and parenchyma tissue of COPD patients. Nuclei (blue) were stained with Hoechst. Representative confocal images acquired at 63X. B) HDAC6 expression in human lung tissue was determined by densiometric analysis of immunoblots. Data are mean ± SE of 4-5 samples and statistical analysis was performed by student's unpaired *t* test compared to the never smoker control.

6.2 HDAC6 DEFICIENCY PROMOTES CS-INDUCED ACCUMULATION OF MISFOLDED PROTEIN AGGREGATES

To determine if CS induces misfolded protein accumulation in epithelial cells, ProteoStat™ protein aggregation dye was used to assay for protein aggregates in MTEC cultures treated with 50 and 100 mg/m^3 CS TPM (**Figure 12A**). A dose dependent induction of inclusion bodies was observed in these cultures, suggesting that CS is a potent inducer of misfolded protein stress. Since HDAC6 promotes autophagic degradation of protein aggregates and is upregulated in response to CS in the lung, we investigated the importance of this protein using HDAC6$^{-/Y}$ derived MTEC cultures (198, 206, 207). Consistent with these previous findings, HDAC6$^{-/Y}$ cultures contained more inclusion bodies basally and following CS treatment compared to controls (**Figure 12A**). Despite these differences, MTEC cultures generated from these mice appeared to have similar disruption of culture integrity following CS-treatment. There were no statistically significant differences in resistance in the HDAC6$^{-/Y}$ or HDAC6$^{+/Y}$ at baseline or following CS exposure (**Figure 12B**). These data indicate that this protein does not play a critical role in the events leading to CS induced cell-cell contact disruption. Surprisingly, immunoblot analysis of the MTEC cultures revealed low baseline activation of apoptosis in the HDAC6$^{-/Y}$ cultures by cleaved caspase 3 immunoblot; however, cell death following lethal treatment with 100 mg/m^3 CS TPM was slightly abrogated in these cells (**Figure 12C**). The simplest interpretation of these data would be that HDAC6 plays an as yet unknown role in CS-induced cell death, possibly by potentiating CS-induced autophagic cell death pathways. Consistent with the wildtype cultures being more injured by 100 mg/m^3 CS, p62 SDS-insoluble aggregates and Beclin-1 cleavage associated with cell death, were more abundant in the HDAC6$^{+/Y}$ cells. Finally, since HDAC6 plays a critical role in primary cilia regulation expression of the cilia marker centrin-1 was also investigated in these cultures (210). While this cilia marker was depleted in the HDAC6$^{+/Y}$ cultures treated with 100 mg/m^3 CS TPM, the HDAC6$^{-/Y}$ cells appeared protected. These data indicate that HDAC6 plays a critical role in cellular homeostasis and the removal of misfolded proteins by autophagy. While the HDAC6$^{-/Y}$ cells appeared vulnerable to cell death basally, the abrogation of apoptosis following lethal CS treatment suggests a specific function in the execution of CS-induced cell death.

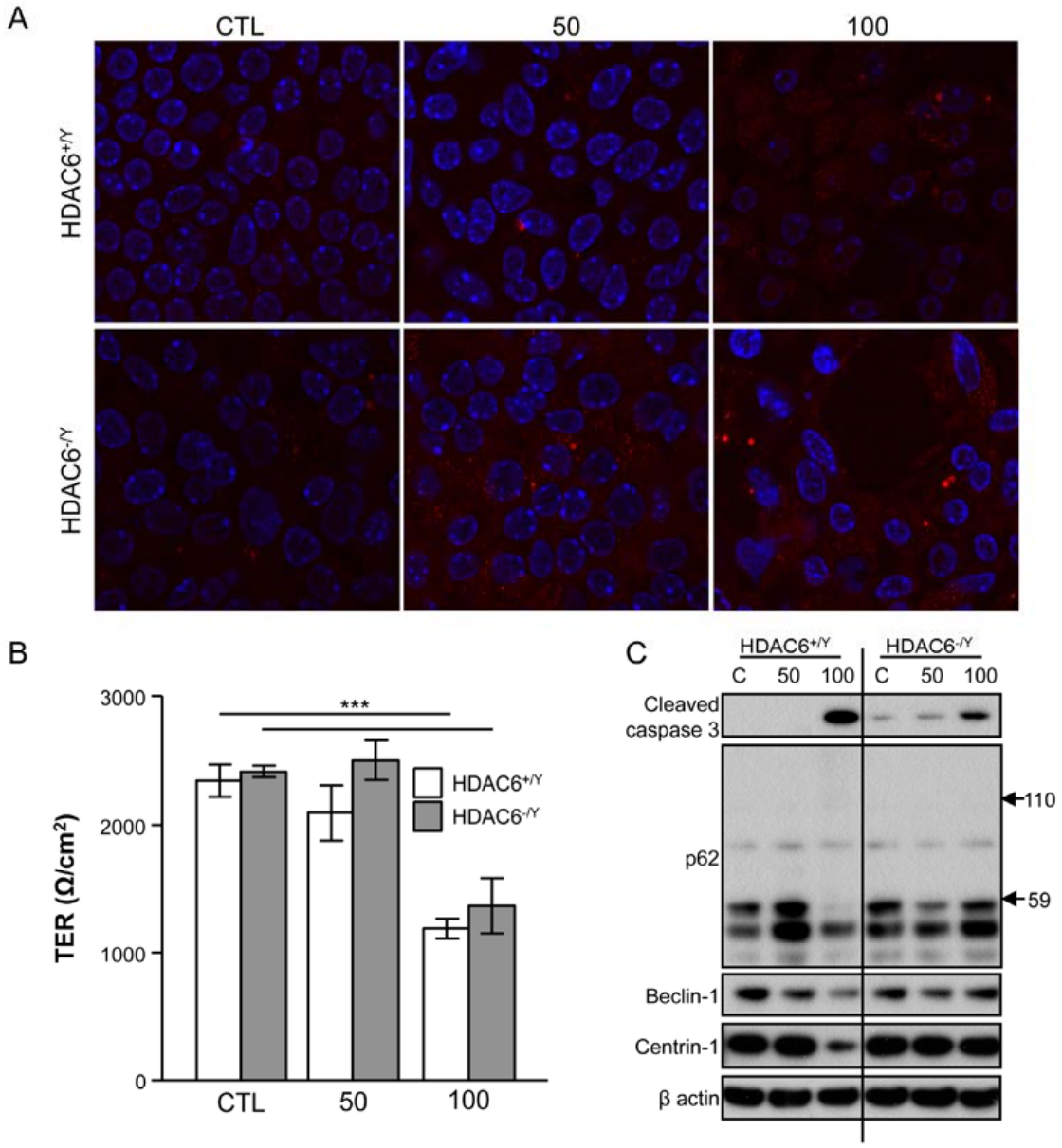

Figure 12. Increased baseline cell death and misfolded protein accumulation in HDAC6$^{-/Y}$ MTEC cultures. A-C) Analysis of MTEC cultures 24 h after exposure to the indicated concentrations of CS TPM (mg/m^3) A) Protein aggregates (red) were stained in MTEC cultures using ProteoStat™ and nuclei (blue) were stained with Hoechst. Representative images were selected from fields acquired at 63X by confocal microscopy. B) TER was measured to assess culture integrity. C) Immunoblot analysis of autophagic, apoptotic and cilia markers. Molecular weights (kDa) are indicated to the right of the blots.

6.3 EMPHYSEMATOUS CHANGES AND APOPTOTIC MARKERS ARE ENHANCED IN AUTOPHAGY DEFICIENT HDAC6 MICE FOLLOWING 6 MONTHS OF CS EXPOSURE *IN VIVO*

As observed in the MTEC cultures *in vitro*, the HDAC6$^{-/Y}$ mice were also predisposed to protein aggregate accumulation *in vivo*. Protein aggregates visualized with the ProteoStat^{TM} protein aggregation dye were robustly induced by CS in HDAC6$^{-/Y}$ mice exposed to CS for 1 wk (**Figure 13A**).

In order to more fully elucidate the role of HDAC6 in ameliorating CS induced stress *in vivo*, mice were exposed for 2 h/d to 150-200 mg/m^3 CS 5 d/wk for 6 mo. The HDAC6$^{-/Y}$ mice displayed a comparable inability to gain weight as compared to the HDAC6$^{+/Y}$ mice, suggesting that the nicotine effects on metabolism are similar in these mouse strains (**Figure 13B**). In the HDAC6$^{+/Y}$ mice there was a 10% increase in mean chord length and in the HDAC6$^{-/Y}$ mice there was a 13% increase in mean chord length, a morphometric indices of emphysematous airspace enlargement (**Figure 13C**). While CS induced a statistically significant increase in airspace in both mouse strains, the airspace enlargement was not significantly different between the two strains treated with CS. Consistent with this observation there was a moderate enhancement of apoptotic markers in the HDAC6$^{-/Y}$ lung homogenates compared to CS exposed HDAC6$^{+/Y}$ (**Figure 22D**). Autophagic activity was assessed in the mice following 6 mo of CS exposure. Autophagic flux was significantly decreased in the HDAC6$^{-/Y}$ mice exposed to CS, while there was not a significant difference observed between the RA and CS wildtype mice (**Figure 22E**). These are the first data demonstrating that autophagy may play a cytoprotective function in epithelial cells exposed to CS, in which is efficient clearance of misfolded protein aggregates is a potential mechanism.

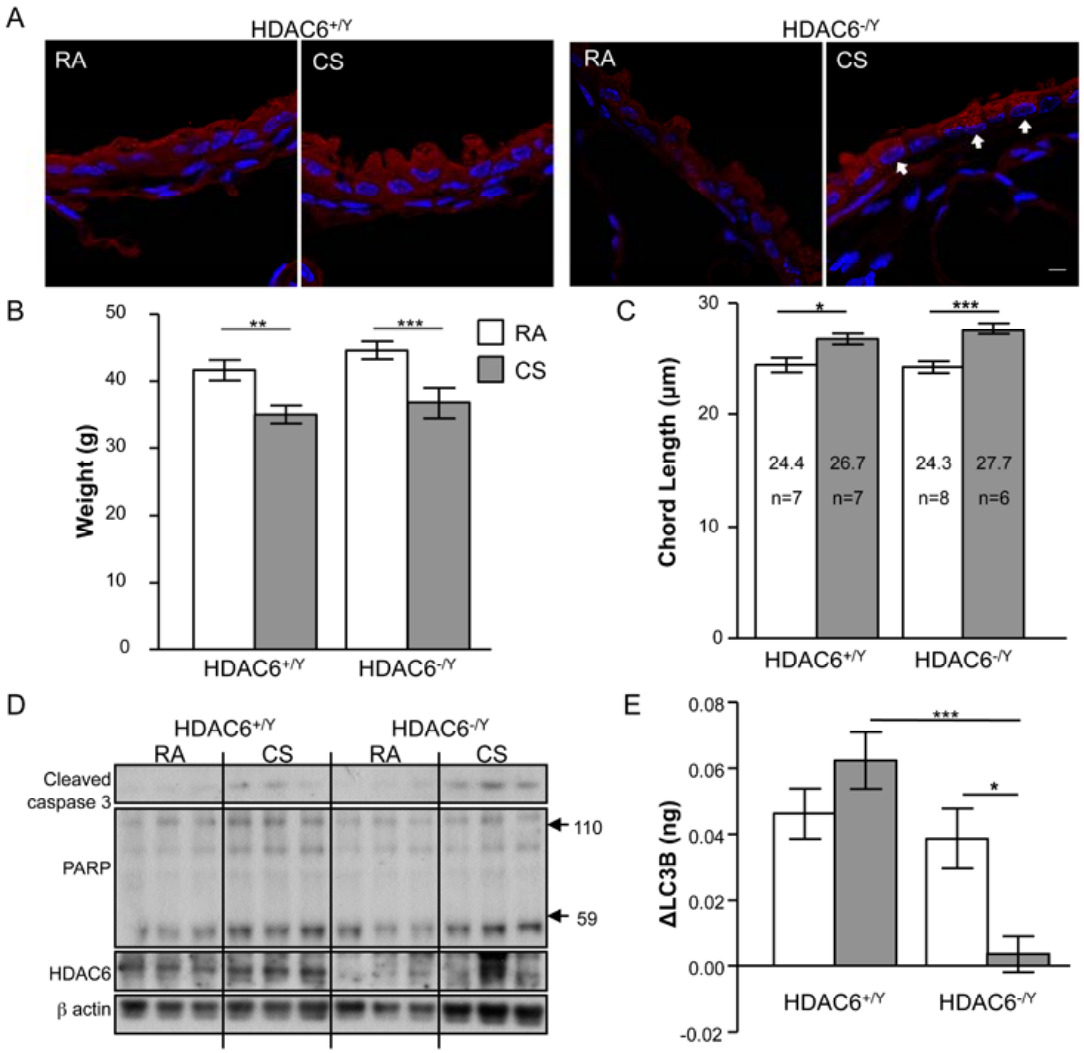

Figure 13. HDAC6$^{-/Y}$ mice are autophagy deficient and moderately more susceptible to CS induced injury. A) Airway cells containing numerous protein aggregate puncta (red; white arrows) in mice exposed to CS for 1 wk were visualized using ProteoStat™ and nuclei (blue) were stained with Hoechst. Representative images were acquired at 63X by confocal microscopy (bar = 10 µm). B-E) Mice were exposed to 150-200 mg/m^3 CS for 2 h/d 5 d/wk for 6 months. All data are presented as the mean ± SE and statistical significance was determined by using a two-way ANOVA and Bonferroni post test. B) Mice were weighed following 6 mo of CS exposure. C) Emphysematous changes caused by CS exposure were assessed by morphometric assessment of chord lengths. D) Apoptotic markers and HDAC6 protein expression was assessed in mouse lung homogenates. Molecular weights (kDa) are inidcated to the right of the blots. E) *In vivo* autophagic flux was assessed in the HDAC6$^{+/Y}$ and HDAC6$^{-/Y}$ mice following 6 mo of CS treatment. The mice were given an *i.p*. injection of 40 mg/kg leupeptin or vehicle within 3 h of the final smoke exposure and sacrificed in parallel 2 h later. Data are densiometric analyses using a GFP-LC3 standard curve of LC3B accumulation in lysosome enriched protein fractions, determined by subtracting the average amount of LC3B present in the vehicle treated mice from the amount of LC3 accumulated in each of the leupeptin treated animals (n = 3-5 mice per group).

6.4 CILIA PROTEINS AS TARGETS OF CS-INDUCED AUTOPHAGIC DEGRADATION

Since CS promotes misfolding of proteins, which are degraded by proteasomal or autophagic mechanisms, enhanced protein turnover would be most detrimental to dynamic structures requiring continual protein input, such as the motile cilia of the respiratory tract. In particular, cilia shortening is observed even in healthily smokers, suggesting either enhanced turnover over of cilia proteins or what may be more likely a lack of essential building blocks (88). In order to determine if cilia components are targets of autophagic degradation, cilia and autophagy markers were assessed following CS exposure in MTEC cultures. Immunofluoresence analysis suggested that 50 mg/m^3 promoted LC3B localization to the cilia, while 100 mg/m^3 was associated with accumulation of autophagosome puncta (**Figure 14A**). Since autophagic flux was most active following treatment with 50 mg/m^3 CS TPM, these data indicate a CS-inducible association between this organelle and essential autophagy proteins in a context when autophagic flux is enhanced. In order to more fully determine if cilia components are actually encapsulated in autophagosomes to be degraded by autophagy following CS treatment, subcellular fractionation was performed to acquire a LE fraction (**Figure 14B**). The cilia marker centrin-1, which was decreased in MTEC cultures in which cilia were significantly diminished by CS treatment, was primarily localized to the cytoplasmic (Cyto) cell fraction in control cells. In the cells treated with 50 mg/m^3 a faint centrin-1 positive band appeared in the LE fraction, in which selective autophagic flux was active. Centrin-1 was robustly relocalized to the LE fraction following treatment with 100 mg/m^3 CS TPM, in which CS-induced flux inhibition would be expected to enhance the signal of autophagic targets. These data suggest that CS induces the autophagic degradation of cilia components following smoke exposure, and may promote the cilia loss and shortening that leave smokers' lungs vulnerable to infections that promote COPD pathogenesis.

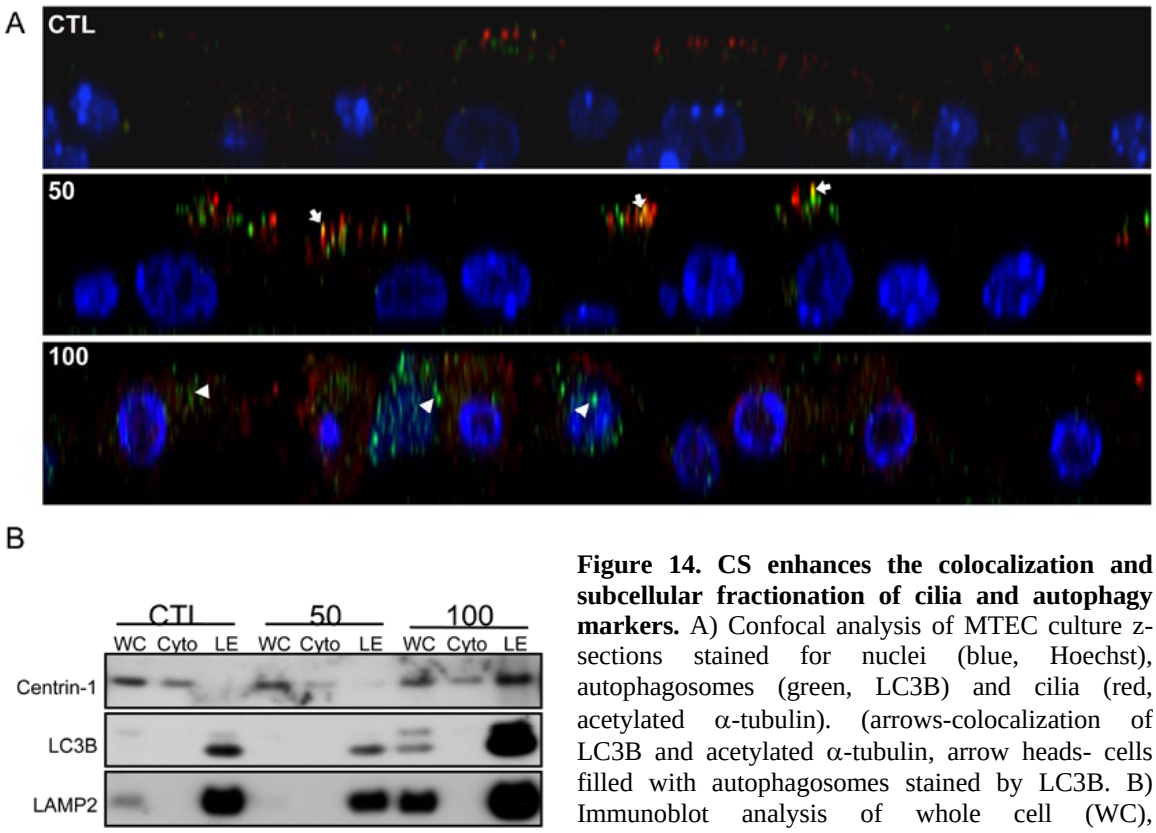

Figure 14. CS enhances the colocalization and subcellular fractionation of cilia and autophagy markers. A) Confocal analysis of MTEC culture z-sections stained for nuclei (blue, Hoechst), autophagosomes (green, LC3B) and cilia (red, acetylated α-tubulin). (arrows-colocalization of LC3B and acetylated α-tubulin, arrow heads- cells filled with autophagosomes stained by LC3B. B) Immunoblot analysis of whole cell (WC), cytoplasmic (Cyto), and lysosome enriched fractions (LE) for cilia, autophagosome, and lysosome markers following subcellular fractionation of MTEC cultures treated for 24 h with the indicated dose of CS (mg/m^3 TPM).

7.0 RESULTS- THE FUNCTIONAL ROLE OF AUTOPHAGY PROTEINS IN THE RESPONSE OF EPITHELIAL CELLS TO CS: LC3B

7.1 LC3B REGULATES CS-INDUCED AUTOPHAGY, APOPTOSIS, AND EMPHYSEMATOUS AIRSPACE ENLARGEMENT

$LC3B^{-/-}$ mice were used to investigate the role of this autophagy protein in the response of epithelial cells to CS. MTEC cultures generated from $LC3B^{-/-}$ mice were exposed to 50 and 100 mg/m^3 CS TPM and assessed for autophagy and apoptotic markers (**Figure 15A**). Consistent with previous findings LC3B promotes CS-induced cell death, as $LC3B^{-/-}$ MTEC cultures had less active cleaved caspase 3 and proapoptotic Bax cleavage fragment accumulation by immunoblot compared to MTEC cultures generated from wildtype mice (6). The enhanced accumulation of p62 SDS-insoluble protein aggregates in the $LC3B^{-/-}$ MTEC cultures is evidence that autophagic flux is defective in these mice. To further evaluate the role of LC3B in the cellular response to CS, emphysema development was evaluated in $LC3B^{-/-}$ mice, wildtype littermates ($LC3B^{+/+}$), or C57BL/6 mice exposed to CS for 3 mo. Following this exposure, airspace enlargement, apoptosis, and autophagy markers were assessed in the lung. Consistent with previous observations, C57BL/6 wildtype mice displayed marked increases in lung airspace after 3 mo of CS exposure relative to RA controls as determined by comparative histological examination and mean linear intercept (Lm) measurements (**Figure 15B**) (294, 295). Similarly, $LC3B^{+/+}$ wildtype littermate mice exposed to CS for 3 mo displayed marked increases in lung airspace after CS exposure relative to air-treated controls. In contrast, airspace was not increased in $LC3B^{-/-}$ mouse lungs by CS exposure relative to air-treated controls; however, the $LC3B^{-/-}$ mice exhibited significant basal airspace enlargement relative to wildtype littermate mice by Lm (**Figure 15B**).

Airspace enlargement caused by CS exposure in $LC3B^{-/-}$ and wildtype mice was also assessed separately by measuring the equivalent diameter of alveolar airspaces using a previously published automated image processing algorithm (296). Consistent with the Lm measurements, the equivalent diameter of CS-exposed $LC3B^{+/+}$ mice (31.5 ± 1.5 μm) was significantly greater than air-treated $LC3B^{+/+}$ mice (27.9 ± 1.4 μm; p=0.001), whereas the equivalent diameter of CS-exposed $LC3B^{-/-}$ mice (30.7 ± 1.8 μm) was not different from the RA LC3B mice (29.0 ± 3.1 μm). The equivalent diameter of air-treated $LC3B^{-/-}$ mice was greater than that of the air-treated $LC3B^{+/+}$ mice; however, the increase was not statistically significant.

To investigate lung cell death, apoptotic indices were measured, including cleaved caspase 9 and Bax/Bcl-2 ratio (**Figure 15C**). These markers were significantly increased in the lungs of the $LC3B^{+/+}$ mice by CS exposure, but were not increased in the CS-exposed $LC3B^{-/-}$ mice. Furthermore, CS induced the accumulation of autophagic vacuoles (AVs) as determined by TEM, in the lungs of wildtype ($LC3B^{+/+}$) mice (**Figure 15D**). In contrast, a reduced number of AVs were detected in the lung after CS exposure in the $LC3B^{-/-}$ mice. These data suggest that LC3B promotes CS-induced cell death both *in vitro* and *in vivo*.

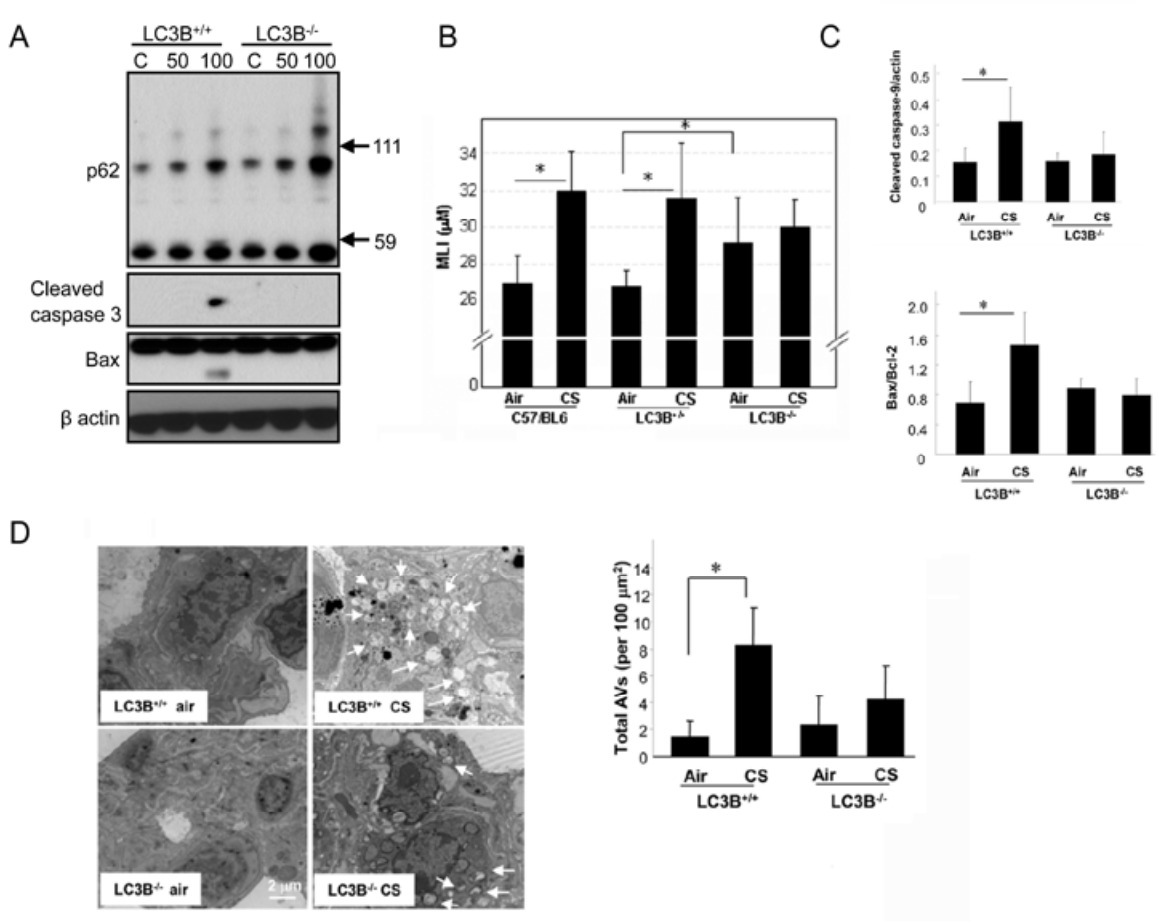

Figure 15. LC3B regulates CS-induced autophagy and apoptosis *in vitro* and *in vivo*. A) MTEC cultures derived from wildtype C57BL/6 and LC3B$^{-/-}$ mice were assessed for autophagic and apoptotic markers 24 h after exposure to 50 or 100 mg/m^3 CS TPM. B-E) Wildtype C57BL/6, LC3B$^{+/+}$ or LC3B$^{-/-}$ mice were exposed to chronic CS of RA for 3 mo (C57BL/6: n = 9 RA & n = 8 CS, LC3B$^{+/+}$: n = 6 RA & n = 9 CS, LC3B$^{-/-}$ n = 9 RA & n = 9 CS). B) Quantification of MLIs (*P<0.01, by student's unpaired *t* test) C) Densitometric analysis of immunoblots generated from lung protein samples for the apoptotic markers cleaved caspase 9 and the ratio of proapoptotic Bax to antiapoptotic Bcl-2. D) Representative TEM images of mouse lung sections. (Arrows: autophagic vacuoles; AVs) E) TEM images were scored for number of AVs. The data are represented as AVs per 100 μm^2, n=20 representative images of each group; *p<0.05 by student's unpaired *t* test.

7.2 LC3B INTERACTS WITH CAVEOLIN-1 AND FAS TO REGULATE CSE-INDUCED AUTOPHAGY AND APOPTOTIC CELL DEATH

To explore the mechanisms by which LC3B regulates CS-induced epithelial cell apoptosis, immunoprecipitation experiments were performed to identify apoptosis-related factors that interact with LC3B. In mammalian cells, the extrinsic apoptotic pathway responds to stimuli via activation of death receptor family proteins (297, 298). Stimulation with aqueous CS extract (CSE) induced the extrinsic apoptotic pathway in lung epithelial (Beas-2B) cells, involving death-inducing signaling complex (DISC) formation, caspase 8 activation, and Bax activation (8, 60). We examined whether LC3B can interact with mediators of this pathway. LC3B interacted with Fas under basal conditions in Beas-2B cells whereas this interaction was rapidly disrupted after exposure to CSE (**Figure 16A & B**). Confocal imaging revealed that LC3B and Fas colocalized in the plasma membrane under basal conditions, whereas the merged complex of LC3B and Fas at the cell membrane was disrupted by CSE treatment (**Figure 16B**).

Fas-mediated apoptosis involves the association of Fas with accessory molecules (i.e. procaspase 8, FADD). Recent studies show that Fas can localize to lipid rafts in the plasma membrane (60, 299). We therefore examined whether LC3B localizes to lipid rafts. Subcellular fractionation experiments demonstrated that LC3B and Fas also localized to low-density caveolin-1 (Cav-1) containing fractions under basal conditions in Beas-2B cells and lung fibroblasts (**Figure 16C**). Cav-1 serves as a structural component of caveolae, which are plasma membrane domains rich in cholesterol and glycosphingolipids. As Cav-1 interacts with several membrane-associated signaling proteins, the role of this protein in mediating the LC3B-Fas interaction at the plasma membrane was investigated (300). Cav-1, under basal conditions, interacted with both LC3B and Fas by co-immunoprecipitation assays (**Figure 16D**). Interestingly, both Cav-1-Fas and LC3B-Cav-1 complexes dissociated after CSE treatment. These data provide novel evidence for LC3B, Cav-1 and Fas interacting at lipid rafts in the plasma membrane, and the regulated disruption of this interaction by CS.

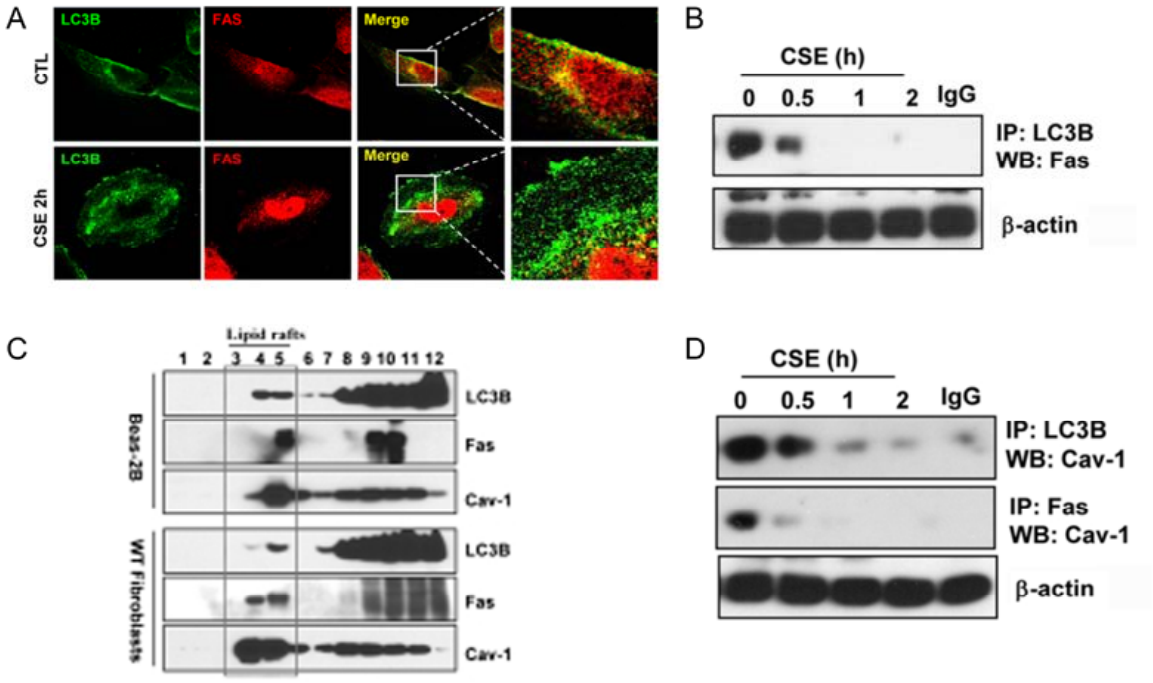

Figure 16. LC3B-Cav-1-Fas interactions regulate CSE-induced autophagy and apoptotic cell death. A) Representative immunofluorescence images of LC3B and Fas staining in Beas-2B cells. Colocalization is indicated by yellow staining in the merged images. B) Beas-2B cells were treated with 10% CSE for the indicated times and the interaction between LC3B and Fas was assessed by immunoprecipitation with LC3B and immunoblotting for Fas. β-actin served as the loading standard. C) Beas-2B and wildtype fibroblasts were fractionated by sucrose gradient ultracentrifugation and the fractions were immunoblotted for Fas, LC3B and Cav-1. D) Beas-2B cells were expoed to 10% CSE for the indicated times and the lysates were subjected to immunoprecipitation with LC3B and Fas antibodies, and analyzed by immunoblot for Cav-1. β-actin served as the loading standard.

7.3 LC3B REGULATES FAS-MEDIATED APOPTOSIS IN CSE-TREATED BEAS-2B CELLS THROUGH INTERACTIONS WITH CAV-1

In order to probe the effect of LC3B on Cav-1 interactions with Fas, Beas-2B cells were treated with LC3B siRNA. LC3B knockdown enhanced the basal interaction of Fas with Cav-1 (**Figure 17A**). Furthermore, Beas-2B cells transfected with LC3B-siRNA exhibited reduced DISC formation and Bax activation in response to CSE relative to control siRNA treated cells (**Figure 17A**).

Proteins that bind Cav-1 typically contain a canonical Cav-1-binding motif (CBM), ΦXΦXXXXΦ or ΦXXXXΦXXΦ, where Φ is an aromatic amino acid and X is any nonaromatic amino acid. Proteins without such motifs are also capable of binding to Cav-1 (301). The primary structure of LC3B contains a sequence, ^{108}FLYMVYASQETF^{109} , which is a potential CBM. Amino acid substitution mutants of LC3B at position Y113 were created to examine whether this sequence mediates the LC3B-Cav-1 interaction. Interestingly, the Y113A mutation abolished the basal LC3B-Cav1 interaction (**Figure 17B**). Similar to observations made with LC3B-siRNA, transfection with the LC3B Y113A enhanced Cav-1-Fas interaction (**Figure 17B**). Overexpression of wildtype LC3B in Beas-2B cells markedly augmented cell death in response to CSE treatment. By comparison, overexpression of LC3B Y113A also induced cell death, although to a lesser degree than the WT LC3B construct (**Figure 17C**). These experiments suggest that LC3B promotes CSE-induced cell death in part through a mechanism dependent on the Cav-1-binding motif.

To further explore the mechanism by which Cav-1 facilitates Fas and LC3B interaction, we confirmed that LC3B binding to Cav-1 was dependent upon the Cav-1 scaffolding domain (CSD), which mediates interactions with the CBMs of other proteins. The interaction between LC3B and Cav-1 was assessed by co-immunoprecipitation following transfection of Beas-2B cells with either wildtype Cav-1 or Cav-1 cells bearing a mutated CSD (ΔCSD) (**Figure 17D**). Cells transfected with the Cav-1 ΔCSD showed decreased interaction between LC3B and Cav-1 compared to cells transfected with WT Cav-1. Fas binding was not affected by the ΔCSD mutation. These data confirm the importance of the LC3B CBM and Cav-1 CSD domains for mediating the interaction between these two proteins. While Fas expression was slightly increased in Cav-1$^{-/-}$ lung fibroblasts, the LC3B Fas interaction was diminished, suggesting an intermediate role for Cav-1 in complex formation (**Figure 17E**).

Since Fas-Cav-1 binding was not affected by expression of the ΔCSD mutation, additional sites of interaction were explored. Cav-1 has three sites of palmitoylation in proximity to the C-terminus. The Cav-1-Fas interaction was disrupted in Beas-2B cells treated with 2-bromopalmitate, a general palmitoylation inhibitor (**Figure 17F**). Fas is also palmitoylated on cysteine 199, this modification was required for mediating the Fas-Cav-1 interaction, as transfection with mutant Fas C199S abolished the interaction (**Figure 17G**). Surprisingly, Fas siRNA diminished the Cav-1-LC3B interaction. Cav-1 appears to mediate the interaction

between Fas and LC3B; however, Fas promotes LC3B binding to Cav-1, while LC3B hinders Fas binding to Cav-1. These data suggest a complicated interdependence of all three factors in complex formation and suggest that loss of LC3B may enhance survival by increasing the Fas Cav-1 interaction (**Figure 17H**).

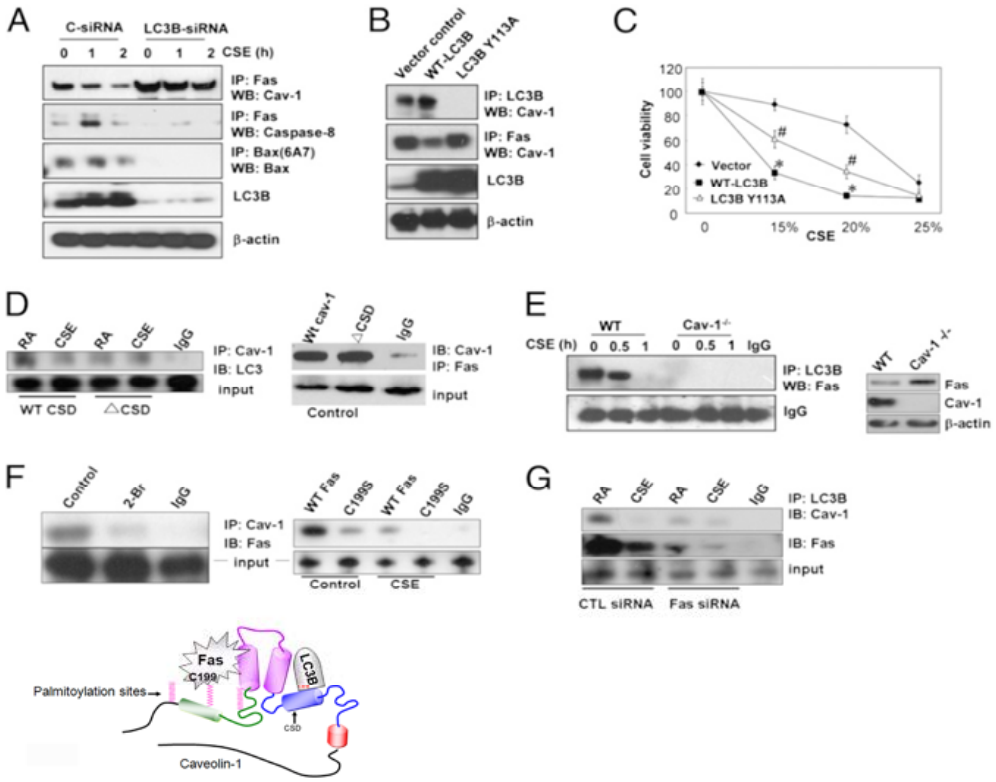

Figure 17. Mapping the LC3B-Cav-1-Fas interaction. A) Beas-2B cells were pretreated with control siRNA (C-siRNA) or LC3B siRNA for 48 h and then treated with 10% CSE for the indicated times. The lysates were then subjected to the indicated immunopercipitation and immunoblot analysis. B) Beas-2B cells were transfected with wildtype LC3B or Y113A LC3B for 48 h and the interaction between LC2B-Cav-1-Fas was then assessed by immunopercipitation and immunoblot analysis. C) Beas-2B cells were transfected with vector, wildtype LC3B, or Y113A LC3B for 48 h and viability was then assessed by MTT assay after treating the cells with the indicated concentration of CSE for an additional 24 h. Data represent mean ± SD; *p<0.05 vs corresponding vector control values; #P<0.05 vs corresponding values for wildtype-LC3B overexpression. D) Wildtype Cav-1 and ΔCSD Cav-1 expression clones were transfected into Beas-2B cells for 36 h and then the cells were exposed to 10% CSE for 1 h. The LC3B-Cav-1-Fas interaction was then assessed by immunopercipitation and immunoblot. The data are representative of three independent experiments. E) Cell lysates from wildtype or Cav-$^{-/-}$ fibroblasts treated with 10% CSE for the indicated times were subjected to immunopercipitation for LC3B and immunoblot of Fas. A nonspecific IgG band served as the standard. Cav-1 and Fas expression was assessed by immunoblot in the wildtype and Cav-1$^{-/-}$ fibroblasts. F) Beas-2B cells were treated with 100 μM 2-bromopalmitate (2-Br), a general palmitoylation inhibitor, or DMSO for one hour and subjected to coimmunoprecipitation assays for Cav-1-Fas interaction (left). Beas-2B cells were transfected for 36 h with wildtype Fas and C199S Fas. The cells were exposed to 10% CSE for 1 h and subjected to immunoprecipitation and immunoblot analysis for Fas-Cav-1 interaction (Right). Representative immunoblot data from three independent experiments. G) Beas-2B cells were pretreated with CTL siRNA or Fas siRNA for 48 h, followed by exposure to 10% CSE for the indicated times. The lysates were subjected to immunoprecipitation and immunoblot analysis. H) A schematic of the proposed LC3B-Cav-1-Fas complex, in which the Fas interaction with Cav-1 is dependent upon Fas palmityolation at cystein 199, while LC3B interacts through the Cav-1 scaffold domain (CSD).

7.4 LC3B INTERACTING PROTEIN, CAV-1, SUPPRESSES CSE-INDUCED AUTOPHAGY AND APOPTOTIC CELL DEATH IN BEAS-2B CELLS

The role of Cav-1 in pulmonary disease remains controversial, since Cav-1 has been shown to play protective and deleterious functions in various models of lung disease (302-306). Furthermore, the role of Cav-1 in COPD pathogenesis remains poorly understood. Cav-1 appears to regulate CS-induced autophagy and cell death. In order to more fully elucidate the role of Cav-1 in this these processes, Beas-2B cells were transfected with Cav-1 siRNA and treated with CSE to determine the effects on autophagic and apoptotic markers (**Figure 18**). Cav-1 siRNA enhanced the accumulation of AVs observed in Beas-2B cells basally and following CSE treatment (**Figure 18A**). Autophagosome accumulation was also apparent in Cav1-siRNA treated cells by LC3B II immunoblot (**Figure 18B**). Cav-1 siRNA also enhanced CSE induced markers of cell death including cleaved caspase 3 and PARP cleavage in Beas-2B cells (**Figure 18C**). Consistent with induction of apoptotic markers, cell viability in response to increasing concentrations of CSE was significantly decreased in Cav-1 siRNA treated cells compared to controls (**Figure 18D**). These data suggest that Cav-1 is an important negative regulator of both autophagy and apoptosis.

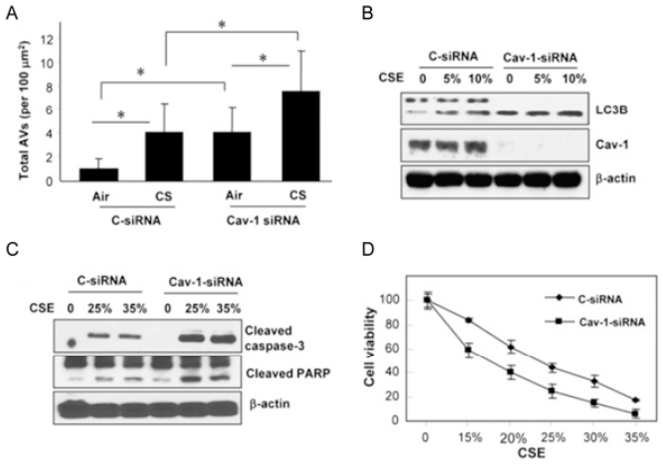

Figure 18. Cav-1 suppresses CSE-induced autophagy and apoptotic cell death *in vitro*. A-D) Cells were transfected with siRNA for 48 h and treated with the indicated concentrations of CSE for 24 h. A) AVs were quantified by TEM. The data are represented as AVs per 100 μm^2 with n=20 representative images for each group. Data are presented as mean ± SD; *p < 0.05 by student's unpaired *t* test. B) Immunoblot analysis of LC3B and Cav-1 following siRNA treatment. B-actin was the loading standard. C) Apoptotic markers were assessed in Beas-2B cells treated with Cav-1 siRNA following CSE exposure. D) The effects of Cav-1 knockdown on cell viability was determined by MTT assay following treatment with the indicated concentrations of CSE.

7.5 LC3B INTERACTING PROTEIN, CAV-1, REGULATES CS-INDUCED AUTOPHAGY AND APOPTOSIS *IN VIVO*

To further elucidate the role of Cav-1 in mediating cellular responses to CS, Cav-$1^{-/-}$ and wildtype mice were exposed to CS for 3 mo. Consistent with the *in vitro* findings, CS-exposed Cav$1^{-/-}$ mice exhibited significantly higher levels autophagic vacuole accumulation by TEM and LC3B II immunoblot (**Figure 19 A & B**). Cav-$1^{-/-}$ mice also exhibited significantly higher levels of apoptosis, as evidenced by activation of caspase 9 in the lungs following CS exposure (**Figure 19C**). Although the Cav-$1^{-/-}$ mice had basal lung airspace enlargement, they were more susceptible to CS-induced lung injury and displayed a further enlargement of airspace (**Figure 19D**). These data indicate that Cav-1 is a critical regulator of CS-induced autophagy and apoptosis *in vivo*.

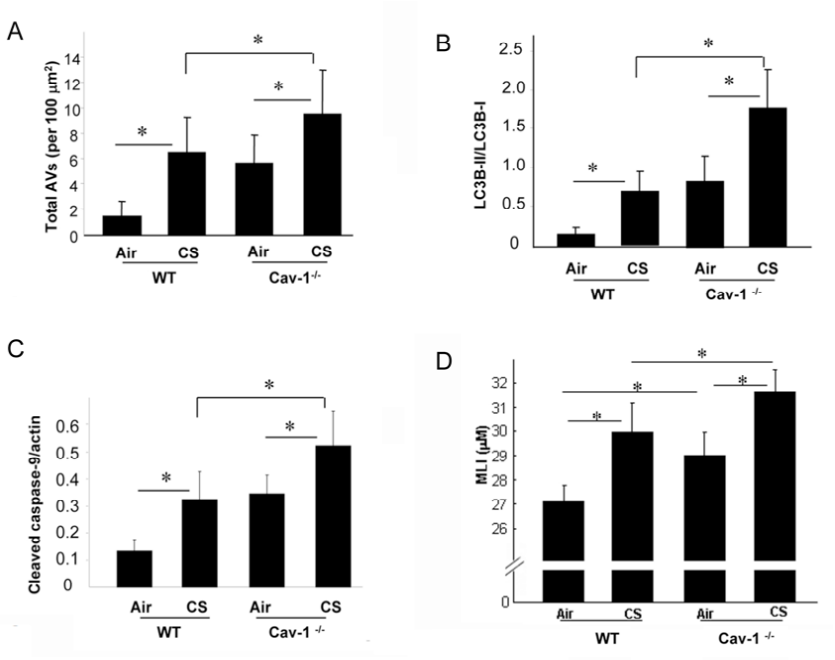

Figure 19. Cav-1 regulates CS-induced autophagy and apoptosis *in vivo*. A-D) Wildtype C57BL/6 or Cav-$1^{-/-}$ mice were exposed to CS for 3 mo (n = 5 for each group). A) AVs were quantified per area from 20 representative TEM images for each group. B) Densiometric analysis of immunoblots quantifying the LC3BII/LC3BI ratio in mouse lung tissue. C) Apoptotic marker, cleaved caspase 9, quantification by immunoblot densitometry from mouse lung tissue samples. D) MLI morphometric analysis of airspace enlargement in mouse lungs. Data represented as mean ± SD; *p < 0.05 by student's unpaired *t* test.

8.0 RESULTS- THE FUNCTIONAL ROLE OF AUTOPHAGY PROTEINS IN THE RESPONSE OF EPITHELIAL CELLS TO CS: BECLIN-1

8.1 BECLIN-1 PROMOTES CS-INDUCED DISRUPTION OF INTERCELLULAR INTERACTIONS AND CILIATED CELL LOSS

To better understand the role of autophagy in the response of airway epithelial cells to CS, MTEC cultures were generated from Beclin-$1^{+/-}$ mice. Morphological changes were assessed by fluorescence microscopy using F-actin and acetylated α-tubulin as markers. While the cells appeared morphologically similar following treatment with 50 mg/m^3, Beclin-$1^{+/+}$ cells treated with 100 mg/m^3 showed marked disruption of intercellular contacts and cilia compared to the Beclin-$1^{+/-}$ cells (**Figure 20A**). SEM confirmed the immunofluorescence observations, in which the untreated control cells appear grossly similar in the Beclin-$1^{+/+}$ and Beclin-$1^{+/-}$, suggesting that Beclin-1 does not play a critical role in epithelium and/or cilia formation and maintenance. There was clear protection of the epithelial cell layer in the Beclin-$1^{+/-}$ treated with 100 mg/m^3 (**Figure 20B**). In addition, there was a significantly higher percentage of ciliated cells that survive following 100 mg/m^3 CS exposure in the Beclin-$1^{+/-}$ MTEC cultures (**Figure 20C**). Since autophagic flux was acutely inhibited following CS treatment with 100 mg/m^3 in MTEC cultures, these data suggest that Beclin-$1^{+/-}$ cells may be protected from CS-induced injury by a mechanism independent of autophagic degradation.

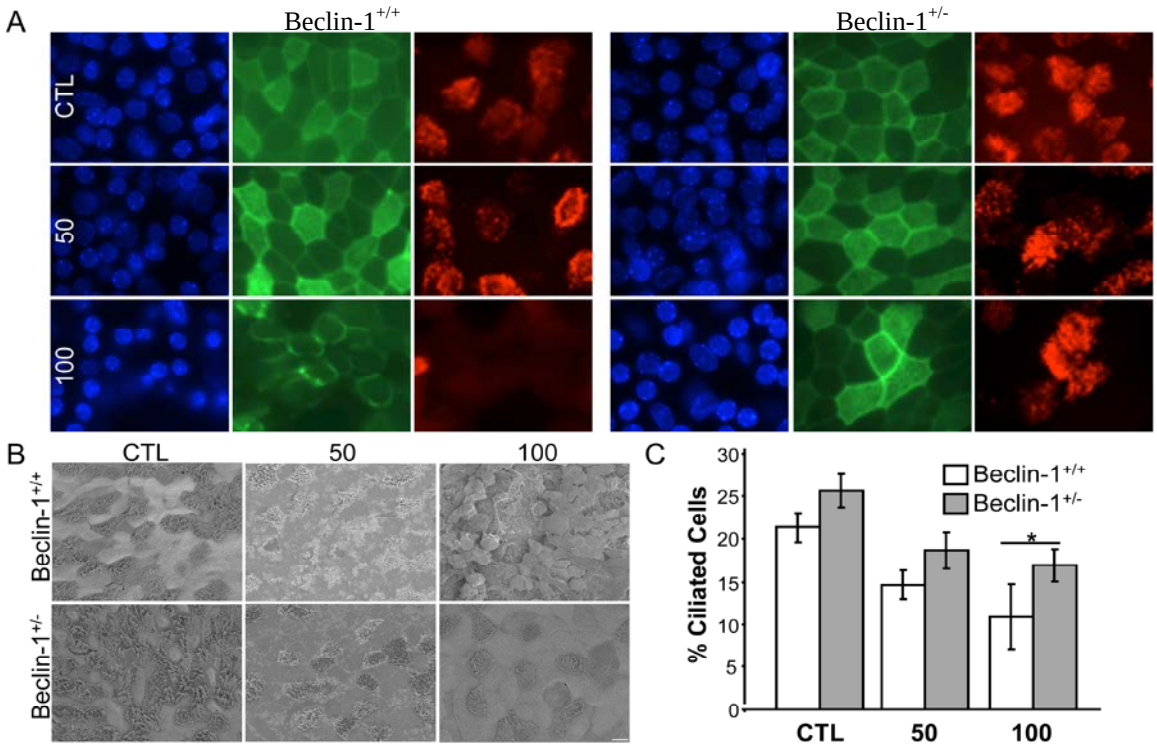

Figure 20. MTECs derived from Beclin-1$^{+/-}$ mice are protected from CS-induced injury. A) Disruption of intercelluar contacts and cilia was monitored by epifluoresence imaging of cells stained for nuclei (blue; Hoescht 33258), cytoskeletal F-actin (green, phalloidin conjugated to Alexa-488), and cilia (red, acetylated α-tubulin). Images were acquired at 100X in the same field at different focal planes. B) Scanning electron microscopy was implemented to directly visualize the apical surface of the epithelial layer following treatment with 50 and 100 mg/m^3 TPM (bar=10um). C) The percentage of ciliated cells in the Beclin-1$^{+/+}$ and Beclin-1$^{+/-}$ was determined by quantifying ciliated cells to total nuclei in 5-10 random fields from 4 independent experiments. Statistical significance was determined by two-way ANOVA *p<0.05

8.2 BECLIN-1 PROMOTES CS-INDUCED AUTOPHAGOSOME ACCUMULATION

TEM was implemented to assess the cellular morphology and autophagic response of Beclin-$1^{+/-}$ compared to Beclin-$1^{+/+}$ MTEC cultures. Representative TEM images demonstrate that overall cellular morphology and cilia formation was similar in the cultures (**Figure 21A**). From these analyses double membrane autophagosomes containing lipid material reminiscent of lamellar bodies was observed in both types of cultures basally. In the Beclin-$1^{+/+}$ cells 50 mg/m^3 CS TPM treatment caused an accumulation of large aggregates composed primarily of these lamellar bodies. As previously demonstrated, 100 mg/m^3 caused cell death associated with autophagic vacuole accumulation and loss of ciliary axonemes in the Beclin-$1^{+/+}$ MTEC cultures (**Figure 8A & Figure 21A**). In contrast, the Beclin-$1^{+/-}$ MTEC cultures were resistant to cell death and were not characterized by an accumulation of numerous cytoplasmic vacuoles or cilia loss. Quantitative analysis of the TEM images indicated that autophagosomes were equally prevalent in the Beclin-$1^{+/+}$ and Beclin-$1^{+/-}$ cultures in control conditions, suggesting that basal formation of autophagosomes is not significantly altered by heterozygous deletion of this critical autophagy protein (**Figure 21B**). However, CS-induced accumulation of autophagosomes is reduced in the Beclin-$1^{+/-}$ cultures following treatment with 50 mg/m^3 CS TPM. These data confirm that Beclin-1 is not critical for epithelial cell morphology or cilia formation. While basal autophagosome formation was similar in both Beclin-$1^{+/+}$ and Beclin-$1^{+/-}$ cultures, there is repression of autophagosome accumulation in the Beclin-$1^{+/-}$ cells following CS exposure.

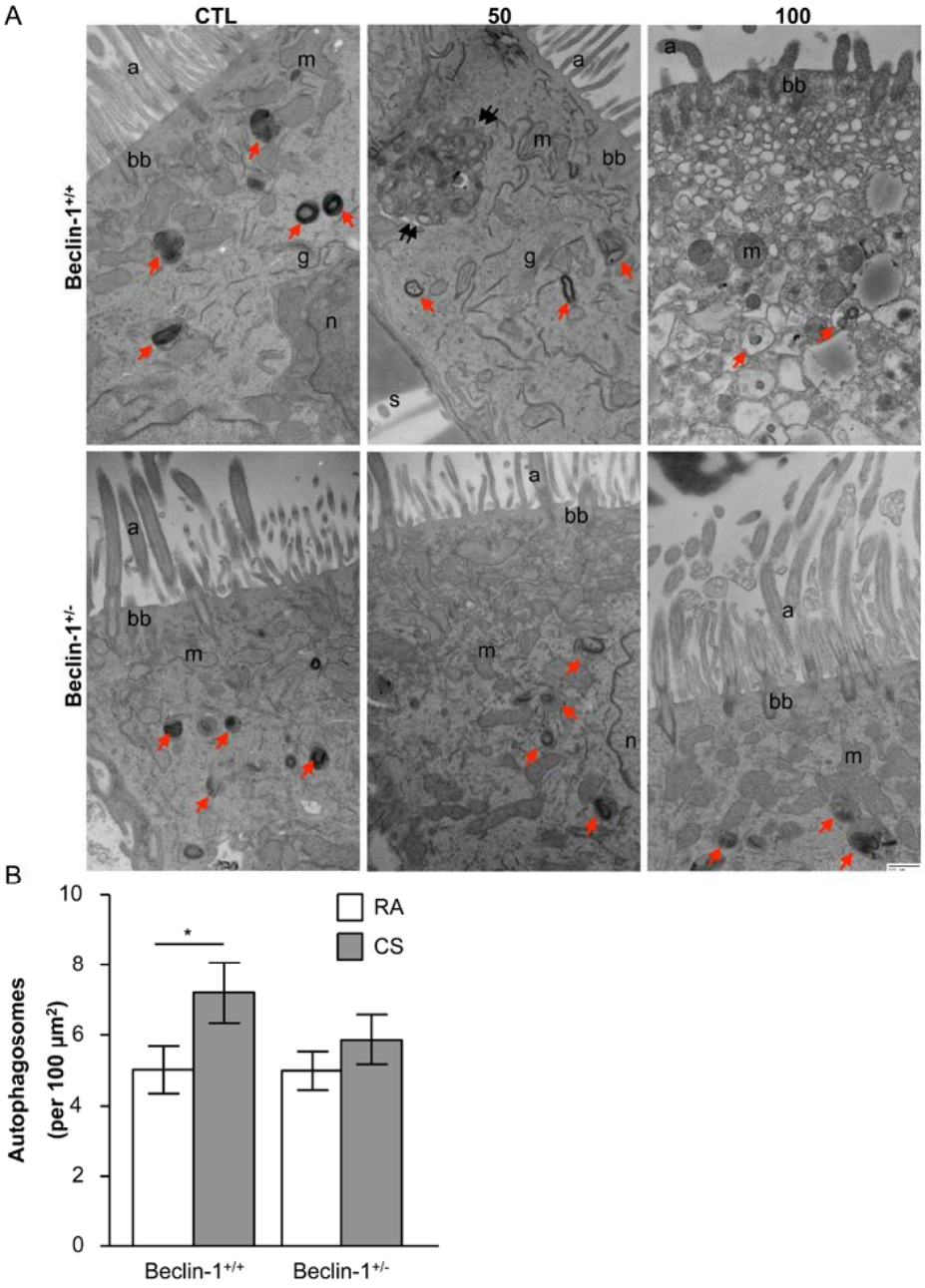

Figure 21. Beclin-1$^{+/-}$ MTEC ciliated cells are resistant to CS induced autophagosome accumulation. A) Representative TEM images of MTEC cultures 24 h after exposure to the indicated concentration of CS (red arrows-autophagosomes, black double arrows- large aggregation of lipid-based materials, a-axoneme, bb-basal bodies, m-mitochondria, n-nucleus, Bar = 500 nm). B) Autophagosomes were quantified in cells exposed to RA or 50 mg/m^3 CS TPM from 20 images acquired at 6500X. Data are presented as the mean number of autophagosomes per unit area ± SE. Statistical significance *p<0.05 was determined by two-way ANOVA and Bonferroni post test.

8.3 BECLIN-1 PROMOTES CS-INDUCED CELL DEATH

To further characterize and confirm the nature of Beclin-$1^{+/-}$ MTEC culture protection from CS-induced injury, the resistance was measured 24 h after exposure to 50 and 100 mg/m^3 CS TPM. Consistent with the imaging data the integrity of the epithelial layer was significantly protected in the Beclin-$1^{+/-}$ MTEC cultures (**Figure 22A**). CS-induced cytotoxicity was determined by measuring LDH in the basal media (**Figure 22B**). There was significantly less LDH activity, suggesting that the Beclin-$1^{+/-}$ MTEC are resistant to CS induced cell death. Immunoblot analysis of protein samples generated from the cultures treated with 50 and 100 mg/m^3 CS TPM and harvested 24 h later was used to assess autophagic, apoptotic, oxidative and cilia markers (**Figure 22C**). Active, cleaved caspase 3 was not detected in any of the Beclin-$1^{+/-}$ cultures treated with CS, while 100 mg/m^3 induced caspase 3 cleavage in the wildtype cells, thereby corroborating the findings of the LDH assay. The autophagic marker p62 demonstrated the usual SDS-insoluble high molecular weight aggregate in the wildtype culture treated with 100 mg/m^3. Surprisingly these high molecular weight bands, which usually indicate inhibited autophagic flux, were not enhanced in the Beclin-$1^{+/-}$ cultures. Beclin-1 protein expression was moderately reduced in Beclin-$1^{+/-}$ cultures; however, the appearance of a Beclin-1 reactive band at ~35 kDa in highly apoptotic Beclin-$1^{+/+}$ cultures is noteworthy. A C-terminal fragment of Beclin-1 at this molecular weight was previously implicated as serving a proapoptotic function at the mitochondrial membrane (138, 268-270, 307). Since Beclin-1 is a BH3-only domain containing protein that interacts with Bcl-2, reduced levels of Beclin-1 protein may alter and potentially enhance the antiapoptotic role of Bcl-2 in the CS exposed cells (308, 309). Consistent with this postulation, in cultures treated with 100 mg/m^3 CS TPM Bcl-2 protein expression is decreased in Beclin-$1^{+/+}$ cultures, while this protein is increased in the Beclin-$1^{+/-}$ cultures. Finally, autophagy regulates the antioxidant Nrf-2 pathway, and many studies have noted enhanced antioxidant capacity with autophagy deficiency (224, 310). In support of these prior findings, Nrf-2 appears to be slightly upregulated in the Beclin-$1^{+/-}$ MTEC cultures. Finally, consistent with quantification of ciliated cells, the basal body protein centrin-1 expression is decreased in the highly apoptotic Beclin-$1^{+/+}$ cultures, while the protein steady-state protein expression is not altered in the Beclin-$1^{+/-}$ cultures. These analyses suggest that the Beclin-$1^{+/-}$ MTEC cultures are protected from CS-induced injury at many levels and may employ a number of molecular

mechanisms both dependent and independent of autophagic activity to exert this protective effect.

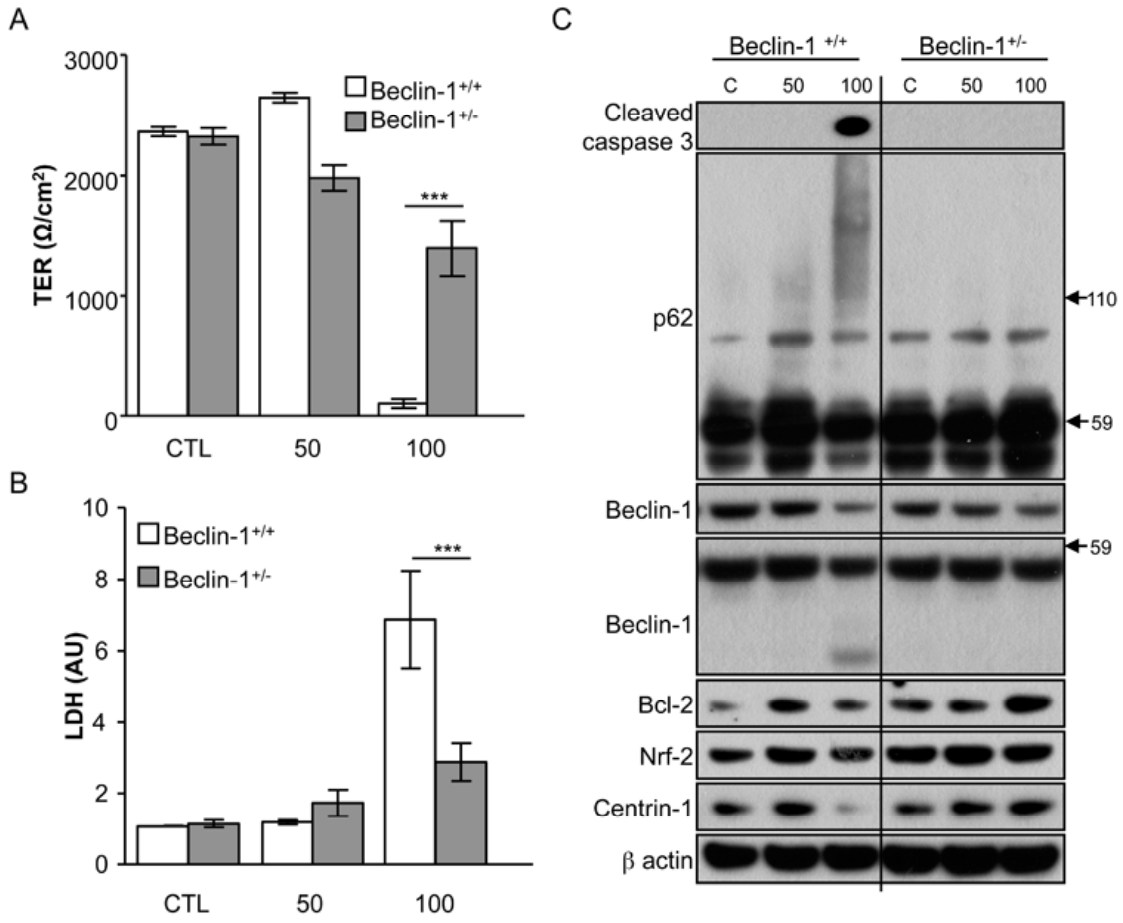

Figure 22. MTECs derived from Beclin-1$^{+/-}$ mice are protected from CS-induced cell death. A) TER, a measure of culture integrity, was measured 24 h following CS treatment with 50 and 100 mg/m^3 TPM. **p<0.001 by two-way ANOVA with Bonferroni post test B) Cytotoxicity was measured by assaying LDH in the basal media 24 h after CS exposure. Quantities are in arbitrary units (AU). Statistical significance ***p<0.001 was determined by two-way ANOVA and Bonferroni post test. C) Representative immunoblot analysis of autophagic, apoptotic, oxidative stress, and cilia markers in MTEC cultures 24 h after CS treatment. Apparent molecular weights (kDa) are indicated to the right of the blots.

8.4 BECLIN-1$^{+/-}$ MICE EXPOSED TO CS FOR 6 MONTHS ARE AUTOPHAGY DEFICIENT AND RESISTANT TO EMPHYSEMATOUS CHANGES

To further elucidate the role of Beclin-1 in the response of epithelial cells to CS, Beclin-1 $^{+/+}$ and $^{+/-}$ mice were exposed to CS for 6 mo *in vivo*. Since mouse strains susceptible to emphysematous changes show a significant difference in weights between RA and CS mice, the mice in all four groups were weighed at the end of the 6 mo exposure (**Figure 23A**). While there was a statistically significant difference in weights between RA and CS mice, there was not a significant difference between the Beclin-1 wildtype and heterozygous mice. These data indicate that the neuroendocrine and metabolic effects of nicotine on the mice are not significantly altered in the Beclin-1$^{+/-}$ strain. Since the purpose of using Beclin-1$^{+/-}$ mice is to have a defect in autophagy, autophagic flux was assessed in these mice *in vivo* (**Figure 23B**). Similar to the prior MTEC findings, Beclin-1$^{+/-}$ flux was significantly reduced in the CS treated mice, while basal flux in the RA mice was similar to the wildtype controls (**Figure 23B**). At this time point there was no longer a significant difference in autophagic activity in the wildtype RA and 6 month CS exposed mice, in contrast to the prior flux analysis of the 1 wk and 2 mo CS exposed mice (**Figure 10B**). The flux of the smoked mice was not altered significantly between these experiments, but the RA mice have more autophagic activity in the 6 mo CS experiment. Previous *in vitro* studies have proposed a model in which cells show greater reliance on autophagic degradation over the UPS with senescence (175, 179).

Consistent with the findings that Beclin-1$^{+/-}$ cultures were protected from CS-induced injury, Beclin-1$^{+/-}$ mice were resistant to CS-induced emphysematous changes (**Figure 23C**). While the wildtype littermates had a 13% increase in airspace caused by CS the airspace of the Beclin-1$^{+/-}$ CS exposed mice increased less than 1% compared to the RA controls. Finally, immunoblot analysis of apoptotic indices was used to assess cell death in lung protein homogenates. The expression pattern of Bcl-2 in tissue exactly recapitulated the *in vitro* findings, in which Bcl-2 expression decreases with smoke treatment in wildtype mice and increases in the heterozygous mice (**Figure 23C**). Finally, PARP cleavage fragments were more abundant in the Beclin-1$^{+/+}$ compared to the Beclin-1$^{+/-}$ lungs following CS exposure. These data confirm that there is defective autophagy in Beclin-1$^{+/-}$ mice and that this protein plays a critical role in mediating CS-induced injury.

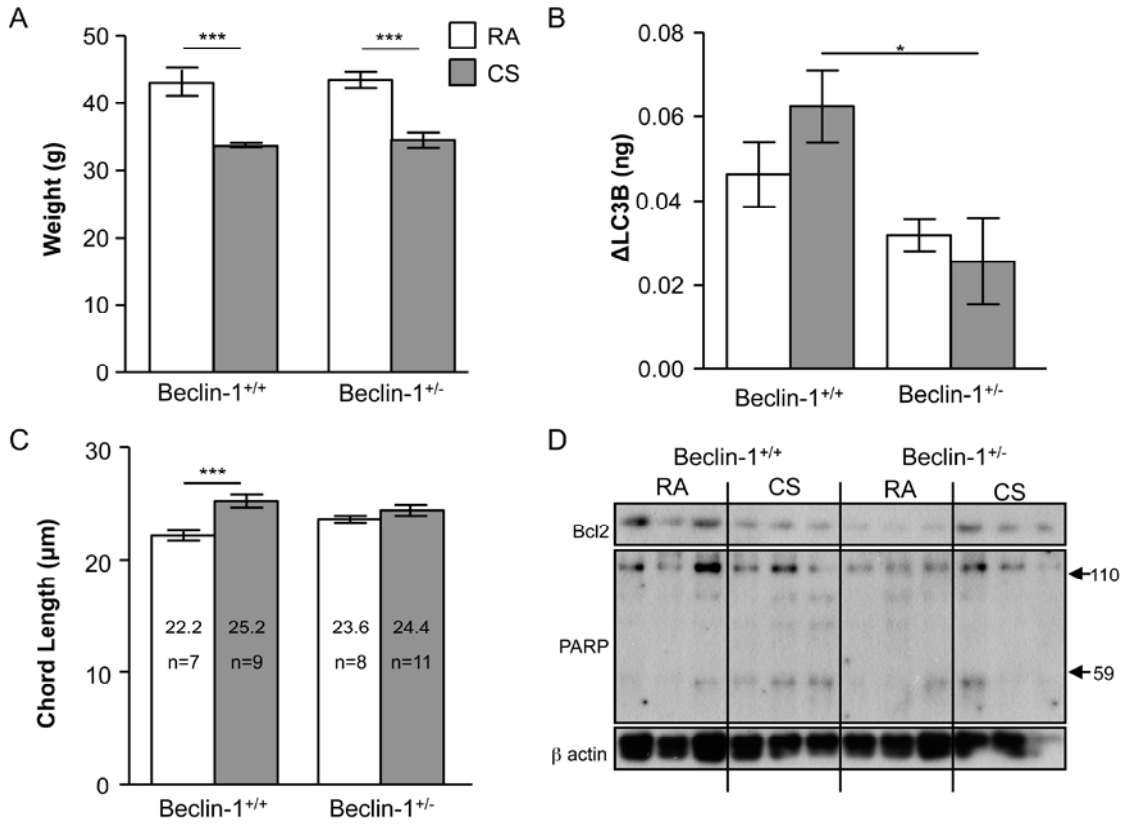

Figure 23. Assessment of injury in Beclin-1$^{+/-}$ mice exposed to CS for 6 months. A) Beclin-1$^{+/+}$ and Beclin-1$^{+/-}$ mice were weighed following 6 mo of CS exposure along with RA controls. Data are presented as the mean ± SE and statistical significance was determined by two-way ANOVA with Bonferroni post tests (***p < 0.001) B) *In vivo* autophagic flux was assessed in the Beclin-1$^{+/+}$ and Beclin-1$^{+/-}$ mice following 6 mo of CS treatment. The mice were given an *i.p.* injection of 40 mg/kg leupeptin or vehicle within 3 ho of the final smoke exposure and sacrificed in parallel 2 h later. Data are presented as densitometric analyses using a GFP-LC3 standard curve of LC3B accumulation in lysosome enriched protein fractions, determined by subtracting the average amount of LC3B present in the vehicle treated mice from the amount of LC3 accumulated in each of the leupeptin treated animals (n=3-5 mice per group). Data are presented as the mean ± SE and statistical significance was determined by using a two-way ANOVA and Bonferroni post test. C) Emphysematous changes were assessed by measuring airspace chord lengths. A chord length value for each mouse was determined by analyzing 5-10 randomly selected 20X fields. The data are presented as the mean ± SE and statistical significance was determined by two-way ANOVA with Bonferroni post test. D) Immunoblot analysis of apoptotic indices in mouse lung tissue. Representative data of n=3 mice for each treatment group. Apparent molecular weights (kDa) are indicated to the right of the blots.

9.0 DISCUSSSION

The purpose of this study was to elucidate the functional significance of autophagy in lung epithelial cells exposed to CS, to gain insights into COPD pathogenesis. A physiologically relevant model of the airways, MTEC cultures grown at an ALI, was developed to assess the contribution of autophagy in the morphological alterations observed in the epithelium following CS exposure. Since little is known about autophagic activity in the lung, autophagic flux was first assessed following acute and chronic CS exposure *in vitro* using the MTEC cultures, as well as *in vivo*. In order to explore the importance of CS in determining the targets of autophagic degradation, HDAC6, which was previously implicated in clearance of misfolded aggregates and cilia regulation, was also investigated. As cilia undergo remodeling in response to CS exposure, the colocalization of cilia and autophagic markers was investigated to determine whether cilia components might be targets of autophagic degradation. Finally regulation and function of autophagy in CS-induced cell death was assessed, with particular focus on the autophagy proteins of LC3B and Beclin-1. By probing autophagic activity, autophagic substrates, and the functions of multiple autophagy proteins in mediating the cellular response to CS, a more comprehensive understanding of the autophagic process in the lung is emerging that may provide important insights into CS-induced cell death and COPD pathogenesis.

9.1 MTEC CULTURES AS A PHYSIOLOGICAL MODEL OF CS EXPOSURE *IN VITRO*

In this study a physiologically relevant *in vitro* model was developed of CS exposure, which recapitulated the intercellular junction remodeling, cilia injury/loss, autophagosome accumulation and cell death observed *in vivo* (**Figures 4-7**). Unlike cells grown using standard

submerged cultures, the MTEC cultures are highly differentiated and can be treated with mainstream whole smoke, mimicking the *in vivo* milieu. The purity of the epithelial cell population allows for a clearer interpretation of the significance of these cells in the response to CS, without contamination from cells of parenchymal, endothelial, or mesenchymal origin. Since immune cells are excluded from the cultures, this system allows for direct determination of epithelial cell involvement in the CS-induced inflammatory cascade. The cultures are also amenable for distinguishing between apical, and basolateral mediator release, imaging analysis and acquisition of protein samples. Furthermore, the use of mouse-derived cells allows for direct comparisons between transgenic and knockout strains. While this model system is labor intensive, produces a low cell yield, and requires 4 wk to fully differentiate before experimentation, this model is more relevant than previous models using CSE and the only *in vitro* model in which the effects of CS can be determined on a specific cell type in the airways, as transformed lung-derived cell lines are not well differentiated.

9.2 REGULATION OF AUTOPHAGIC FLUX BY CS

As described previously, flux is generally assessed by comparing the turnover of a protein (i.e. p62 or LC3B) specifically targeted for autophagic degradation in control and treated cells. This assay requires four treatment groups, control and treated cells without an inhibitor of autophagolysosome degradation and control and treated cells with an inhibitor of autophagolysosome degradation. The difference between the basal and inhibitor treated cells indicates the autophagic flux for that particular treatment. The greater the difference between the basal and autophagic inhibitor treated cells, the more autophagic flux.

9.2.1 Effects of CS on autophagic flux *in vitro*

Previous studies have demonstrated that CS induces autophagosome accumulation, imlying that CS has a direct effect on the autophagic process. In this study, CS-induced autophagosome accumulation was assessed in MTEC cultures treated acutely with CS to confirm these prior findings (**Figure 8**). In order to more fully elucidate the regulation of autophagy in this model,

autophagic flux was also assessed in MTEC cultures following acute and chronic CS treatments (**Figure 9**).

LC3B turnover was not significantly induced by CS treatment in any of the MTEC cultures, reflecting the high catabolic status of the control cells (**Figure 9**). This finding is consistent with previous observations that confluent, quiescent cells generally have higher rates of basal autophagic activity than proliferating cells *in vitro*. Selective autophagy mediated by p62 was found to be increased by 50 mg/m^3 CS TPM following both acute and chronic exposure regimens (**Figure 9**). CS-induced transcriptional upregulation of p62 may contribute to the observed increase in turnover, as this protein is regulated by an Nrf-2 antioxidant response element (188). These data indicate that low doses of CS induce selective autophagy in MTEC cultures.

9.2.2 Effects of CS on autophagic flux *in vivo*

In this study autophagic activity was assessed in mice exposed to CS. A time dependent induction of autophagic activity as measured by LC3B turnover in mice exposed to CS for 1 wk and 2 mo, which was sustained 24h following CS exposure, was observed (**Figure 10**). These data indicate that CS may have a prolonged effect in the lung that persists even after the initial insult is removed. In addition, the time dependent induction of autophagic activity from 1 wk to 2 mo, suggests that there may be positive feedback loops enhancing the autophagic response with continued stimulus. In contrast to the findings of mice treated for 1 wk and 2 mo, autophagic flux was no longer significantly upregulated in wildtype mice exposed to 6 m of CS compare to RA controls (**Figure 13E & 23B**). These are the first *in vivo* flux assays to demonstrate the effects of CS on autophagy in the lung, and these data suggest an important dependence between autophagic activity and duration of CS exposure.

9.3 HDAC6 MEDIATES CLEARANCE OF MISFOLDED PROTEINS IN THE LUNG

Consistent with the finding that chronic smoke exposure may lead to an attenuation or dysregulation of autophagy, protein aggregate accumulation in the airways and parenchyma of

patient tissues appeared to correlate with COPD severity (**Figure 11A**). Furthermore, HDAC6, a protein implicated in the efficient clearance of misfolded protein aggregates and mediating autophagosome-lysosome fusion, is upregulated as a fundamental physiological response to CS in lung tissues from patients (**Figure 11B**). These human data corroborate the recent findings in which UPR activation and ubiquitin aggregate accumulation demonstrated a positive correlation with severity of emphysema (237). The deleterious effects of misfolded proteins have been described in numerous organ systems, such as the brain and liver, which are now being elucidated in the lung (237, 242, 311). The importance of protein folding stress in the lung has been demonstrated in a number of studies. For example, mutations leading to aggregation of SP-C have been implicated in interstitial lung disease and misfolded proteins also accumulate in the lung in models of sepsis and acute lung injury (311-313). However, little is known about the contribution of CS-induced protein aggregates in the pathogenesis of COPD. Since degradation of these protein aggregates is primarily mediated by autophagy, significant insights may be gained by studying the contribution of CS, misfolded protein aggregates and autophagy in COPD pathogenesis.

In this study CS was found to induce the accumulation of misfolded proteins aggregates in MTEC cultures *in vitro* and *in vivo* (**Figure 12A & 13A**). Consistent with the hypothesis that HDAC6 plays a role in CS-induced protein aggregate clearance, HDAC6$^{-/Y}$ cells and lungs appeared to have increased numbers of misfolded protein aggregates, which was further augmented by CS (**Figure 12A & 13A**). These data are consistent with prior findings, in which HDAC6 was previously implicated in the aggregation of mutant CFTR near the microtubule organizing center and protection of A549 cells from the toxic effects of expressing this misfolded protein (198). HDAC6 deacetylase activity has been previously show to be sufficient to confer protection from protein aggregation and UPS inhibition in drosophila, and to promote autophagosome-lysosome fusion through deacetylation of cortactin (194, 207). The findings of this study and those of prior studies suggest that HDAC6 may be an integral mediator of the autophagic clearance of misfolded proteins, particularly those produced by CS exposure.

The accumulation of misfolded proteins in untreated MTEC cultures suggests that HDAC6 is critical for removing these aggregates even in the basal state. The high levels of basal apoptosis observed in the HDAC6$^{-/Y}$ cultures, supports the importance of this protein in cellular homeostasis (**Figure 12C**). Cell death assessed by cleaved caspase 3 was enhanced further by

treatment with 50 mg/m^3 cells. Surprisingly, this stress did not potentiate CS-induced cell death, which was mitigated relative to the wildtype cells treated with 100 mg/m^3 CS TPM (**Figure 12C**). HDAC6 is a complex protein with many targets; therefore, these data suggest that this protein may have a dual role, promoting homeostasis in basal conditions and cell death under stress, or that loss of this protein induces compensatory mechanisms that mitigate CS-induced stress.

9.4 CS-INDUCED AUTOPHAGY AND CILIATED CELL INJURY

CS-induced challenges to protein folding and enhanced protein degradation may also contribute to cilia shortening and loss observed in smokers. Cilia are dynamic organelles with continuous protein input and turnover, which is mediated by ubiquitination of ciliary proteins in the cilium and degradation in the cytoplasm (94). The *in vitro* data from this study indicate that there are at least two mechanisms promoting cilia/ciliated cell loss by smoking: 1) desquamation with loss of intercellular contacts and 2) cilia shortening/scarcity with maintenance of intercellular integrity (**Figure 5**).

Cilia shortening was observed in MTEC cultures treated with 50 mg/m^3 CS TPM. By SEM these cells had fewer or shorter cilia per cell and maintained intercellular contacts. At this dose of CS there was also an increase in the colocalization of LC3B and acetylated α-tubulin in the cilia implicating autophagy in cilia turnover during CS exposure (**Figure 5B & 14A**).

In these studies desquamation, in which ciliated cells succumbed to cell death and shed out of the epithelium, may disrupt apical-basal polarity cues leading to significant morphological changes in the remaining viable epithelial cells (**Figure 5**). Previous studies demonstrated that proportions of shed ciliated cells directly correlated with ciliary dynein, suggesting that CS does not induce significant axoneme shedding (87). Since cell death is a major contributing factor for this mechanism of CS-induced ciliated cell loss, cell vulnerability to cell death plays a major role in the observed cilia phenotype. The basal body marker of cilia, centrin-1, was significantly decreased in cells treated with 100 mg/m^3 CS TPM; however, this cilia marker was protected in HDAC6$^{-/Y}$ and Beclin-1$^{+/-}$ cells, which were resistant to CS-induced cell death (**Figure 12C & 22C**).

At both doses, 50 and 100 mg/m^3 CS TPM, centrin-1 was recovered in the LE fraction (**Figure 14B**). The signal was particularly strong in the cells treated with 100 mg/m^3, in which ciliated cell death occurred with complete loss of ciliary axonemes, as well as, decreased autophagic flux, which would augment the signal of proteins targeted for autophagic turnover. These data suggest that autophagy and autophagy associated proteins may exert effects on the ciliated cells of the respiratory epithelium at two points, by mediating CS-induced cell death and direct degradation of cilia proteins.

9.5 AUTOPHAGIC FLUX IN CS-INDUCED CELL DEATH

To assess the role of autophagic activity in CS-induced cell death, MTEC cultures were treated with 100 mg/m^3 rapidly, which rapidly induced apoptosis (**Figure 6**). Time dependent induction of autophagic and apoptotic markers were observed following this lethal CS treatment. There was an acute accumulation of LC3B II, which proceeded the generation of cleaved caspase 3 (**Figure 8D**). Similarly, there was an accumulation of p62 SDS-insoluble high molecular weight aggregates, which is generally interpreted a marker of impaired autophagic activity (**Figure 8D**). By TEM, cells filled with autophagic vacuoles undergoing apoptosis were observed 24 h after CS exposure (**Figure 8A**). Upon assaying for flux in these cells we determined that autophagic activity is acutely inhibited by this treatment in an ATP-independent manner (**Figure 9A & 9B**). Based on the observation that LC3B and p62 levels are slightly decreased after 6 h of CQ, despite inhibition of flux, these data suggest that global transcriptional downregulation may be the primary mechanism by which flux is acutely inhibited in this model (**Figure 9A**).

In the chronic MTEC model, in which cells were treated for up to 3 d with 50 mg/m^3 CS TPM, cell death was also induced following the final 24 h exposure. In contrast to the acute model, selective autophagic flux was upregulated in these cells. (**Figure 7 & Figure 9C**). Since the flux assay was conducted in the first three hours after CS treatment and apoptosis was evident at 24 h, autophagic activity upon execution of cell death was not determined in this model.

These data demonstrate the importance of CS dose on the autophagic response. While flux is inhibited in the acute model, possibly via stress induced global inhibition of protein

synthesis, chronic CS exposure may prime cells for cell death associated with increased autophagic activity.

9.6 AUTOPHAGIC PROTEINS MEDIATE CROSSTALK TO APOPTOSIS

9.6.1 LC3B promotes CS-induced extrinsic apoptosis

The results of the *in vitro* CSE experiments suggest that LC3B plays a regulatory role in extrinsic apoptosis activation, through a dynamic interaction with Fas mediated by Cav-1. These results are consistent with our previous observations that siRNA knockdown of LC3B conferred protection, while LC3B overexpression promoted epithelial cell apoptosis induced by CSE (6). The interaction of LC3B and Fas was facilitated by Cav-1 and acutely disrupted by CSE treatment. The requirement for Cav-1 in LC3B/Fas interaction, as well as reciprocal complex formation between Cav-1 and LC3B or Fas, suggests the formation of a multiprotein complex composed of all three proteins. While Fas and LC3B bound to Cav-1 via different sites, the data support allosteric regulation, in which LC3B levels negatively correlate with Fas sequestration by Cav-1.

Mutation of the Cav-1-binding site in LC3B (Y113A) resulted in loss of LC3B/Cav-1 interaction *in vitro*. Transfection of LC3B Y113A resulted in reduced apoptosis in response to CS relative to wildtype LC3B. These results indicate that the interaction of LC3B with Cav-1 is required for the proapoptotic function of LC3B in this model. The reduced effectiveness of LC3B Y113A relative to wildtype LC3B at promoting apoptosis may be a result of the apparent increase in the Cav-1/Fas interaction, which consequently reduces the activation of the extrinsic apoptotic pathway (**Figure 17B & 17C**). The dissociation of LC3B and Fas from Cav-1 is stimulated by CSE, which permits further progression of the extrinsic apoptotic pathway. The elucidation of the molecular mechanism(s) for the dissociation of these regulatory complexes by pro-death stimuli requires further investigation.

The studies also suggest that Cav-1 can exert a functional role in CS-induced emphysema development by downregulating autophagic and apoptotic pathways. This observation appears to be a general mechanism, since Cav-1 has been implicated in the sequestration and inactivation of

a diverse group of signaling molecules at caveolae, including Src, Ras, epidermal growth factor receptor (EGFR), and platelet derived growth factor (PDGF) (314). In the current study, we show that Cav-$1^{-/-}$ mice are more susceptible to CS-induced cell death and AV accumulation in lung tissue. In agreement with our current findings, a recent study has also demonstrated increased autophagy in several organs in the Cav-$1^{-/-}$ mice (315). In summary, we demonstrate that dynamic interaction of the autophagic protein LC3B with Cav-1 and Fas regulate CS-induced lung epithelial cell apoptosis.

9.6.2 Beclin-1 promotes CS-induced apoptosis

Beclin-1 is an integral autophagic protein, which functions in the initial formation of the phagophore (**Figure 3**). While Beclin-$1^{-/-}$ mice are embryonic lethal, suggesting a critical role for this protein in development, Beclin-$1^{+/-}$ mice are viable and have an increased propensity for tumor formation (316, 317). While basal protein expression is not appreciably decreased in the Beclin-$1^{+/-}$ mice, the mice demonstrate phenotypic variations when a stressor is applied (318). Consistent with these findings we also observed modest changes in protein expression and demonstrate that basal autophagosome formation and flux appear intact in the Beclin-$1^{+/-}$ mice, while CS exposed cells and mice lack stress-induced autophagy compared to wildtype controls (**Figure 22C, 21 & 23B**).

Previous reports have described autophagy independent functions for Beclin-1. Beclin-1 was originally identified as a BH3 domain-containing protein that interacts with the antiapoptotic Bcl-2 protein family, and more recently a c-terminal fragment of Beclin-1 generated by active caspases has been shown to localize to mitochondria to potentiate MOMP and cell death (270, 279, 309). While the interaction of Bcl-2 with Beclin-1 has been shown to inhibit autophagy, the interaction thus far has been primarily one directional since overexpression of Beclin-1 has not been implicated in promoting apoptosis through the sequestration of Bcl-2 (271, 309). Previously we have demonstrated that CSE causes a time dependent reduction in Bcl-2 levels (8). In this study this effect was found to be completely reversed in Beclin-$1^{+/-}$ MTEC cultures. While in the Beclin-$1^{+/+}$ cultures Bcl-2 decreased, in the Beclin-$1^{+/-}$ cultures Bcl-2 increased after 100 mg/m^3 CS TPM treatment (**Figure 22C**). Furthermore these results were confirmed *in vivo* (**Figure 23D**). In addition to the Beclin-$1^{+/-}$ MTEC cultures expressing higher levels of antiapoptotic Bcl-

2 upon smoke exposure, Beclin-$1^{+/+}$ MTEC cultures treated with 100 mg/m^3 produced more of the proapoptotic C-terminal cleavage fragment than the Beclin-$1^{+/-}$ cultures (**Figure 22C**). Since Beclin-1 has been implicated as a scaffold protein mediating many protein-protein interactions, this autophagy protein is likely to play a complex role in cell fate decisions. These data provide strong evidence for Beclin-1 promoting cell death via autophagy independent mechanisms.

9.7 REGULATION OF AIRSPACE ENLARGEMENT BY AUTOPHAGIC PATHWAYS *IN VIVO*

The murine model of CS exposure remains the preeminent model of COPD because the initiating insult is most relevant to the human disease (38, 42, 43). While the development of emphysema requires at least 3 mo of chronic CS exposure, depending on the mouse strain, acute exposures are frequently utilized for mechanistic studies (7). Since smoking pathology is extremely complex with many redundant injurious pathways involved, identifying critical mediators that demonstrate significant modulation of the disease process *in vivo* is a challenge.

To assess the contribution of autophagic pathways implicated by the *in vitro* models in the regulation of cellular responses to CS *in vivo*, a number of murine CS exposures were carried out in this study using the following mouse strains: LC3B$^{-/-}$, Beclin-$1^{+/-}$, Cav-$1^{-/-}$, and HDAC6$^{-/Y}$. CS-induced airspace enlargement was significantly attenuated in the LC3B$^{-/-}$ and Beclin-$1^{+/-}$ mice, suggesting that these proteins are critical mediators of alveolar cell destruction (**Figure 15B & 23C**). In contrast, Cav-$1^{-/-}$ mice were more susceptible to CS-induced airspace enlargement suggesting that this protein serves a protective function in epithelial cells following CS-induced cellular stress (**Figure19D**). These *in vivo* data implicate autophagy proteins in promoting CS-induced cell death and Cav-$1^{-/-}$ as a negative regulator of CS-induced injury.

While autophagic flux was decreased in both the Beclin-$1^{+/-}$ and HDAC6$^{-/Y}$ mice, the HDAC6$^{-/Y}$ mice demonstrated a modest increase in susceptibility to airspace enlargement and induction of apoptotic indices (**Figure 13**). Although the airspace enlargement in the HDAC6$^{-/Y}$ mice was not statistically significant, the lack of a significant effect was not surprising given that there are a number of redundant proteins implicated in both selective autophagic degradation of ubiquitinated proteins and autophagosome-lysosome fusion (194, 319, 320). While cell death

was attenuated in the acute *in vitro* model, these *in vivo* data implicate HDAC6 in executing primarily protective functions following chronic exposure to CS. These data are consistent with the findings in literature that accumulation of misfolded proteins in the cytosol is detrimental to epithelial cell function and survival (280, 321, 322).

HDAC6$^{-/Y}$ and Beclin-1$^{-/+}$ mice and the respective wildtype control mice treated with CS for 6 mo weighed significantly less than the RA control mice, suggesting that these mutant mice have a metabolic response to CS that is not significantly different from wildtype mice (**Figure 13B & 23A**). Mice become rapidly hypophagic in response to CS and previous studies have demonstrated that CS exposure for 7 wk will cause a significant decrease in organ fat mass, and serum glucose, leptin, and insulin concentrations (323). These studies clearly demonstrate a connection between CS and metabolism, which is mediated through the central nervous system (324). Although the systemic metabolic effects of CS is beyond the scope of this thesis, this finding is highly relevant to this research, as starvation and calorie restriction are potent inducers of autophagy.

These *in vivo* data support the mechanistic *in vitro* findings, and provide strong evidence for the autophagy proteins, LC3B and Beclin-1, exerting pro-pathogenic functions with respect to CS-induced emphysema development, by promoting apoptotic cell death. However, a cytoprotective function for autophagy, potentially through the mitigation of misfolded protein stress, is also suggested by these studies.

9.8 CONCLUSIONS

These data implicate autophagy and autophagic proteins in mediating lung epithelial cell fate following CS exposure. We have demonstrated that CS acutely induces autophagic activity *in vitro* and *in vivo*, and induces autophagic protein expression and autophagosome accumulation in these models. The data also indicate that the autophagic response to CS can be profoundly different depending on the dose and duration of exposure.

Misfolded protein accumulation appeared to be a feature of COPD severity and CS exposure *in vivo* and *in vitro*. HDAC6 appeared to function in misfolded protein removal and play a role in cellular homeostasis. These observations support the speculation that HDAC6

mediated misfolded protein degradation by autophagy is an important homeostatic process that may contribute to cytoprotection in the context of CS-induced protein folding stress.

Imaging analysis suggested that CS induces cilia shortening/loss and ciliated cell loss by two mechanisms: 1) ciliated cell shedding associated with loss of intercellular contacts and 2) reduced cilia numbers and length with maintained intercellular junction integrity. The data suggest that by mediating CS-induced cell death and direct degradation of cilia proteins, autophagy and autophagic proteins may contribute to the disruption of mucociliary clearance, which has been implicated in infection vulnerability thereby exacerbating COPD pathogenesis

Both LC3B and Beclin-1 were implicated in CS-induced cell death. While autophagy may play an active role in cell death by reducing the cells to bare essentials, these particular autophagy proteins appear to promote cell death by additional mechanisms. LC3B disrupted an antiapoptotic interaction between Fas and Cav-1, thereby regulating CS-induced extrinsic apoptosis, while Beclin-1 expression modulated the expression of antiapoptotic Bcl-2 and produced a proapoptotic cleavage fragment known to potentiate cell death in response to CS.

From these studies a complex model of autophagy in COPD pathogenesis is emerging, in which autophagy proteins are initially upregulated to promote cytoprotection via misfolded protein removal, possibly leading to cilia shortening and loss as collateral damage, and mitigate CS-induced injury. Ultimately CS exposure may prime cells for cell death via many mechanism, which may not dependent on an active autophagic process. These data suggest that even if there were a decline in autophagic activity with late stage disease, the upregulation of these proteins would make the cells more vulnerable to cell death.

In conclusion, CS-induced autophagy is not entirely “good” or “bad” and is dependent on dose and duration of exposure; therefore, targeting specific autophagy proteins particularly those with direct crosstalk to apoptosis may yield the greatest therapeutic benefits.

10.0 FUTURE DIRECTIONS

While these studies have provided significant insights into the impact of CS on autophagic regulation and the subsequent functions of autophagy in the modulation of epithelial cell morphology and cell fate, there are many mechanistic pathways warranting further investigation.

Further insights into the function of autophagy in cytoprotection in the lung, could be elucidated utilizing the HDAC6$^{-/Y}$ mice. To this end, the effects of HDAC6 on the accumulation of misfolded proteins and autophagic flux could be probed following CS treatment *in vitro*. Additional markers of cellular toxicity caused by misfolded protein accumulation could be determined by assaying LDH and epithelial cytokines in basal media from HDAC6$^{-/Y}$ MTEC cultures. Chemical modulators, which diminish and enhance misfolded proteins are abundant, and could be used to determine the effects on cell viability in HDAC6$^{-/Y}$ MTEC cultures. In the long-term, mice with a protein conformational disease of the lung could be assessed for CS-induced emphysema with autophagy modulating drug intervention.

Many studies on CS-induced cilia changes are impeded by the use of *in vivo* models; therefore, the MTEC cultures are a unique opportunity to finally address an underlying mechanism. While desquamation was a significant contributing factor to CS-induced ciliated cell loss, further morphometric analysis of SEM images to quantitatively evaluate the effects of CS on cilia loss and shortening at the subtoxic dose of 50 mg/m^3 would provide a better understanding of the more subtle effects of CS on cilia. Once a morphometric rubric is established, the functional role of HDAC6 and Beclin-1 on CS induced cilia loss could then be evaluated. Furthermore, there is a possibility that cilia proteins comprise a proportion of the misfolded protein aggregates; therefore, autophagic proteins may not be directly involved in the regulation of cilia loss and agents that promote protein folding may be better targets of intervention. Exogenous addition of chemical chaperones has been shown to promote protein folding in contexts of cell stress (325).

While hypophagia observed in mice is consistent with human smoker behavior, calorie restriction is a confounding factor for measuring the direct impact of CS on autophagic activity in these mice. Either removing or blocking the appetite suppressing nicotinic compounds from the CS would allow for a clearer assessment of CS-induced autophagy. This finding in particular suggests that a greater understanding of metabolism in smokers and smokers that develop COPD is necessary.

These studies provide substantial evidence demonstrating that Beclin-1 and LC3B promote CS-induced cell death. Previously published literature and our own findings indicate that the molecular mechanisms by which these proteins promote apoptosis may not depend on autophagy. However, we have consistently found that cells exposed to CS die with an accumulation of autophagosomes, whether flux is increased or not, may not be as essential as the role of encapsulation and packaging of cytoplasmic material for phagocytosis. Recent work has demonstrated that phagocytosis of autophagosome filled 3T3 cells promotes inflammasome activation (326). Future work on the functional significance of epithelial cells succumbing to cell death filled with autophagic vacuoles may yield important insights into disease pathology.

There is widespread skepticism at this time with regard to autophagic cell death, but the CS model is one in which knockdown and overexpression with multiple autophagy proteins consistently demonstrates a contribution of autophagy in mediating apoptotic cell death. While inhibition of both autophagy and apoptosis promote cell survival following CS treatment, the contribution of both pathways should be more decisively determined in order to elucidate the potential synergy between these pathways and identify molecular mechanisms that regulate the switch from cytoprotection to cell death.

Furthermore, our studies using $LC3B^{-/-}$ and $Beclin\text{-}1^{+/-}$ are not completely autophagy deficient. The requirement for autophagy in CS-induced cell death, would be greatly bolstered by using a model in which autophagy is inhibited completely. Recently lung specific inducible deletion of Atg7 was described; however, there was a gross disruption of airway morphology (310). A more viable method for inhibiting autophagy may require the acquisition of the Tat-Atg5 (K130R) construct, which is a membrane-crossing dominant negative protein that suppresses the autophagic process (327). Use of this construct would be logistically feasible in the MTEC cultures, and assessing the effects of complete autophagy deficiency would make the contribution of autophagic flux in CS-induced cell death more convincing.

Autophagy deficiency has recently been linked to enhanced antioxidant protein expression, via p62-mediated sequestration of Keap1 and subsequent nuclear localization of Nrf-2 (189, 190, 224). Recently the specific deletion of Atg7 in the airways was shown to similarly induced transcription of antioxidant proteins (310). Since oxidant-antioxidant imbalance is a major contributing factor to COPD, enhanced Nrf-2 transcriptional activity may be enough to provide the survival advantage observed in the autophagy deficient mice.

The field of autophagy is exciting and perplexing. The contribution of this process in lung disease is only beginning to be elucidated and based on the modulation of autophagy by CS there is great potential for identification of therapeutic targets.

APPENDIX A

CURRICULUM VITAE

CURRICULUM VITAE
University of Pittsburgh
School of Medicine

BIOGRAPHICAL

Name:	Hilaire C. Lam	Birth Date:	June 19, 1984
Home Address:	24 Elderwood Drive Stoughton, MA	Birth Place: Citizenship:	Boston, MA USA
Cell Phone:	(617) 595-6408		
Business Address:	Brigham and Women's Hospital Thorn 821 75 Francis Street Boston, MA 02115	Email:	hcl1@pitt.edu
Business Phone:	(617) 525-6504	Fax:	(617) 264-5133

EDUCATION

GRADUATE:

2006 – Present	University of Pittsburgh Graduate School of Medicine Pittsburgh, PA GPA: 3.95/4.00	Cellular & Molecular Pathology Laboratory Dr. Augustine MK Choi Area of study: Investigating the role of autophagy in cigarette smoke induced airway remodeling, which is associated with chronic obstructive pulmonary disease (COPD).

UNDERGRADUATE:

2002 - 2006	Wellesley College Wellesley, MA GPA: 3.79/4.00	BA 2006	Major: Biological Chemistry graduated *magna cum laude* with honors

INTERNSHIPS

2004-2006	Wellesley College Wellesley, MA Laboratory of Dr. T. Kaye Peterman	STUDENT RESEARCHER Investigated the function of patellin1 (PATL1) by studying the effects of overexpression in yeast and conducting a yeast-two hybrid screen for interacting proteins.

MEMBERSHIP in PROFESSIONAL and SCIENTIFIC SOCIETIES

American Thoracic Society (ATS)	2007-Present
Sigma Xi	2006
Phi Beta Kappa	2006
American Society of Plant Biologists (ASPB)	2005

AWARDS and HONORS

Adelaide Niles Belyea Botany Prize (Wellesley College)	2006
First-year Distinction (Wellesley College)	2003

PEER-REVIEWED PUBLICATIONS

1. Nakahira K, Haspel JA, Rathinam VA, Lee SJ, Dolinay T, **Lam HC**, Englert JA, Rabinovich M, Cernadas M, Kim HP, Fitzgerald KA, Ryter SW, Choi AM. Autophagy proteins regulate innate immune responses by inhibiting the release of mitochondrial DNA mediated by the NALP3 inflammasome. Nat Immunol. 2010 Dec 12 (Epub ahead of print) PubMed PMID:21151103

2. **Lam HC***, Chen ZH*, Jin Y, Kim HP, Cao J, Lee SJ, Ifedigbo E, Parameswaran H, Ryter SW, Choi AM. Autophagy protein microtubule-associated protein 1 light chain-3B (LC3B) activates extrinsic apoptosis during cigarette smoke-induced emphysema. Proc Natl Acad Sci USA. 2010 Nov 2: 107(44):18880-5 PubMed PMID: 20956295

3. **Lam HC**, Choi AMK, Ryter SW. Isolation of mouse respiratory epithelial cells and exposure to environmental cigarette smoke at air liquid interface. http://www.jove.com/details.stp?id=2513 doi: 10 .3791/2513. J Vis Exp. 2011 Feb:48

* Authors made equal contributions

PUBLICATIONS (other)

1. Ryter SW, **Lam HC**, Chen ZH, Choi AM. Deadly triplex: smoke, autophagy, and apoptosis. Autophagy. 2011 April 1;7(4). (Epub ahead of print) PubMed PMID: 21200154

POSTERS and PRESENTATIONS

1. **Lam, H.**, Choi, A.M.K. The role of autophagy in cigarette smoke-mediated epithelial cell cilia loss and injury: Implications for Chronic Obstructive Pulmonary Disease. Cilia, Mucus, Mucociliary Interactions Gordon Conference 2011, Ventura, CA

2. **Lam**, **H**., Kim, H.P., Chen, Z., Choi, A.M.K. The role of autophagy in cigarette smoke-induced cilia loss: Implications for chronic obstructive pulmonary disease. American Thoracic Society Annual Conference 2010, New Orleans, LA

3. **Lam, H**., Chen, Z., Kim, H.P., Choi, A.M.K. Autophagy precedes and promotes cilia loss and cell death in cigarette smoke models of chronic obstructive pulmonary disease. Keystone Symposia Cell Death Pathways: Apoptosis, Autophagy and Necrosis 2010, Vancouver, Canada

4. **Lam**, **H**., Kim, H.P., Chen, Z., Choi, A.M.K. Caveolin-1 regulates ciliated epithelial cell stress responses to cigarette smoke. ATS Annual Conference 2009, San Diego, CA

5. **Lam**, **H**., Kim, H.P., Chen, Z., Choi, A.M.K. The role of autophagy in cilia degradation: Implications for chronic obstructive pulmonary disease. ATS Annual Conference 2008, Toronto, Canada

6. Peterman, K., Sequira, A., **Leavitt, H**., Oddone, A., Kremer, M. Genome-wide analysis of the patellin family of Arabidopsis. ASPB Plant Biology Annual Meeting 2006, Boston, MA

PROFESSIONAL ACTIVITIES

Institution	Grant Number	Grant Type	Title	Funding Dates
NIH	HL007118	T32 (K08, RO1)	Training in Interdisciplinary Pulmonary Sciences	03/01/2008-02/28/2009
AHA	09PRE2250120	Predoctoral	The Role of Autophagy in Cilia Degradation: Implications for Chronic Obstructive Pulmonary Disease	Period 1:07/01/09-06/30/2010 Period 2: 07/01/10-06/30/2010

BIBLIOGRAPHY

1. Lopez AD & Murray CC (1998) The global burden of disease, 1990-2020. *Nature medicine* 4(11):1241-1243.
2. Rabe KF, *et al.* (2007) Global strategy for the diagnosis, management, and prevention of chronic obstructive pulmonary disease: GOLD executive summary. *American journal of respiratory and critical care medicine* 176(6):532-555.
3. Yoshida T & Tuder RM (2007) Pathobiology of cigarette smoke-induced chronic obstructive pulmonary disease. *Physiological reviews* 87(3):1047-1082.
4. Ryter SW, Lee SJ, & Choi AM (2010) Autophagy in cigarette smoke-induced chronic obstructive pulmonary disease. *Expert review of respiratory medicine* 4(5):573-584.
5. Hwang JW, *et al.* (2010) Cigarette smoke-induced autophagy is regulated by SIRT1-PARP-1-dependent mechanism: implication in pathogenesis of COPD. *Archives of biochemistry and biophysics* 500(2):203-209.
6. Chen ZH, *et al.* (2008) Egr-1 regulates autophagy in cigarette smoke-induced chronic obstructive pulmonary disease. *PloS one* 3(10):e3316.
7. Yoshida T, *et al.* (2010) Rtp801, a suppressor of mTOR signaling, is an essential mediator of cigarette smoke-induced pulmonary injury and emphysema. *Nature medicine* 16(7):767-773.
8. Kim HP, *et al.* (2008) Autophagic proteins regulate cigarette smoke-induced apoptosis: protective role of heme oxygenase-1. *Autophagy* 4(7):887-895.
9. Silverman EK, *et al.* (2011) Opportunities and challenges in the genetics of COPD 2010: an International COPD Genetics Conference report. *COPD* 8(2):121-135.
10. Wan ES & Silverman EK (2009) Genetics of COPD and emphysema. *Chest* 136(3):859-866.
11. Joos L (2004) COPD and genetics--what's new? *Swiss medical weekly* 134(31-32):437-439.
12. Vestbo J & Hogg JC (2006) Convergence of the epidemiology and pathology of COPD. *Thorax* 61(1):86-88.
13. Wright JL & Churg A (2006) Advances in the pathology of COPD. *Histopathology* 49(1):1-9.
14. Turato G, Zuin R, & Saetta M (2001) Pathogenesis and pathology of COPD. *Respiration; international review of thoracic diseases* 68(2):117-128.
15. Duvoix A, *et al.* (2011) Evaluation of full-length, cleaved and nitrosylated serum surfactant protein D as biomarkers for COPD. *COPD* 8(2):79-95.
16. Liu Y, Gao W, & Zhang D (2010) Effects of cigarette smoke extract on A549 cells and human lung fibroblasts treated with transforming growth factor-beta1 in a coculture system. *Clinical and experimental medicine* 10(3):159-167.
17. Man SF, *et al.* (2009) The effects of inhaled and oral corticosteroids on serum inflammatory biomarkers in COPD: an exploratory study. *Therapeutic advances in respiratory disease* 3(2):73-80.
18. Pinto-Plata V, *et al.* (2007) Profiling serum biomarkers in patients with COPD: associations with clinical parameters. *Thorax* 62(7):595-601.

19. Sidney S, *et al.* (2005) COPD and incident cardiovascular disease hospitalizations and mortality: Kaiser Permanente Medical Care Program. *Chest* 128(4):2068-2075.
20. Curkendall SM, *et al.* (2006) Cardiovascular disease in patients with chronic obstructive pulmonary disease, Saskatchewan Canada cardiovascular disease in COPD patients. *Annals of epidemiology* 16(1):63-70.
21. Mannino DM, Thorn D, Swensen A, & Holguin F (2008) Prevalence and outcomes of diabetes, hypertension and cardiovascular disease in COPD. *The European respiratory journal : official journal of the European Society for Clinical Respiratory Physiology* 32(4):962-969.
22. Parappil A, Depczynski B, Collett P, & Marks GB (2010) Effect of comorbid diabetes on length of stay and risk of death in patients admitted with acute exacerbations of COPD. *Respirology* 15(6):918-922.
23. Tharappel JC, *et al.* (2010) Effects of cigarette smoke on the activation of oxidative stress-related transcription factors in female A/J mouse lung. *Journal of toxicology and environmental health. Part A* 73(19):1288-1297.
24. Blake DJ, *et al.* (2010) Deletion of Keap1 in the lung attenuates acute cigarette smoke-induced oxidative stress and inflammation. *American journal of respiratory cell and molecular biology* 42(5):524-536.
25. Singh A, *et al.* (2009) Nrf2-dependent sulfiredoxin-1 expression protects against cigarette smoke-induced oxidative stress in lungs. *Free radical biology & medicine* 46(3):376-386.
26. Profita M, *et al.* (2005) Muscarinic receptors, leukotriene B4 production and neutrophilic inflammation in COPD patients. *Allergy* 60(11):1361-1369.
27. de Boer WI, *et al.* (2000) Monocyte chemoattractant protein 1, interleukin 8, and chronic airways inflammation in COPD. *The Journal of pathology* 190(5):619-626.
28. Yamamoto C, *et al.* (1997) Airway inflammation in COPD assessed by sputum levels of interleukin-8. *Chest* 112(2):505-510.
29. Maeno T, *et al.* (2007) CD8+ T Cells are required for inflammation and destruction in cigarette smoke-induced emphysema in mice. *Journal of immunology* 178(12):8090-8096.
30. Shapiro SD, *et al.* (2003) Neutrophil elastase contributes to cigarette smoke-induced emphysema in mice. *The American journal of pathology* 163(6):2329-2335.
31. Hautamaki RD, Kobayashi DK, Senior RM, & Shapiro SD (1997) Requirement for macrophage elastase for cigarette smoke-induced emphysema in mice. *Science* 277(5334):2002-2004.
32. Ferry G, *et al.* (1997) Activation of MMP-9 by neutrophil elastase in an in vivo model of acute lung injury. *FEBS letters* 402(2-3):111-115.
33. Rubin RL, *et al.* (2005) Effect of cigarette smoke on autoimmunity in murine and human systemic lupus erythematosus. *Toxicological sciences : an official journal of the Society of Toxicology* 87(1):86-96 .
34. Talamo RC, Blennerhassett JB, & Austen KF (1966) Familial emphysema and alpha-1-antitrypsin deficiency. *The New England journal of medicine* 275(23):1301-1304.
35. Betsuyaku T, Takeyabu K, Tanino M, & Nishimura M (2002) Role of secretory leukocyte protease inhibitor in the development of subclinical emphysema. *The European respiratory journal : official journal of the European Society for Clinical Respiratory Physiology* 19(6):1051-1057.

36. Mercer PF, *et al.* (2005) MMP-9, TIMP-1 and inflammatory cells in sputum from COPD patients during exacerbation. *Respiratory research* 6:151.
37. Cataldo D, *et al.* (2001) Matrix metalloproteinases and TIMP-1 production by peripheral blood granulocytes from COPD patients and asthmatics. *Allergy* 56(2):145-151.
38. Shapiro SD (2000) Animal models for COPD. *Chest* 117(5 Suppl 1):223S-227S.
39. Shapiro SD (2000) Animal models for chronic obstructive pulmonary disease: age of klotho and marlboro mice. *American journal of respiratory cell and molecular biology* 22(1):4-7.
40. Shapiro SD, Demeo DL, & Silverman EK (2004) Smoke and mirrors: Mouse models as a reflection of human chronic obstructive pulmonary disease. *American journal of respiratory and critical care medicine* 170(9):929-931.
41. Churg A, Sin DD, & Wright JL (2011) Everything Prevents Emphysema: Are Animal Models of Cigarette Smoke-Induced COPD Any Use? *American journal of respiratory cell and molecular biology*.
42. Wright JL & Churg A (2010) Animal models of cigarette smoke-induced chronic obstructive pulmonary disease. *Expert review of respiratory medicine* 4(6):723-734.
43. Wright JL & Churg A (2008) Animal models of COPD: Barriers, successes, and challenges. *Pulmonary pharmacology & therapeutics* 21(5):696-698.
44. Hamakawa H, *et al.* (2010) Structure-function Relations in an Elastase-induced Mouse Model of Emphysema. *American journal of respiratory cell and molecular biology*.
45. Brass DM, *et al.* (2008) Chronic LPS inhalation causes emphysema-like changes in mouse lung that are associated with apoptosis. *American journal of respiratory cell and molecular biology* 39(5):584-590.
46. Tuder RM, *et al.* (2003) Oxidative stress and apoptosis interact and cause emphysema due to vascular endothelial growth factor receptor blockade. *American journal of respiratory cell and molecular biology* 29(1):88-97.
47. Kasahara Y, *et al.* (2001) Endothelial cell death and decreased expression of vascular endothelial growth factor and vascular endothelial growth factor receptor 2 in emphysema. *American journal of respiratory and critical care medicine* 163(3 Pt 1):737-744.
48. Tuder RM, Kasahara Y, & Voelkel NF (2000) Inhibition of vascular endothelial growth factor receptors causes emphysema in rats. *Chest* 117(5 Suppl 1):281S.
49. Guerassimov A, *et al.* (2004) The development of emphysema in cigarette smoke-exposed mice is strain dependent. *American journal of respiratory and critical care medicine* 170(9):974-980.
50. Krimmer DI & Oliver BG (2010) What can in vitro models of COPD tell us? *Pulmonary pharmacology & therapeutics*.
51. Ochiai Y, Sakurai E, Nomura A, Itoh K, & Tanaka Y (2006) Metabolism of nicotine in rat lung microvascular endothelial cells. *The Journal of pharmacy and pharmacology* 58(3):403-407.
52. Heusch WL & Maneckjee R (1998) Signalling pathways involved in nicotine regulation of apoptosis of human lung cancer cells. *Carcinogenesis* 19(4):551-556.
53. Weidauer E, Lehmann T, Ramisch A, Rohrdanz E, & Foth H (2004) Response of rat alveolar type II cells and human lung tumor cells towards oxidative stress induced by hydrogen peroxide and paraquat. *Toxicology letters* 151(1):69-78.

54. Dandrea T, *et al.* (2004) The transcriptosomal response of human A549 lung cells to a hydrogen peroxide-generating system: relationship to DNA damage, cell cycle arrest, and caspase activation. *Free radical biology & medicine* 36(7):881-896.
55. Lim SK, *et al.* (2010) Formaldehyde induces apoptosis through decreased Prx 2 via p38 MAPK in lung epithelial cells. *Toxicology* 271(3):100-106.
56. Persoz C, Achard S, Leleu C, Momas I, & Seta N (2010) An in vitro model to evaluate the inflammatory response after gaseous formaldehyde exposure of lung epithelial cells. *Toxicology letters* 195(2-3):99-105.
57. Speit G, Schmid O, Neuss S, & Schutz P (2008) Genotoxic effects of formaldehyde in the human lung cell line A549 and in primary human nasal epithelial cells. *Environmental and molecular mutagenesis* 49(4):300-307.
58. Moktar A, *et al.* (2011) Cigarette smoke condensate-induced oxidative DNA damage and its removal in human cervical cancer cells. *International journal of oncology* 39(4):941-947.
59. Veljkovic E, Jiricny J, Menigatti M, Rehrauer H, & Han W (2011) Chronic exposure to cigarette smoke condensate in vitro induces epithelial to mesenchymal transition-like changes in human bronchial epithelial cells, BEAS-2B. *Toxicology in vitro : an international journal published in association with BIBRA* 25(2):446-453.
60. Park JW, *et al.* (2008) Protein kinase C alpha and zeta differentially regulate death-inducing signaling complex formation in cigarette smoke extract-induced apoptosis. *Journal of immunology* 180(7):4668-4678.
61. Sugiura H, *et al.* (2007) Prostaglandin E(2) protects human lung fibroblasts from cigarette smoke extract-induced apoptosis via EP(2) receptor activation. *Journal of cellular physiology* 210(1):99-110.
62. Kim H, *et al.* (2004) Reversible cigarette smoke extract-induced DNA damage in human lung fibroblasts. *American journal of respiratory cell and molecular biology* 31(5):483-490.
63. Carnevali S, *et al.* (2003) Cigarette smoke extract induces oxidative stress and apoptosis in human lung fibroblasts. *American journal of physiology. Lung cellular and molecular physiology* 284(6):L955-963.
64. Kim SE, *et al.* (2009) Simvastatin inhibits induction of matrix metalloproteinase-9 in rat alveolar macrophages exposed to cigarette smoke extract. *Experimental & molecular medicine* 41(4):277-287.
65. Kreutmayer SB, *et al.* (2011) Dynamics of heat shock protein 60 in endothelial cells exposed to cigarette smoke extract. *Journal of molecular and cellular cardiology*.
66. Csordas A, *et al.* (2011) Cigarette smoke extract induces prolonged endoplasmic reticulum stress and autophagic cell death in human umbilical vein endothelial cells. *Cardiovascular research*.
67. Yang YM & Liu GT (2004) Damaging effect of cigarette smoke extract on primary cultured human umbilical vein endothelial cells and its mechanism. *Biomedical and environmental sciences : BES* 17(2):121-134.
68. Su Y, Cao W, Han Z, & Block ER (2004) Cigarette smoke extract inhibits angiogenesis of pulmonary artery endothelial cells: the role of calpain. *American journal of physiology. Lung cellular and molecular physiology* 287(4):L794-800.

69. Wang H, Ye Y, Zhu M, & Cho C (2000) Increased interleukin-8 expression by cigarette smoke extract in endothelial cells. *Environmental toxicology and pharmacology* 9(1-2):19-23.
70. Tuder RM, Wood K, Taraseviciene L, Flores SC, & Voekel NF (2000) Cigarette smoke extract decreases the expression of vascular endothelial growth factor by cultured cells and triggers apoptosis of pulmonary endothelial cells. *Chest* 117(5 Suppl 1):241S-242S.
71. Lam HC, Choi AM, & Ryter SW (2011) Isolation of mouse respiratory epithelial cells and exposure to experimental cigarette smoke at air liquid interface. *Journal of visualized experiments : JoVE* (48).
72. Olivera D, Knall C, Boggs S, & Seagrave J (2010) Cytoskeletal modulation and tyrosine phosphorylation of tight junction proteins are associated with mainstream cigarette smoke-induced permeability of airway epithelium. *Experimental and toxicologic pathology : official journal of the Gesellschaft fur Toxikologische Pathologie* 62(2):133-143.
73. Maunders H, Patwardhan S, Phillips J, Clack A, & Richter A (2007) Human bronchial epithelial cell transcriptome: gene expression changes following acute exposure to whole cigarette smoke in vitro. *American journal of physiology. Lung cellular and molecular physiology* 292(5):L1248-1256.
74. Coggins CR, Fouillet XL, Lam R, & Morgan KT (1980) Cigarette smoke induced pathology of the rat respiratory tract: a comparison of the effects of the particulate and vapour phases. *Toxicology* 16(2):83-101.
75. Jeffery PK & Reid LM (1981) The effect of tobacco smoke, with or without phenylmethyloxadiazole (PMO), on rat bronchial epithelium: a light and electron microscopic study. *The Journal of pathology* 133(4):341-359.
76. Frasca JM, Auerbach O, Parks VR, & Jamieson JD (1968) Electron microscopic observations of the bronchial epithelium of dogs. II. Smoking dogs. *Experimental and molecular pathology* 9(3):380-399.
77. Chen YT, *et al.* (2010) Cigarette smoke induces epidermal growth factor receptor-dependent redistribution of apical MUC1 and junctional beta-catenin in polarized human airway epithelial cells. *The American journal of pathology* 177(3):1255-1264.
78. Zhao H, Yang J, Shan L, & Jorgensen ED (2011) Measuring the impact of cigarette smoke on the UPR. *Methods in enzymology* 489:147-164.
79. Jorgensen E, *et al.* (2008) Cigarette smoke induces endoplasmic reticulum stress and the unfolded protein response in normal and malignant human lung cells. *BMC cancer* 8:229.
80. McMillan DH, *et al.* (2011) Lung-Targeted Overexpression of the NF-kappaB Member RelB Inhibits Cigarette Smoke-Induced Inflammation. *The American journal of pathology* 179(1):125-133.
81. Li YT, He B, Wang YZ, & Wang J (2009) Effects of intratracheal administration of nuclear factor-kappaB decoy oligodeoxynucleotides on long-term cigarette smoke-induced lung inflammation and pathology in mice. *Respiratory research* 10:79.
82. Bhalla DK, Hirata F, Rishi AK, & Gairola CG (2009) Cigarette smoke, inflammation, and lung injury: a mechanistic perspective. *Journal of toxicology and environmental health. Part B, Critical reviews* 12(1):45-64.

83. Rajendrasozhan S, *et al.* (2008) Deacetylases and NF-kappaB in redox regulation of cigarette smoke-induced lung inflammation: epigenetics in pathogenesis of COPD. *Antioxidants & redox signaling* 10(4):799-811.
84. Parsanejad R, Fields WR, Morgan WT, Bombick BR, & Doolittle DJ (2008) The time course of expression of genes involved in specific pathways in normal human bronchial epithelial cells following exposure to cigarette smoke. *Experimental lung research* 34(8):513-530.
85. Liu X, *et al.* (2008) NF-kappaB mediates the survival of human bronchial epithelial cells exposed to cigarette smoke extract. *Respiratory research* 9:66.
86. Ballenger JJ (1960) Experimental effect of cigarette smoke on human respiratory cilia. *The New England journal of medicine* 263:832-835.
87. Sisson JH, *et al.* (1994) Smoke and viral infection cause cilia loss detectable by bronchoalveolar lavage cytology and dynein ELISA. *American journal of respiratory and critical care medicine* 149(1):205-213.
88. Leopold PL, *et al.* (2009) Smoking is associated with shortened airway cilia. *PloS one* 4(12):e8157.
89. Simet SM, *et al.* (2010) Long-term cigarette smoke exposure in a mouse model of ciliated epithelial cell function. *American journal of respiratory cell and molecular biology* 43(6):635-640.
90. Follit JA, Tuft RA, Fogarty KE, & Pazour GJ (2006) The intraflagellar transport protein IFT20 is associated with the Golgi complex and is required for cilia assembly. *Molecular biology of the cell* 17(9):3781-3792.
91. Dute R & Kung C (1978) Ultrastructure of the proximal region of somatic cilia in Paramecium tetraurelia. *The Journal of cell biology* 78(2):451-464.
92. Satir P & Christensen ST (2008) Structure and function of mammalian cilia. *Histochemistry and cell biology* 129(6):687-693.
93. Satir P & Christensen ST (2007) Overview of structure and function of mammalian cilia. *Annual review of physiology* 69:377-400.
94. Huang K, Diener DR, & Rosenbaum JL (2009) The ubiquitin conjugation system is involved in the disassembly of cilia and flagella. *The Journal of cell biology* 186(4):601-613.
95. Schmid A, *et al.* (2007) Soluble adenylyl cyclase is localized to cilia and contributes to ciliary beat frequency regulation via production of cAMP. *The Journal of general physiology* 130(1):99-109.
96. Cohen NA, *et al.* (2009) Cigarette smoke condensate inhibits transepithelial chloride transport and ciliary beat frequency. *The Laryngoscope* 119(11):2269-2274.
97. Tamashiro E, *et al.* (2009) Cigarette smoke exposure impairs respiratory epithelial ciliogenesis. *American journal of rhinology & allergy* 23(2):117-122.
98. Antoniu SA (2011) New therapeutic options in the management of COPD - focus on roflumilast. *International journal of chronic obstructive pulmonary disease* 6:147-155.
99. Singh S, Loke YK, & Furberg CD (2010) Outpatient management of severe COPD. *The New England journal of medicine* 363(5):493-494; author reply 494-495.
100. Celli BR, Cote CG, Lareau SC, & Meek PM (2008) Predictors of Survival in COPD: more than just the FEV1. *Respiratory medicine* 102 Suppl 1:S27-35.
101. Poole PJ (2006) Role of mucolytics in the management of COPD. *International journal of chronic obstructive pulmonary disease* 1(2):123-128.

102. Dekhuijzen PN & van Beurden WJ (2006) The role for N-acetylcysteine in the management of COPD. *International journal of chronic obstructive pulmonary disease* 1(2):99-106.
103. Scullion JE (2007) The development of anticholinergics in the management of COPD. *International journal of chronic obstructive pulmonary disease* 2(1):33-40.
104. Walker PP, Mitchell P, Diamantea F, Warburton CJ, & Davies L (2006) Effect of primary-care spirometry on the diagnosis and management of COPD. *The European respiratory journal : official journal of the European Society for Clinical Respiratory Physiology* 28(5):945-952.
105. Seemungal TA & Wedzicha JA (2006) Integrated care: a new model for COPD management? *The European respiratory journal : official journal of the European Society for Clinical Respiratory Physiology* 28(1):4-6.
106. Huang WP & Klionsky DJ (2002) Autophagy in yeast: a review of the molecular machinery. *Cell structure and function* 27(6):409-420.
107. Mizushima N & Levine B (2010) Autophagy in mammalian development and differentiation. *Nature cell biology* 12(9):823-830.
108. Levine B & Ranganathan R (2010) Autophagy: Snapshot of the network. *Nature* 466(7302):38-40.
109. Ahlberg J & Glaumann H (1985) Uptake--microautophagy--and degradation of exogenous proteins by isolated rat liver lysosomes. Effects of pH, ATP, and inhibitors of proteolysis. *Experimental and molecular pathology* 42(1):78-88.
110. Kunz JB, Schwarz H, & Mayer A (2004) Determination of four sequential stages during microautophagy in vitro. *The Journal of biological chemistry* 279(11):9987-9996.
111. Kaushik S, *et al.* (2011) Chaperone-mediated autophagy at a glance. *Journal of cell science* 124(Pt 4):495-499.
112. Arias E & Cuervo AM (2011) Chaperone-mediated autophagy in protein quality control. *Current opinion in cell biology* 23(2):184-189.
113. Bandyopadhyay U, Sridhar S, Kaushik S, Kiffin R, & Cuervo AM (2010) Identification of regulators of chaperone-mediated autophagy. *Molecular cell* 39(4):535-547.
114. Eskelinen EL (2008) New insights into the mechanisms of macroautophagy in mammalian cells. *International review of cell and molecular biology* 266:207-247.
115. Petiot A, Pattingre S, Arico S, Meley D, & Codogno P (2002) Diversity of signaling controls of macroautophagy in mammalian cells. *Cell structure and function* 27(6):431-441.
116. Heath RJ & Xavier RJ (2009) Autophagy, immunity and human disease. *Current opinion in gastroenterology* 25(6):512-520.
117. Huang J & Klionsky DJ (2007) Autophagy and human disease. *Cell cycle* 6(15):1837-1849.
118. Levine B, Mizushima N, & Virgin HW (2011) Autophagy in immunity and inflammation. *Nature* 469(7330):323-335.
119. Shang L & Wang X (2011) AMPK and mTOR coordinate the regulation of Ulk1 and mammalian autophagy initiation. *Autophagy* 7(8):924-926.
120. Narita M, *et al.* (2011) Spatial coupling of mTOR and autophagy augments secretory phenotypes. *Science* 332(6032):966-970.
121. Egan D, Kim J, Shaw RJ, & Guan KL (2011) The autophagy initiating kinase ULK1 is regulated via opposing phosphorylation by AMPK and mTOR. *Autophagy* 7(6):643-644.

122. Kim J, Kundu M, Viollet B, & Guan KL (2011) AMPK and mTOR regulate autophagy through direct phosphorylation of Ulk1. *Nature cell biology* 13(2):132-141.
123. Mitroulis I, Kourtzelis I, Kambas K, Chrysanthopoulou A, & Ritis K (2011) Evidence for the involvement of mTOR inhibition and basal autophagy in familial Mediterranean fever phenotype. *Human immunology* 72(2):135-138.
124. Yu L, *et al.* (2010) Termination of autophagy and reformation of lysosomes regulated by mTOR. *Nature* 465(7300):942-946.
125. Jung CH, Ro SH, Cao J, Otto NM, & Kim DH (2010) mTOR regulation of autophagy. *FEBS letters* 584(7):1287-1295.
126. Ganley IG, *et al.* (2009) ULK1.ATG13.FIP200 complex mediates mTOR signaling and is essential for autophagy. *The Journal of biological chemistry* 284(18):12297-12305.
127. Jung CH, *et al.* (2009) ULK-Atg13-FIP200 complexes mediate mTOR signaling to the autophagy machinery. *Molecular biology of the cell* 20(7):1992-2003.
128. Nicklin P, *et al.* (2009) Bidirectional transport of amino acids regulates mTOR and autophagy. *Cell* 136(3):521-534.
129. Ravikumar B, *et al.* (2004) Inhibition of mTOR induces autophagy and reduces toxicity of polyglutamine expansions in fly and mouse models of Huntington disease. *Nature genetics* 36(6):585-595.
130. Scherz-Shouval R & Elazar Z (2011) Regulation of autophagy by ROS: physiology and pathology. *Trends in biochemical sciences* 36(1):30-38.
131. Dewaele M, Maes H, & Agostinis P (2010) ROS-mediated mechanisms of autophagy stimulation and their relevance in cancer therapy. *Autophagy* 6(7):838-854.
132. Bensaad K, Cheung EC, & Vousden KH (2009) Modulation of intracellular ROS levels by TIGAR controls autophagy. *The EMBO journal* 28(19):3015-3026.
133. Scherz-Shouval R & Elazar Z (2007) ROS, mitochondria and the regulation of autophagy. *Trends in cell biology* 17(9):422-427.
134. Sarkar S & Rubinsztein DC (2006) Inositol and IP3 levels regulate autophagy: biology and therapeutic speculations. *Autophagy* 2(2):132-134.
135. Crawford AC, Riggins RB, Shajahan AN, Zwart A, & Clarke R (2010) Co-inhibition of BCL-W and BCL2 restores antiestrogen sensitivity through BECN1 and promotes an autophagy-associated necrosis. *PloS one* 5(1):e8604.
136. Lorin S, Pierron G, Ryan KM, Codogno P, & Djavaheri-Mergny M (2010) Evidence for the interplay between JNK and p53-DRAM signalling pathways in the regulation of autophagy. *Autophagy* 6(1):153-154.
137. Criollo A, Dessen P, & Kroemer G (2009) DRAM: a phylogenetically ancient regulator of autophagy. *Cell cycle* 8(15):2319-2320.
138. Russo R, *et al.* (2011) Calpain-mediated cleavage of Beclin-1 and autophagy deregulation following retinal ischemic injury in vivo. *Cell death & disease* 2:e144 .
139. Yousefi S, *et al.* (2006) Calpain-mediated cleavage of Atg5 switches autophagy to apoptosis. *Nature cell biology* 8(10):1124-1132.
140. Harr MW & Distelhorst CW (2010) Apoptosis and autophagy: decoding calcium signals that mediate life or death. *Cold Spring Harbor perspectives in biology* 2(10):a005579.
141. Sarkar S, Korolchuk V, Renna M, Winslow A, & Rubinsztein DC (2009) Methodological considerations for assessing autophagy modulators: a study with calcium phosphate precipitates. *Autophagy* 5(3):307-313.

142. Cottam EM, *et al.* (2011) Coronavirus nsp6 proteins generate autophagosomes from the endoplasmic reticulum via an omegasome intermediate. *Autophagy* 7(11).
143. Polson HE, *et al.* (2010) Mammalian Atg18 (WIPI2) localizes to omegasome-anchored phagophores and positively regulates LC3 lipidation. *Autophagy* 6(4).
144. Juhasz G & Neufeld TP (2006) Autophagy: a forty-year search for a missing membrane source. *PLoS biology* 4(2):e36.
145. Chan EY (2009) mTORC1 phosphorylates the ULK1-mAtg13-FIP200 autophagy regulatory complex. *Science signaling* 2(84):pe51.
146. Hosokawa N, *et al.* (2009) Nutrient-dependent mTORC1 association with the ULK1-Atg13-FIP200 complex required for autophagy. *Molecular biology of the cell* 20(7):1981-1991.
147. Thoresen SB, Pedersen NM, Liestol K, & Stenmark H (2010) A phosphatidylinositol 3-kinase class III sub-complex containing VPS15, VPS34, Beclin 1, UVRAG and BIF-1 regulates cytokinesis and degradative endocytic traffic. *Experimental cell research* 316(20):3368-3378.
148. Funderburk SF, Wang QJ, & Yue Z (2010) The Beclin 1-VPS34 complex--at the crossroads of autophagy and beyond. *Trends in cell biology* 20(6):355-362.
149. Furuya N, Yu J, Byfield M, Pattingre S, & Levine B (2005) The evolutionarily conserved domain of Beclin 1 is required for Vps34 binding, autophagy and tumor suppressor function. *Autophagy* 1(1):46-52.
150. Zhong Y, Wang QJ, & Yue Z (2009) Atg14L and Rubicon: yin and yang of Beclin 1-mediated autophagy control. *Autophagy* 5(6):890-891.
151. Matsunaga K, *et al.* (2009) Two Beclin 1-binding proteins, Atg14L and Rubicon, reciprocally regulate autophagy at different stages. *Nature cell biology* 11(4):385-396.
152. Zhong Y, *et al.* (2009) Distinct regulation of autophagic activity by Atg14L and Rubicon associated with Beclin 1-phosphatidylinositol-3-kinase complex. *Nature cell biology* 11(4):468-476.
153. Zalckvar E, *et al.* (2009) DAP-kinase-mediated phosphorylation on the BH3 domain of beclin 1 promotes dissociation of beclin 1 from Bcl-XL and induction of autophagy. *EMBO reports* 10(3):285-292.
154. Feng W, Huang S, Wu H, & Zhang M (2007) Molecular basis of Bcl-xL's target recognition versatility revealed by the structure of Bcl-xL in complex with the BH3 domain of Beclin-1. *Journal of molecular biology* 372(1):223-235.
155. Maiuri MC, *et al.* (2007) Functional and physical interaction between Bcl-X(L) and a BH3-like domain in Beclin-1. *The EMBO journal* 26(10):2527-2539.
156. Cadwell K, Patel KK, Komatsu M, Virgin HWt, & Stappenbeck TS (2009) A common role for Atg16L1, Atg5 and Atg7 in small intestinal Paneth cells and Crohn disease. *Autophagy* 5(2):250-252.
157. Kang MR, *et al.* (2009) Frameshift mutations of autophagy-related genes ATG2B, ATG5, ATG9B and ATG12 in gastric and colorectal cancers with microsatellite instability. *The Journal of pathology* 217(5):702-706.
158. Hanada T, *et al.* (2007) The Atg12-Atg5 conjugate has a novel E3-like activity for protein lipidation in autophagy. *The Journal of biological chemistry* 282(52):37298-37302.

159. Jounai N, *et al.* (2007) The Atg5 Atg12 conjugate associates with innate antiviral immune responses. *Proceedings of the National Academy of Sciences of the United States of America* 104(35):14050-14055.
160. Noda NN, Fujioka Y, Ohsumi Y, & Inagaki F (2008) Crystallization of the Atg12-Atg5 conjugate bound to Atg16 by the free-interface diffusion method. *Journal of synchrotron radiation* 15(Pt 3):266-268.
161. Li M, *et al.* (2011) Kinetics comparisons of mammalian Atg4 homologues indicate selective preferences toward diverse Atg8 substrates. *The Journal of biological chemistry* 286(9):7327-7338.
162. Kouno T, *et al.* (2005) Solution structure of microtubule-associated protein light chain 3 and identification of its functional subdomains. *The Journal of biological chemistry* 280(26):24610-24617.
163. Sugawara K, *et al.* (2004) The crystal structure of microtubule-associated protein light chain 3, a mammalian homologue of Saccharomyces cerevisiae Atg8. *Genes to cells : devoted to molecular & cellular mechanisms* 9(7):611-618.
164. Tanida I, *et al.* (2004) HsAtg4B/HsApg4B/autophagin-1 cleaves the carboxyl termini of three human Atg8 homologues and delipidates microtubule-associated protein light chain 3- and GABAA receptor-associated protein-phospholipid conjugates. *The Journal of biological chemistry* 279(35):36268-36276.
165. Zhou B, Boudreau N, Coulber C, Hammarback J, & Rabinovitch M (1997) Microtubule-associated protein 1 light chain 3 is a fibronectin mRNA-binding protein linked to mRNA translation in lamb vascular smooth muscle cells. *The Journal of clinical investigation* 100(12):3070-3082.
166. Kabeya Y, *et al.* (2004) LC3, GABARAP and GATE16 localize to autophagosomal membrane depending on form-II formation. *Journal of cell science* 117(Pt 13):2805-2812.
167. McLeland CB, Rodriguez J, & Stern ST (2011) Autophagy monitoring assay: qualitative analysis of MAP LC3-I to II conversion by immunoblot. *Methods in molecular biology* 697:199-206.
168. Mostowy S & Cossart P (2011) Autophagy and the cytoskeleton: new links revealed by intracellular pathogens. *Autophagy* 7(7):780-782.
169. Monastyrska I, Rieter E, Klionsky DJ, & Reggiori F (2009) Multiple roles of the cytoskeleton in autophagy. *Biological reviews of the Cambridge Philosophical Society* 84(3):431-448.
170. Reggiori F, Monastyrska I, Shintani T, & Klionsky DJ (2005) The actin cytoskeleton is required for selective types of autophagy, but not nonspecific autophagy, in the yeast Saccharomyces cerevisiae. *Molecular biology of the cell* 16(12):5843-5856.
171. Lin MG & Zhong Q (2011) Interaction between small GTPase Rab7 and PI3KC3 links autophagy and endocytosis: A new Rab7 effector protein sheds light on membrane trafficking pathways. *Small GTPases* 2(2):85-88.
172. Yang Z, Huang J, Geng J, Nair U, & Klionsky DJ (2006) Atg22 recycles amino acids to link the degradative and recycling functions of autophagy. *Molecular biology of the cell* 17(12):5094-5104.
173. Singh R & Cuervo AM (2011) Autophagy in the cellular energetic balance. *Cell metabolism* 13(5):495-504.

174. Kovsan J, Bashan N, Greenberg AS, & Rudich A (2010) Potential role of autophagy in modulation of lipid metabolism. *American journal of physiology. Endocrinology and metabolism* 298(1):E1-7.
175. Gamerdinger M, Carra S, & Behl C (2011) Emerging roles of molecular chaperones and co-chaperones in selective autophagy: focus on BAG proteins. *Journal of molecular medicine*.
176. Behl C (2011) BAG3 and friends: co-chaperones in selective autophagy during aging and disease. *Autophagy* 7(7):795-798.
177. Rosati A, Graziano V, De Laurenzi V, Pascale M, & Turco MC (2011) BAG3: a multifaceted protein that regulates major cell pathways. *Cell death & disease* 2:e141 .
178. Gamerdinger M, Kaya AM, Wolfrum U, Clement AM, & Behl C (2011) BAG3 mediates chaperone-based aggresome-targeting and selective autophagy of misfolded proteins. *EMBO reports* 12(2):149-156.
179. Gamerdinger M, *et al.* (2009) Protein quality control during aging involves recruitment of the macroautophagy pathway by BAG3. *The EMBO journal* 28(7):889-901.
180. Carra S, Seguin SJ, Lambert H, & Landry J (2008) HspB8 chaperone activity toward poly(Q)-containing proteins depends on its association with Bag3, a stimulator of macroautophagy. *The Journal of biological chemistry* 283(3):1437-1444.
181. Lamark T, Kirkin V, Dikic I, & Johansen T (2009) NBR1 and p62 as cargo receptors for selective autophagy of ubiquitinated targets. *Cell cycle* 8(13):1986-1990.
182. Kirkin V, Lamark T, Johansen T, & Dikic I (2009) NBR1 cooperates with p62 in selective autophagy of ubiquitinated targets. *Autophagy* 5(5):732-733.
183. Kirkin V, *et al.* (2009) A role for NBR1 in autophagosomal degradation of ubiquitinated substrates. *Molecular cell* 33(4):505-516.
184. Zheng YT, *et al.* (2009) The adaptor protein p62/SQSTM1 targets invading bacteria to the autophagy pathway. *Journal of immunology* 183(9):5909-5916.
185. Larsen KB, *et al.* (2010) A reporter cell system to monitor autophagy based on p62/SQSTM1. *Autophagy* 6(6):784-793.
186. Stepkowski TM & Kruszewski MK (2011) Molecular cross-talk between the NRF2/KEAP1 signaling pathway, autophagy, and apoptosis. *Free radical biology & medicine* 50(9):1186-1195.
187. Fan W, *et al.* (2010) Keap1 facilitates p62-mediated ubiquitin aggregate clearance via autophagy. *Autophagy* 6(5).
188. Jain A, *et al.* (2010) p62/SQSTM1 is a target gene for transcription factor NRF2 and creates a positive feedback loop by inducing antioxidant response element-driven gene transcription. *The Journal of biological chemistry* 285(29):22576-22591.
189. Lau A, *et al.* (2010) A noncanonical mechanism of Nrf2 activation by autophagy deficiency: direct interaction between Keap1 and p62. *Molecular and cellular biology* 30(13):3275-3285.
190. Komatsu M, *et al.* (2010) The selective autophagy substrate p62 activates the stress responsive transcription factor Nrf2 through inactivation of Keap1. *Nature cell biology* 12(3):213-223.
191. Riley BE, Kaiser SE, & Kopito RR (2011) Autophagy inhibition engages Nrf2-p62 Ub-associated signaling. *Autophagy* 7(3):338-340.

192. Riley BE, *et al.* (2010) Ubiquitin accumulation in autophagy-deficient mice is dependent on the Nrf2-mediated stress response pathway: a potential role for protein aggregation in autophagic substrate selection. *The Journal of cell biology* 191(3):537-552.
193. Inami Y, *et al.* (2011) Persistent activation of Nrf2 through p62 in hepatocellular carcinoma cells. *The Journal of cell biology* 193(2):275-284.
194. Lee JY, *et al.* (2010) HDAC6 controls autophagosome maturation essential for ubiquitin-selective quality-control autophagy. *The EMBO journal* 29(5):969-980.
195. Boyault C, Sadoul K, Pabion M, & Khochbin S (2007) HDAC6, at the crossroads between cytoskeleton and cell signaling by acetylation and ubiquitination. *Oncogene* 26(37):5468-5476.
196. Zhang X, *et al.* (2007) HDAC6 modulates cell motility by altering the acetylation level of cortactin. *Molecular cell* 27(2):197-213.
197. Tran AD, *et al.* (2007) HDAC6 deacetylation of tubulin modulates dynamics of cellular adhesions. *Journal of cell science* 120(Pt 8):1469-1479.
198. Kawaguchi Y, *et al.* (2003) The deacetylase HDAC6 regulates aggresome formation and cell viability in response to misfolded protein stress. *Cell* 115(6):727-738.
199. Hubbert C, *et al.* (2002) HDAC6 is a microtubule-associated deacetylase. *Nature* 417(6887):455-458.
200. Kovacs JJ, Cohen TJ, & Yao TP (2005) Chaperoning steroid hormone signaling via reversible acetylation. *Nuclear receptor signaling* 3:e004.
201. Zhao Z, Xu H, & Gong W (2010) Histone deacetylase 6 (HDAC6) is an independent deacetylase for alpha-tubulin. *Protein and peptide letters* 17(5):555-558.
202. Parmigiani RB, *et al.* (2008) HDAC6 is a specific deacetylase of peroxiredoxins and is involved in redox regulation. *Proceedings of the National Academy of Sciences of the United States of America* 105(28):9633-9638.
203. Luxton GW & Gundersen GG (2007) HDAC6-pack: cortactin acetylation joins the brew. *Developmental cell* 13(2):161-162.
204. Su M, *et al.* (2011) HDAC6 regulates aggresome-autophagy degradation pathway of alpha-synuclein in response to MPP+-induced stress. *Journal of neurochemistry* 117(1):112-120.
205. Boyault C, *et al.* (2006) HDAC6-p97/VCP controlled polyubiquitin chain turnover. *The EMBO journal* 25(14):3357-3366.
206. Pandey UB, Batlevi Y, Baehrecke EH, & Taylor JP (2007) HDAC6 at the intersection of autophagy, the ubiquitin-proteasome system and neurodegeneration. *Autophagy* 3(6):643-645.
207. Pandey UB, *et al.* (2007) HDAC6 rescues neurodegeneration and provides an essential link between autophagy and the UPS. *Nature* 447(7146):859-863.
208. Slepecky NB, Henderson CG, & Saha S (1995) Post-translational modifications of tubulin suggest that dynamic microtubules are present in sensory cells and stable microtubules are present in supporting cells of the mammalian cochlea. *Hearing research* 91(1-2):136-147.
209. Webster DR & Borisy GG (1989) Microtubules are acetylated in domains that turn over slowly. *Journal of cell science* 92 (Pt 1):57-65.
210. Pugacheva EN, Jablonski SA, Hartman TR, Henske EP, & Golemis EA (2007) HEF1-dependent Aurora A activation induces disassembly of the primary cilium. *Cell* 129(7):1351-1363.

211. Matsuyama A, *et al.* (2002) In vivo destabilization of dynamic microtubules by HDAC6-mediated deacetylation. *The EMBO journal* 21(24):6820-6831.
212. Loktev AV, *et al.* (2008) A BBSome subunit links ciliogenesis, microtubule stability, and acetylation. *Developmental cell* 15(6):854-865.
213. Klionsky DJ, Cuervo AM, & Seglen PO (2007) Methods for monitoring autophagy from yeast to human. *Autophagy* 3(3):181-206.
214. Mizushima N, Yoshimori T, & Levine B (2010) Methods in mammalian autophagy research. *Cell* 140(3):313-326.
215. Eskelinen EL, Reggiori F, Baba M, Kovacs AL, & Seglen PO (2011) Seeing is believing: The impact of electron microscopy on autophagy research. *Autophagy* 7(9).
216. Swanlund JM, Kregel KC, & Oberley TD (2010) Investigating autophagy: quantitative morphometric analysis using electron microscopy. *Autophagy* 6(2):270-277.
217. Yla-Anttila P, Vihinen H, Jokitalo E, & Eskelinen EL (2009) Monitoring autophagy by electron microscopy in Mammalian cells. *Methods in enzymology* 452:143-164.
218. Ericsson JL (1969) Studies on induced cellular autophagy. I. Electron microscopy of cells with in vivo labelled lysosomes. *Experimental cell research* 55(1):95-106.
219. Klionsky DJ, *et al.* (2008) Guidelines for the use and interpretation of assays for monitoring autophagy in higher eukaryotes. *Autophagy* 4(2):151-175.
220. Terada M, *et al.* (2010) Double transgenic mice crossed GFP-LC3 transgenic mice with alphaMyHC-mCherry-LC3 transgenic mice are a new and useful tool to examine the role of autophagy in the heart. *Circulation journal : official journal of the Japanese Circulation Society* 74(1):203-206.
221. Mizushima N & Yoshimori T (2007) How to interpret LC3 immunoblotting. *Autophagy* 3(6):542-545.
222. Kabeya Y, *et al.* (2000) LC3, a mammalian homologue of yeast Apg8p, is localized in autophagosome membranes after processing. *The EMBO journal* 19(21):5720-5728.
223. Ichimura Y, Kominami E, Tanaka K, & Komatsu M (2008) Selective turnover of p62/A170/SQSTM1 by autophagy. *Autophagy* 4(8):1063-1066.
224. Komatsu M, *et al.* (2007) Homeostatic levels of p62 control cytoplasmic inclusion body formation in autophagy-deficient mice. *Cell* 131(6):1149-1163.
225. Kuma A, Matsui M, & Mizushima N (2007) LC3, an autophagosome marker, can be incorporated into protein aggregates independent of autophagy: caution in the interpretation of LC3 localization. *Autophagy* 3(4):323-328.
226. Perry CN, *et al.* (2009) Novel methods for measuring cardiac autophagy in vivo. *Methods in enzymology* 453:325-342.
227. Haspel J, *et al.* (2011) Characterization of macroautophagic flux in vivo using a leupeptin-based assay. *Autophagy* 7(6):629-642.
228. Chiang MJ & Massaro D (1979) Protein metabolism in lung. II. Influence of amino acids and glucose on protein degradation. *Journal of applied physiology: respiratory, environmental and exercise physiology* 47(5):1058-1061.
229. Thet LA, Delaney MD, Gregorio CA, & Massaro D (1977) Protein metabolism by rat lung: influence of fasting, glucose, and insulin. *Journal of applied physiology: respiratory, environmental and exercise physiology* 43(3):463-467.
230. Frasca JM, Auerbach O, Carter HW, & Parks VR (1983) Morphologic alterations induced by short-term cigarette smoking. *The American journal of pathology* 111(1):11-20.

231. Coxson HO, *et al.* (2004) Early emphysema in patients with anorexia nervosa. *American journal of respiratory and critical care medicine* 170(7):748-752.
232. Hatzitolios AI, *et al.* (1997) Diffuse soft tissue emphysema as a complication of anorexia nervosa. *Postgraduate medical journal* 73(864):662-664.
233. Overby KJ & Litt IF (1988) Mediastinal emphysema in an adolescent with anorexia nervosa and self-induced emesis. *Pediatrics* 81(1):134-136.
234. Thorburn A (2008) Apoptosis and autophagy: regulatory connections between two supposedly different processes. *Apoptosis : an international journal on programmed cell death* 13(1):1-9.
235. Tagawa Y, *et al.* (2008) Induction of apoptosis by cigarette smoke via ROS-dependent endoplasmic reticulum stress and CCAAT/enhancer-binding protein-homologous protein (CHOP). *Free radical biology & medicine* 45(1):50-59.
236. Hengstermann A & Muller T (2008) Endoplasmic reticulum stress induced by aqueous extracts of cigarette smoke in 3T3 cells activates the unfolded-protein-response-dependent PERK pathway of cell survival. *Free radical biology & medicine* 44(6):1097-1107.
237. Min T, Bodas M, Mazur S, & Vij N (2011) Critical role of proteostasis-imbalance in pathogenesis of COPD and severe emphysema. *Journal of molecular medicine* 89(6):577-593.
238. Nijholt DA, De Kimpe L, Elfrink HL, Hoozemans JJ, & Scheper W (2011) Removing protein aggregates: the role of proteolysis in neurodegeneration. *Current medicinal chemistry* 18(16):2459-2476.
239. Ding WX & Yin XM (2008) Sorting, recognition and activation of the misfolded protein degradation pathways through macroautophagy and the proteasome. *Autophagy* 4(2):141-150.
240. Fortun J, Dunn WA, Jr., Joy S, Li J, & Notterpek L (2003) Emerging role for autophagy in the removal of aggresomes in Schwann cells. *The Journal of neuroscience : the official journal of the Society for Neuroscience* 23(33):10672-10680.
241. Taylor JP, *et al.* (2003) Aggresomes protect cells by enhancing the degradation of toxic polyglutamine-containing protein. *Human molecular genetics* 12(7):749-757.
242. Greene CM & McElvaney NG (2010) Protein misfolding and obstructive lung disease. *Proceedings of the American Thoracic Society* 7(6):346-355.
243. Bouchecareilh M & Balch WE (2011) Proteostasis: a new therapeutic paradigm for pulmonary disease. *Proceedings of the American Thoracic Society* 8(2):189-195.
244. Monick MM, *et al.* (2010) Identification of an autophagy defect in smokers' alveolar macrophages. *Journal of immunology* 185(9):5425-5435.
245. Llambi F & Green DR (2011) Apoptosis and oncogenesis: give and take in the BCL-2 family. *Current opinion in genetics & development* 21(1):12-20.
246. Tait SW & Green DR (2010) Cell survival in tough times: The mitochondrial recovery plan. *Cell cycle* 9(21):4254-4255.
247. Parsons MJ & Green DR (2010) Mitochondria in cell death. *Essays in biochemistry* 47:99-114.
248. Chipuk JE, Moldoveanu T, Llambi F, Parsons MJ, & Green DR (2010) The BCL-2 family reunion. *Molecular cell* 37(3):299-310.
249. Ryter SW, *et al.* (2007) Mechanisms of cell death in oxidative stress. *Antioxidants & redox signaling* 9(1):49-89.

250. Hotchkiss RS, Strasser A, McDunn JE, & Swanson PE (2009) Cell death. *The New England journal of medicine* 361(16):1570-1583.
251. Park JW, Ryter SW, & Choi AM (2007) Functional significance of apoptosis in chronic obstructive pulmonary disease. *COPD* 4(4):347-353.
252. Demedts IK, Demoor T, Bracke KR, Joos GF, & Brusselle GG (2006) Role of apoptosis in the pathogenesis of COPD and pulmonary emphysema. *Respiratory research* 7:53.
253. Petrache I, *et al.* (2006) Ceramide causes pulmonary cell apoptosis and emphysema: a role for sphingolipid homeostasis in the maintenance of alveolar cells. *Proceedings of the American Thoracic Society* 3(6):510.
254. Petrache I, *et al.* (2005) Ceramide upregulation causes pulmonary cell apoptosis and emphysema-like disease in mice. *Nature medicine* 11(5):491-498.
255. Tang K, Rossiter HB, Wagner PD, & Breen EC (2004) Lung-targeted VEGF inactivation leads to an emphysema phenotype in mice. *Journal of applied physiology* 97(4):1559-1566; discussion 1549.
256. Kou YR & Lee TS (2010) Intratracheal siRNA for the in vivo silencing of caspase-3: a novel therapy for acute lung injury? *Critical care medicine* 38(4):1223-1224.
257. Siena L, *et al.* (2011) Reduced apoptosis of CD8+ T-Lymphocytes in the airways of smokers with mild/moderate COPD. *Respiratory medicine* 105(10):1491-1500.
258. Saetta M, *et al.* (1998) CD8+ T-lymphocytes in peripheral airways of smokers with chronic obstructive pulmonary disease. *American journal of respiratory and critical care medicine* 157(3 Pt 1):822-826.
259. Barry M & Bleackley RC (2002) Cytotoxic T lymphocytes: all roads lead to death. *Nature reviews. Immunology* 2(6):401-409.
260. Frisch SM & Screaton RA (2001) Anoikis mechanisms. *Current opinion in cell biology* 13(5):555-562.
261. Vandivier RW, *et al.* (2002) Elastase-mediated phosphatidylserine receptor cleavage impairs apoptotic cell clearance in cystic fibrosis and bronchiectasis. *The Journal of clinical investigation* 109(5):661-670.
262. Powell WC, Fingleton B, Wilson CL, Boothby M, & Matrisian LM (1999) The metalloproteinase matrilysin proteolytically generates active soluble Fas ligand and potentiates epithelial cell apoptosis. *Current biology : CB* 9(24):1441-1447.
263. Boutten A, Goven D, Artaud-Macari E, Boczkowski J, & Bonay M (2011) NRF2 targeting: a promising therapeutic strategy in chronic obstructive pulmonary disease. *Trends in molecular medicine* 17(7):363-371.
264. Rangasamy T, *et al.* (2004) Genetic ablation of Nrf2 enhances susceptibility to cigarette smoke-induced emphysema in mice. *The Journal of clinical investigation* 114(9):1248-1259.
265. Taraseviciene-Stewart L, *et al.* (2006) Is alveolar destruction and emphysema in chronic obstructive pulmonary disease an immune disease? *Proceedings of the American Thoracic Society* 3(8):687-690.
266. Gump JM & Thorburn A (2011) Autophagy and apoptosis: what is the connection? *Trends in cell biology* 21(7):387-392.
267. Norman JM, Cohen GM, & Bampton ET (2010) The in vitro cleavage of the hAtg proteins by cell death proteases. *Autophagy* 6(8):1042-1056.
268. Zhu Y, *et al.* (2010) Beclin 1 cleavage by caspase-3 inactivates autophagy and promotes apoptosis. *Protein & cell* 1(5):468-477.

269. Djavaheri-Mergny M, Maiuri MC, & Kroemer G (2010) Cross talk between apoptosis and autophagy by caspase-mediated cleavage of Beclin 1. *Oncogene* 29(12):1717-1719.
270. Wirawan E, *et al.* (2010) Caspase-mediated cleavage of Beclin-1 inactivates Beclin-1-induced autophagy and enhances apoptosis by promoting the release of proapoptotic factors from mitochondria. *Cell death & disease* 1:e18.
271. Chang NC, Nguyen M, Germain M, & Shore GC (2010) Antagonism of Beclin 1-dependent autophagy by BCL-2 at the endoplasmic reticulum requires NAF-1. *The EMBO journal* 29(3):606-618.
272. Pattingre S, *et al.* (2005) Bcl-2 antiapoptotic proteins inhibit Beclin 1-dependent autophagy. *Cell* 122(6):927-939.
273. Chen ZH, *et al.* (2010) Autophagy protein microtubule-associated protein 1 light chain-3B (LC3B) activates extrinsic apoptosis during cigarette smoke-induced emphysema. *Proceedings of the National Academy of Sciences of the United States of America* 107(44):18880-18885.
274. Debnath J, Baehrecke EH, & Kroemer G (2005) Does autophagy contribute to cell death? *Autophagy* 1(2):66-74.
275. Eum KH & Lee M (2011) Crosstalk between autophagy and apoptosis in the regulation of paclitaxel-induced cell death in v-Ha-ras-transformed fibroblasts. *Molecular and cellular biochemistry* 348(1-2):61-68.
276. Levine B & Kroemer G (2009) Autophagy in aging, disease and death: the true identity of a cell death impostor. *Cell death and differentiation* 16(1):1-2.
277. Mizushima N, Levine B, Cuervo AM, & Klionsky DJ (2008) Autophagy fights disease through cellular self-digestion. *Nature* 451(7182):1069-1075.
278. Levine B & Kroemer G (2008) Autophagy in the pathogenesis of disease. *Cell* 132(1):27-42.
279. Cho DH, *et al.* (2009) Caspase-mediated cleavage of ATG6/Beclin-1 links apoptosis to autophagy in HeLa cells. *Cancer letters* 274(1):95-100.
280. Luciani A, *et al.* (2010) Defective CFTR induces aggresome formation and lung inflammation in cystic fibrosis through ROS-mediated autophagy inhibition. *Nature cell biology* 12(9):863-875.
281. Fu L & Sztul E (2009) ER-associated complexes (ERACs) containing aggregated cystic fibrosis transmembrane conductance regulator (CFTR) are degraded by autophagy. *European journal of cell biology* 88(4):215-226.
282. MS D (1962) Quantitative methods in the study of pulmonary pathology. *Thorax* 17:320-328.
283. ER W (1979) *Sterological Methods* (Academic Press, London).
284. SI T (1945) Linear intercepts, areas and volumes. *Nature* 155(24).
285. You Y, Richer EJ, Huang T, & Brody SL (2002) Growth and differentiation of mouse tracheal epithelial cells: selection of a proliferative population. *American journal of physiology. Lung cellular and molecular physiology* 283(6):L1315-1321.
286. Davidson DJ, *et al.* (2004) Murine epithelial cells: isolation and culture. *Journal of cystic fibrosis : official journal of the European Cystic Fibrosis Society* 3 Suppl 2:59-62.
287. Davidson DJ, Kilanowski FM, Randell SH, Sheppard DN, & Dorin JR (2000) A primary culture model of differentiated murine tracheal epithelium. *American journal of physiology. Lung cellular and molecular physiology* 279(4):L766-778.

288. Olivera DS, Boggs SE, Beenhouwer C, Aden J, & Knall C (2007) Cellular mechanisms of mainstream cigarette smoke-induced lung epithelial tight junction permeability changes in vitro. *Inhalation toxicology* 19(1):13-22.
289. Overgaard CE, *et al.* (2009) Deciliation is associated with dramatic remodeling of epithelial cell junctions and surface domains. *Molecular biology of the cell* 20(1):102-113.
290. Rock JR, Randell SH, & Hogan BL (2010) Airway basal stem cells: a perspective on their roles in epithelial homeostasis and remodeling. *Disease models & mechanisms* 3(9-10):545-556.
291. Rock JR, *et al.* (2009) Basal cells as stem cells of the mouse trachea and human airway epithelium. *Proceedings of the National Academy of Sciences of the United States of America* 106(31):12771-12775.
292. Komatsu M & Ichimura Y (2010) Physiological significance of selective degradation of p62 by autophagy. *FEBS letters* 584(7):1374-1378.
293. Shen D, *et al.* (2011) Novel cell- and tissue-based assays for detecting misfolded and aggregated protein accumulation within aggresomes and inclusion bodies. *Cell biochemistry and biophysics* 60(3):173-185.
294. Suzuki M, *et al.* (2009) Curcumin attenuates elastase- and cigarette smoke-induced pulmonary emphysema in mice. *American journal of physiology. Lung cellular and molecular physiology* 296(4):L614-623.
295. Bartalesi B, *et al.* (2005) Different lung responses to cigarette smoke in two strains of mice sensitive to oxidants. *The European respiratory journal : official journal of the European Society for Clinical Respiratory Physiology* 25(1):15-22.
296. Parameswaran H, Majumdar A, Ito S, Alencar AM, & Suki B (2006) Quantitative characterization of airspace enlargement in emphysema. *Journal of applied physiology* 100(1):186-193.
297. Barnhart BC, Lee JC, Alappat EC, & Peter ME (2003) The death effector domain protein family. *Oncogene* 22(53):8634-8644.
298. Green DR (2005) Apoptotic pathways: ten minutes to dead. *Cell* 121(5):671-674.
299. Gajate C, *et al.* (2004) Intracellular triggering of Fas aggregation and recruitment of apoptotic molecules into Fas-enriched rafts in selective tumor cell apoptosis. *The Journal of experimental medicine* 200(3):353-365.
300. Schlegel A & Lisanti MP (2001) The caveolin triad: caveolae biogenesis, cholesterol trafficking, and signal transduction. *Cytokine & growth factor reviews* 12(1):41-51.
301. Couet J, Sargiacomo M, & Lisanti MP (1997) Interaction of a receptor tyrosine kinase, EGF-R, with caveolins. Caveolin binding negatively regulates tyrosine and serine/threonine kinase activities. *The Journal of biological chemistry* 272(48):30429-30438.
302. Jin Y, *et al.* (2009) Caveolin-1 regulates the secretion and cytoprotection of Cyr61 in hyperoxic cell death. *The FASEB journal : official publication of the Federation of American Societies for Experimental Biology* 23(2):341-350.
303. Jin Y, *et al.* (2008) Deletion of caveolin-1 protects against oxidative lung injury via up-regulation of heme oxygenase-1. *American journal of respiratory cell and molecular biology* 39(2):171-179.
304. Wang XM, *et al.* (2006) Caveolin-1: a critical regulator of lung fibrosis in idiopathic pulmonary fibrosis. *The Journal of experimental medicine* 203(13):2895-2906.

305. Hoetzel A, *et al.* (2009) Carbon monoxide prevents ventilator-induced lung injury via caveolin-1. *Critical care medicine* 37(5):1708-1715.
306. Zhao YY, *et al.* (2009) Persistent eNOS activation secondary to caveolin-1 deficiency induces pulmonary hypertension in mice and humans through PKG nitration. *The Journal of clinical investigation* 119(7):2009-2018.
307. Kang R, Zeh HJ, Lotze MT, & Tang D (2011) The Beclin 1 network regulates autophagy and apoptosis. *Cell death and differentiation* 18(4):571-580.
308. Liang XH, *et al.* (1998) Protection against fatal Sindbis virus encephalitis by beclin, a novel Bcl-2-interacting protein. *Journal of virology* 72(11):8586-8596.
309. Ciechomska IA, Goemans GC, Skepper JN, & Tolkovsky AM (2009) Bcl-2 complexed with Beclin-1 maintains full anti-apoptotic function. *Oncogene* 28(21):2128-2141.
310. Inoue D, *et al.* (2011) Inducible disruption of autophagy in the lung causes airway hyper-responsiveness. *Biochemical and biophysical research communications* 405(1):13-18.
311. Bodas M, Min T, & Vij N (2010) Early-age-related changes in proteostasis augment immunopathogenesis of sepsis and acute lung injury. *PloS one* 5(11):e15480.
312. Maguire JA, Mulugeta S, & Beers MF (2011) Endoplasmic reticulum stress induced by surfactant protein C BRICHOS mutants promotes proinflammatory signaling by epithelial cells. *American journal of respiratory cell and molecular biology* 44(3):404-414.
313. Wang WJ, Mulugeta S, Russo SJ, & Beers MF (2003) Deletion of exon 4 from human surfactant protein C results in aggresome formation and generation of a dominant negative. *Journal of cell science* 116(Pt 4):683-692.
314. Schlegel A, *et al.* (1998) Crowded little caves: structure and function of caveolae. *Cellular signalling* 10(7):457-463.
315. Le Lay S, *et al.* (2010) The lipoatrophic caveolin-1 deficient mouse model reveals autophagy in mature adipocytes. *Autophagy* 6(6):754-763.
316. Aita VM, *et al.* (1999) Cloning and genomic organization of beclin 1, a candidate tumor suppressor gene on chromosome 17q21. *Genomics* 59(1):59-65.
317. Liang XH, *et al.* (1999) Induction of autophagy and inhibition of tumorigenesis by beclin 1. *Nature* 402(6762):672-676.
318. Matsui Y, *et al.* (2007) Distinct roles of autophagy in the heart during ischemia and reperfusion: roles of AMP-activated protein kinase and Beclin 1 in mediating autophagy. *Circulation research* 100(6):914-922.
319. Kirkin V, McEwan DG, Novak I, & Dikic I (2009) A role for ubiquitin in selective autophagy. *Molecular cell* 34(3):259-269.
320. Yao TP (2010) The role of ubiquitin in autophagy-dependent protein aggregate processing. *Genes & cancer* 1(7):779-786.
321. Marambio P, *et al.* (2010) Glucose deprivation causes oxidative stress and stimulates aggresome formation and autophagy in cultured cardiac myocytes. *Biochimica et biophysica acta* 1802(6):509-518.
322. Taylor RC & Dillin A (2011) Aging as an event of proteostasis collapse. *Cold Spring Harbor perspectives in biology* 3(5).
323. Chen H, *et al.* (2007) Detrimental metabolic effects of combining long-term cigarette smoke exposure and high-fat diet in mice. *American journal of physiology. Endocrinology and metabolism* 293(6):E1564-1571.

324. Mineur YS, *et al.* (2011) Nicotine decreases food intake through activation of POMC neurons. *Science* 332(6035):1330-1332.
325. Ozcan U, *et al.* (2006) Chemical chaperones reduce ER stress and restore glucose homeostasis in a mouse model of type 2 diabetes. *Science* 313(5790):1137-1140.
326. Petrovski G, Zahuczky G, Majai G, & Fesus L (2007) Phagocytosis of cells dying through autophagy evokes a pro-inflammatory response in macrophages. *Autophagy* 3(5):509-511.
327. Huang C, *et al.* (2010) Autophagy induced by ischemic preconditioning is essential for cardioprotection. *Journal of cardiovascular translational research* 3(4):365-373.